Coverage Problems in Mobile Sensing

by

Ajay A. Deshpande

B.Tech., M.Tech., Mechanical Engineering
Indian Institute of Technology Bombay, 2001
S.M., Mechanical Engineering
Massachusetts Institute of Technology, 2006
S.M., Electrical Engineering and Computer Science
Massachusetts Institute of Technology, 2006

Submitted to the Department of Mechanical Engineering
in partial fulfillment of the requirements for the degree of

Doctor of Philosophy

at the

MASSACHUSETTS INSTITUTE OF TECHNOLOGY

September 2008

Author .....
Department of Mechanical Engineering
August 28, 2008

Certified by .....
Sanjay E. Sarma
Associate Professor of Mechanical Engineering
Thesis Supervisor

Certified by .....
Daniela Rus
Professor of Electrical Engineering and Computer Science
Thesis Supervisor

Accepted by .....
Lallit Anand
Chairman, Department Committee on Graduate Students

Coverage Problems in Mobile Sensing

by

Ajay A. Deshpande

Submitted to the Department of Mechanical Engineering
on August 28, 2008, in partial fulfillment of the
requirements for the degree of
Doctor of Philosophy

Abstract

Sensor-networks can today measure physical phenomena at spatial and temporal scales that were not achievable earlier, and have shown promise in monitoring the environment, structures, agricultural fields and so on. A key challenge in sensor-networks is the coordination of four actions across the network: measurement (sensing), communication, motion and computation. The term *coverage* is applied to the central question of how *well* a sensor-network senses some phenomenon to make inferences. More formally, a coverage problem involves finding an arrangement of sensors that optimizes a coverage metric.

In this thesis we examine coverage in the context of three sensing modalities. The literature on the topic has thus far focused largely on coverage problems with the first modality: static *event-detection sensors*, which detect purely binary events in their immediate vicinity based on thresholds. However, coverage problems for sensors which measure physical quantities like temperature, pressure, chemical concentrations, light intensity and so on in a network configuration have received limited attention in the literature. We refer to this second modality of sensors as *estimation sensors*; local estimates from such sensors can be used to reconstruct a field. Third, there has been recent interest in deploying sensors on mobile platforms. Mobility has the effect of increasing the effectiveness of sensing actions. We further classify sensor mobility into incidental and intentional motion. Incidentally mobile sensors move passively under the influence of the environment, for instance, a floating sensor drifting in the sea. We define intentional mobility as the ability to control the location and trajectory of the sensor, for example by mounting it on a mobile robot.

We build our analysis on a series of cases. We first analyze coverage and connectivity of a network of floating sensors in rivers using simulations and experimental data, and give guidelines for sensor-network design. Second, we examine intentional mobility and detection sensors. We examine the problem of covering indoor and outdoor pathways with reconfigurable camera sensor-networks. We propose and validate an empirical model for detection behavior of cameras. We propose a distributed algorithm for reconfiguring locations of cameras to maximize detection performance. Finally, we examine more general strategies for the placement of estimation sensors

and ask when and where to take samples in order to estimate an unknown spatio-temporal field with tolerable estimation errors. We discuss various classes of error-tolerant sensor arrangements for trigonometric polynomial fields.

Thesis Supervisor: Sanjay E. Sarma
Title: Associate Professor of Mechanical Engineering

Thesis Supervisor: Daniela Rus
Title: Professor of Electrical Engineering and Computer Science

Acknowledgments

First of all, I would like to thank my advisors, Sanjay Sarma and Daniela Rus, without whose support and invaluable guidance this work would not have been possible.

Words are not enough to express my gratitude towards Sanjay. I have learned so much from him through his unique research-style. He gave me complete freedom in terms of the classes that I took and the problems I chose to work on and I value that a lot. I am simply held in awe by his in-depth understanding of a wide range of areas, his ability to ask *right* questions, his vision and bold approach to research. Besides research, he has given me invaluable advice on various other aspects of life for which I will be forever indebted to him. His energy and enthusiasm are highly contagious. I truly thank him for the TA opportunities he gave me. Sanjay, thanks a lot for everything!

I am truly grateful to Daniela for having given me an opportunity to work in her group. I have learned a great deal from her about research over the last few years. I am amazed by her energy and her ability to successfully run such a large research group. I thank her for providing work-space in Stata Center. I thank her for the opportunity she provided me to collaborate with our collaborators at the University of Southern California. I also thank her for generously funding my conference trips.

I am grateful to Devavrat Shah for being an excellent mentor for the last few years at MIT. I truly appreciate the constructive criticism he gave me on my research. I also thank him for detailed comments on my thesis.

I would like to thank Dr. David Brock for several useful suggestions during the committee meetings and comments on the thesis.

Work discussed in Chapter 4 was done in collaboration with Sameera Poduri and Gaurav Sukhatme at the University of Southern California. I am thankful to them for this great collaboration. I had several fruitful discussions with Sameera during our meetings and over phone. I am thankful to Gaurav for his useful comments on work in the second part of this thesis.

I truly acknowledge pointers provided by Prof. Vivek Goyal on related work in

frame theory.

I thank Prof. Harold Hemond for useful discussion on river work. I would also like to thank David Holtschlag of the USGS for generously providing me with their experimental data used in Chapter 3 of this thesis.

I would like to thank all the current and former members of Sanjay's research group, Rahul Bhattacharyya, Isaac Ehrenberg, Christian Floerkemeier, Patrick Hacker, Stephen Ho, Kashif Khan, Taejung Kim, Sriram Krishnan, Sumeet Kumar, Kirti Mansukhani, Seung-Kil Son and Marty Vona for creating wonderful atmosphere at the workplace. I would like to thank Sriram for being an excellent mentor and a great office mate over the years. I collaborated with Taejung Kim on art-gallery work and learned a lot from him about paper writing. I would like to thank Stephen Ho for proof-reading an early draft of this thesis and providing several useful suggestions. I thank him for several fruitful discussions we have had over the last year. I would like to thank Christian Floerkemeier for several discussions we have had over lunch. I would especially like to thank Christian and Stephen for taking time out to patiently listen to my defense practice presentation and providing so many useful suggestions. I would also like to thank Edmund Schuster for several useful discussions on applications of my work, and his kind and encouraging words.

I would also like to thank the members of Daniela's research group (Distributed Robotics Laboratory), especially Mac Schwager and Marty Vona, for so many useful discussions.

I would like to thank David Rodriguera and Rachel Russell of the Laboratory for Manufacturing and Productivity along with Leslie Regan and Joan Kravit at the Graduate Office of Mechanical Engineering for the incredible support they provided on the administrative front. Because of them I never had to bother about any administrative issues.

I was fortunate enough to have a great set of friends at MIT. I would like to thank Sreekar Bhaviripudi, Shashibhushan Borade, Amit Deshpande, Rohit Karnik, Dhanushkodi Mariappan, Ashish Shah, Vijay Shilpiekandula, Amit Surana, Kripa Varanasi and Murtaza Zafer. I have spent real quality time with these guys and have

learned a lot from each one. I will forever cherish the fun-times we have had together. I have spent countless hours with both the Amits, Vijay, Dhanush and Kripa chatting over afternoon coffee, lunches and dinners. These guys are like my brothers. I would also like to thank my friends in other parts of the world including my school friends and my IIT friends.

I would like to thank all my relatives and friends back in India for their support and love. They have always made my every trip to India a memorable one. I would like to thank Sunita (my brother's wife) for her support and encouragement. I thank Amma-Appa (my in-laws) for treating me like their own son. I thank Prahladh for being a big brother. He has left indelible impressions in my life through his thoughts and actions, and continues to inspire me. If not for him, I would have never met Pavithra, my wife and his sister! Finally I would like to thank my dearest wife Pavithra, my brother Nitin, Aai (Alka Deshpande) and Baba (Ashok Deshpande) for their constant love and endless encouragement. To them I dedicate this thesis. Pavithra, the sweetest dream unfolded before my eyes, brings the spark in my life and is the biggest source of my strength. Nitin has always been my true friend, philosopher and role model in life. Aai-Baba have made countless sacrifices and molded me into what I am today. I attribute my success so far to my parents and my brother.

To Aai, Baba, Nitin

and

Pavithra

Contents

List of Figures

List of Tables

Chapter 1

Introduction

Wireless sensor networks have revolutionized the way we can collect information about the physical world. Advances in three key technologies, integrated circuits, wireless communications, and micro and nano-mechanical systems in the last two decades lead to the advent of cheap, low-power and compact *wireless sensors*. These sensors have shown great promise in monitoring urban and natural environments, structures, agricultural fields, industries, and so on by providing data at spatial and temporal scales that were not achievable before. For example, in structural monitoring applications, wireless sensors regularly monitor the health of structures such as buildings and bridges, and can warn of impending failures. As another example, sensors fixed at traffic signals combined with sensors on automobiles can provide real-time update on traffic conditions in urban environments. In each application, sensors provide real-time mapping of some aspects of the physical world.

Each sensor in a sensor-network embodies three abilities: *sensing*, *communication* and *computation*. If a sensor is mounted on a mobile agent such as a robot, an animal or a float in water, it has yet a yet another ability, *mobility*. In the cost, size and power-regime of sensors that we consider suitable for sensor-networks applications, a sensor is heavily constrained in each of its abilities. Sensors have limited battery-life, memory, computational capacity, and sensing resolution. They are also prone to failures. Power and adverse mobility patterns heavily limit communication ability. The main challenge in a sensor-network is the coordination of sensors' limited abilities

across the network for the desired application. However, despite these limitations, sensor-networks have demonstrated success in quite a few applications. Since its emergence towards the end of the last century, sensor-networks has been an active area of research and still in its early stage.

A central question in sensor-networks is how *well* sensors can sense and map some physical phenomenon. For example, in structural monitoring applications, we may ask how many sensors we may need and where we mount them on a structure or how reliable are the overall inferences about the sensors' measurements. It seems that one configuration might be better over the other configuration of the sensors in the sense of sensing quality. The term *coverage problems* applies to the class of problems that implicitly tries to address these questions. More formally, a coverage problem involves formulating an overall coverage metric based on an individual sensor's behavior and optimizing it over different configurations. This thesis addresses coverage problems in sensor networks with special emphasis on mobile sensing.

1.1 Problems addressed in this Thesis

The overall coverage metric depends on an individual sensor's sensing behavior, which in turn depends on the kind of sensors. The literature on coverage problems thus far has focused on static sensors that detect purely binary events in their immediate vicinity based on thresholds. It is possible to associate a spatial *sensing-performance function* with each sensor. For example, some sensors can detect the presence of an event only within a certain range. The sensing-performance function in this case can be a step function that is 1 over the circular disc of radius equal to the range and 0 everywhere else. This model is known as the *disc model* of coverage in the literature. In yet another example, some sensors can have an explicit sensing performance-function in which performance decreases as a function of distance. We call this type of sensors *event-detection* sensors. Apart from event-detection sensors, there is another type of sensors in which sensors measure physical quantities like temperature, pressure, chemical concentrations, light intensity and so on in a network configuration. We

refer to this type of sensors as *estimation* sensors. In estimation applications, local estimates are used to reconstruct the spatio-temporal *field* of the unknown physical quantity. Coverage problems for such sensors have received limited attention in the literature. In this thesis, we address coverage problems for both event-detection and estimation sensors.

Recently, there has been great interest in deploying sensors on mobile platforms such as robots, floats in water, animals, and cars. Mobility adds another degree of freedom in coverage problems. It has the effect of increasing the effectiveness of sensing actions and can significantly alter the definition of the coverage metric. For example, the coverage of a mobile sensor with the disc model is the area covered by the sweeping of the disc. We classify sensor mobility into *incidental* and *intentional* motion. Incidentally mobile sensors move passively under the influence of the environment, for instance, sensors attached to animals or a floating sensor drifting in the sea. We refer to a sub-class of incidental motion where sensors move under the influence of natural forces as *natural mobility*. We define intentional mobility as the intentional control of the location and trajectory of the sensor. An example is a sensor mounted on a mobile robot. This thesis addresses the three categories of coverage problems at the intersection of both mobility models, incidental and intentional, and both sensor types, detection and estimation. In summary, the problems we address are:

1. **Naturally mobile event-detection sensors in rivers:** We address the coverage of floating sensors moving passively in rivers. We consider event-detection sensors with the disc model. The disc model is also used to model communication between two nodes. Two nodes can communicate with each other if the distance between them is less than the communication range. We analyze the *connectivity* of the moving network.

2. **Reconfigurable camera-networks:** We examine the problem of covering indoor and outdoor pathways using a reconfigurable camera-network where cameras are intentionally mobile. We also address the problem of modeling the

detection behavior of an individual camera.

3. **Sensor arrangement problem:** We introduce the sensor arrangement problem as a kind of coverage problem for the estimation sensors that provide local sample values of a field of some physical quantity. The samples can be used to reconstruct the unknown field. Using the sampling theory and estimation theory, we formulate the coverage metric as the error in the field reconstruction. The error is a function of the geometric arrangement of the sensors. The sensor arrangement problem addresses the question of when and where to take samples in order to estimate an unknown spatio-temporal field with tolerable estimation errors.

The table below shows our categorization of the sensors and mobility types, and the combinations we address.

Table 1.1: Our categorization of sensors and mobility types and the coverage problems addressed in this thesis

Sensor Types	Mobility Types	
	Incidental	Intentional
Event-detection	Coverage and connectivity of a network of floating sensors in rivers	Reconfiguring a network of cameras to cover pathways
Estimation	Sensor Arrangement Problem	

1.2 Summary of our Contributions

A summary of our contributions for each coverage problem is as follows.

1. **Naturally-mobile event-detection sensors in rivers:** We analyze coverage and connectivity under the disc model of a network of floating detection-sensors moving passively in rivers. Our work appears to be one of the first efforts to study the impact of natural mobility on coverage and connectivity. We analyze coverage and connectivity by simulating floating-sensor trajectories in

two situations, 1) an *ideal-channel* river for which we propose a natural mobility model based on hydrodynamics literature, 2) a mesh model obtained using GPS location data for drifting floats in St. Clair River in Michigan at two sites. We assume that the sensors are initially placed uniformly randomly across the transverse cross-section of the river. Here is a summary of our observations.

- **Coverage:** Our choice of the coverage metric is the area swept by the discs around the floating sensors. We show results on coverage versus time for different numbers of nodes. We show that if the number of nodes is large enough, coverage relates to the cross-sectional average of the surface velocity.
- **Connectivity:** We measure network-connectivity in terms of the size of the *largest connected cluster* (LCC). We divide the river into three zones (or more depending on the width of the river) and analyze connectivity in each zone. We observe that connectivity in the central zone sustains for a long duration whereas connectivity in side zones decreases rapidly over time.

In each case, we provide analysis of how coverage and connectivity depends on motion parameters in the limiting sense.

2. **Reconfigurable camera-networks:** The coverage problem involving detection-sensors with spatial sensing-performance functions is formulated as the locational optimization problem in the literature [14], [69], [51]. The Lloyd's descent algorithm yields a locally optimal solution to the locational optimization problem. Intentionally mobile sensors can emulate Lloyd's descent in a distributed way and provide a locally optimal solution to the coverage problem [14]. The work so far deals with the sensors that exhibit identical behavior everywhere. We consider a class of sensors for which the sensing-performance function is location dependent. A camera is an example of such sensors. We formulate the coverage problem for such sensors as a new type of locational optimization problem. We propose a modified form of the Lloyd's descent algorithm and

prove that it guarantees convergence to the local optimal solution. As an application we consider the problem of covering indoor and outdoor pathways with a network of intentionally-mobile Cyclops cameras. We propose an empirical model for the sensing-performance function of the camera, which is location dependent. We present the simulation and experimental results.

3. **Sensor arrangement problem:** In this thesis, we restrict our work to the fields that are modeled as a linear combination of a set of known basis functions. We assume that the sensor measurements are corrupted with additive noise. In this setting, the minimum variance unbiased estimator (MVUE) yields the optimal mean squared error (MSE) for given sample values over all possible estimators [48]. We choose the MSE corresponding to the MVUE as the error metric for the sensor arrangement problem.

   Our approach is to characterize different classes of sensor arrangements and to understand the circumstances under which the MSE satisfies the error tolerance limit. We refer to these classes of arrangements as Error Tolerant Arrangement Classes or ETAC's. In this work we discuss different types of ETAC's for fields that are modeled as 2D trigonometric polynomials: regular grid sensor arrangements, Δ-dense sensor arrangements, incrementally constructed sensor arrangements and random sensor arrangements. With a knowledge of the nature of ETAC's we will have articulated constraints for placing sensors in time and space; furthermore, by identifying possible sampling locations *in advance*, we will also have simplified the planning of the motion of mobile sensors for that field.

1.3 Structure of this Thesis

In Chapter 2 we provide a brief background on sensor-networks and literature review on the problems we address. We divide the rest of the thesis into two parts. In Part I, we discuss two coverage problems related to event-detection sensors. In Part II, we

deal with estimation sensors.

- **Part I:** In Chapter 3, we discuss the coverage and connectivity problems in a network of floating sensors in rivers. In Chapter 4, we deal with the problem of covering indoor and outdoor pathways using a network of reconfigurable cameras.

- **Part II:** We address the sensor arrangement problem for the estimation sensors in this part of the thesis. In Chapter 5, we briefly review the relevant results from frame theory and nonuniform sampling. In Chapter 6, we formally define the sensor arrangement problem and outline our approach. We then discuss a few classes of error-tolerant sensor arrangements for trigonometric polynomials. In Chapter 7, we formulate a couple of optimization problems related to mobility of estimation sensors.

We summarize our contributions in Chapter 8 and outline future work.

Chapter 2

Literature Review

There has been a flurry of papers published on sensor networks in the last decade. Sensor networks have several aspects and providing an overview of these is a monumental task. In this chapter, we attempt to provide a quick overview of sensor networks and its various aspects, and present a brief review of work related to the problems we address in this thesis. The chapter is organized as follows:

Organization: In Section 2.1, we provide an overview of sensor networks including their applications and describe differences with traditional networks. In Section 2.2, we introduce coverage problems in sensor networks. In the same section, we provide our categorizations of sensor types and sensor mobility. The problems we address in this thesis are organized around these categorizations. Subsequently we present a review of existing literature on the coverage problems addressed in this thesis.

2.1 Sensor Networks

Sensor networks came into prevalence in the 1990's. This was enabled by the convergence of three key technologies: integrated circuits, wireless communications and micro-electro mechanical systems (MEMS). Advances in each of these areas led to the development of cheap, low-power and compact sensors, also referred to as sensor nodes or simply nodes. Each node has one or more sensors along with *computation* and

communication capabilities. Early papers in this area, *e.g.*, [23], [66], [47] provided future application scenarios, emphasized the paradigm shift beyond the Internet, put forward sensor network challenges and proposed early solutions. Since then the area of sensor networks has been an active area of research with many open questions. [2] is a comprehensive survey article that discusses applications, factors influencing sensor networks design and contemporary efforts. [89], [67], [50] are examples of books entirely dedicated to this subject.

2.1.1 What is a sensor network?

A sensor network is formed by a group of autonomous sensor nodes that coordinate among themselves through networking to apply themselves on a larger sensing task. Each sensor has an ability to perform low-power signal processing, computation and low-power wireless networking [66]. These nodes differ significantly from traditional sensors. In the traditional sensor paradigm, sensors tended to be very precise, expensive, bulky, hence very few in numbers, tethered to the base station using wires and deployed carefully. Much of the processing is done centrally and there is no protection against sensor failure. Modern sensors are viewed to be cheap, compact, less precise but can be deployed in a large numbers. Wireless networking provides the ability for sensors to coordinate among themselves. Sensors are prone to failures due to power constraints. These fundamental changes in operational settings have not only opened up avenues for several potential applications but also need to address new challenges.

A sensor has three key abilities, *sensing*, *communication* and *computation*. There is a range of open problems in each of these areas as well as at the intersections of these. Sometimes a sensor has an additional ability, *mobility*. In some applications, mobility provides an alternative to having a large number of static sensors, whereas in some applications, the environment itself is dynamic and makes sensors move. Examples include sensors moving with water, wind currents, sensors attached to humans, animals, robots, *etc.* This opens a new set of challenges. In this thesis, we mainly address the problems at the intersection of two abilities, sensing and mobility.

2.1.2 Applications

Sensor networks have shown a great promise in monitoring events by providing measurements at scales that was not possible with traditional sensors. This has enabled a wide range of applications in domains such as military, health, urban and natural environments, agriculture, industries, civil infrastructures. It is seen as a great tool to advance research in other scientific communities such as geology, biology, ecology. Below we cite a few examples from recent deployments in different application domains.

- Habitat monitoring: In two deployments, first 32 and then 150 UC Berkeley sensor motes, known as *mica* motes were deployed on Great Duck Island, off Maine coast, to monitor seabird nesting and behavior. Motes formed an *ad hoc* network among themselves to upload data every few minutes to a few motes who had access to the Internet. The data on temperature, humidity and local images could be remotely seen live on the Internet. For details, we refer readers to [55] and [75]. More than 100 nodes were deployed as a part of the Extensible Sensing System (ESS) at the University of California James Reserve in the San Jacinto Mountains to monitor animal presence. Micro-climate data consisting of sunlight, temperature, humidity, air pressure was collected above and below the ground level [76]. Other examples of research efforts related to habitat monitoring applications are [5] and [65].

- Environmental monitoring: In [19] and [88], the authors consider deployment of a network of a few static sensors and mobile robotic boats equipped with sensors in a lake to study growth of micro-organisms. In [88], the authors report on experimental results in sampling temperature and chlorophyll concentration levels in a lake. Other examples of research efforts related to environmental monitoring applications are [1], [65] and [73].

- Structural monitoring: A wireless sensor system called *Wisden* consisting of vibration sensors was deployed on a seismic test structure to test reliable recovery of structural vibration data [63], [86].

- Agriculture: 65 nodes were deployed in a wine grape vineyard, for 6 months to collect with agricultural significance [6]. In vineyard low temperatures can significantly damage the crop. In the past only a single measurement station was used although local temperatures vary considerably. The dense multi-hop sensor network was shown to reliably collect data. In [8], the idea of using humans, animals operating in the vineyard as *data mules* carrying sensors was proposed. The authors, in agricultural settings, suggest the need for carrying our human-centered research.

- Underwater applications: Water bodies including oceans, rivers and lakes constitute 70% of ocean sampling. Monitoring these systems manually is virtually impossible [82]. An underwater sensor network platform consisting of static sensors, *Aquaflecks* and mobile nodes, *Starbug* and *Amour* was developed in [82] for long-term monitoring of coral reefs and fisheries. Optical and acoustic networking protocol are presented for underwater communications. A mobile sensor network consisting of five *spray* gliders and ten *Slocum* gliders was deployed in Monterey Bay to collect data based on an adaptive data sampling strategy [52].

- Traffic monitoring: A traffic surveillance system consisting of a wireless sensor network and access point was proposed in [11]. *Traffic-Dot* node proposed in this system consists of a magnetometer sensor to detect vehicles and MICA2MOTE, a mote in the family of Berkeley motes. *CarTel* is a distributed sensor computing system designed to process data from sensors attached to mobile units such as automobiles [45]. In addition to the obvious application of road traffic monitoring, CarTel is also seen useful in environmental monitoring using pollution sensors, civil infrastructure monitoring, geo-imaging.

2.1.3 Differences with Traditional Network Design

Sensor networks were seen as an answer to the question, what next beyond personal computers and the Internet [47], [23]. Although lessons learnt from the Internet and

mobile network design are applicable, sensor networks present some unique challenges [23] which demand different design paradigms. We summarize a few of the differences compared with the traditional network design below [23], [2].

- The *sheer number* of sensor nodes deployed without any control naturally poses scalability challenges.
- Sensors are limited in power, computational capacity and memory.
- Sensors are prone to failure.
- Topology of the network keeps changing frequently because of sensor failures or mobility of nodes.
- Individual sensors may have IDs but the overall interest is in global identification.
- Sensor nodes mainly use broadcast communication paradigm as opposed to point-to-point communications.

These factors influence the design of a sensor network demanding re-thinking of conventional algorithms.

2.2 Coverage Problems in Sensor Networks

The main challenge in sensor networks is to coordinate four abilities, sensing, communication, computation and mobility, across the nodes for sensing a phenomenon. This leads to a flurry of problems pertaining to the individual ability as well as the combinations of two or more abilities. This thesis mostly focuses on an issue related to sensing termed as with emphasis on mobile sensors. A central question in sensing a how *well* sensor networks can sense a particular phenomenon. This question relates to the notion of *quality of sensing* (QoS) and is addressed under a class of problems called as *coverage problems* in sensor networks.

Coverage problems are not unique to the field of sensor networks. They arise frequently in other areas such as theory of computation, computational geometry and robotics. In theory of computation, set cover and a related vertex cover problems are examples of coverage problems. Both minimum set cover and vertex cover problems are NP-hard [74]. In computational geometry, art gallery problems are examples coverage problem. The classic art gallery problem involves finding the minimum number of guards and their locations in an art gallery such that every point in the gallery is *guarded* by at least one guard [62]. There are a number of variations on this problem and optimization version of most of these problems are NP-hard [62], [72], [80] and [22]. In robotics, the problem of mapping and exploring an unknown environment using mobile robots is a type of coverage problem. In [26], Gage presents classification of different types of coverage problems in many-robot systems. A typical coverage problem in sensor networks involves finding a geometric configuration or an *arrangement* of sensors that guarantees *good* QoS. More formally, a coverage problem involves finding an arrangement that optimizes some coverage metric. This metric is based on behavior of an individual sensor. In this thesis we address coverage problems in sensor networks with emphasis on mobile sensors. Through the rest of this chapter we present a detailed literature review related to the coverage problems we address in this thesis. First, we provide categorization of sensors into two types based on sensing functionality.

2.2.1 Sensors Classification

Depending on the applications, sensor networks consist of various types of sensors such as thermal, visual, infra-red, acoustic, seismic [2]. Some sensors' functionality involves scanning space around them to detect an event of interest whereas some sensors simply measure physical quantities locally. Based on this observation we categorize sensors into two types: *event detection* and *estimation*. In event detection, sensors remotely scan the space around them and detect binary events based on thresholds. In estimation applications, sensors provide a local measure of a physical quantity like temperature, pressure, chemical concentrations, light intensity and so

on.

Examples of detection sensors include infra-red sensors, cameras, motion-detection sensors, etc. In such sensors, detection-ability of sensors degrades with distance. In formulation of coverage problems related to such sensors, different models have been proposed to characterize behavior of such sensors [83], [85], [15], [44], [49], [64], etc. The most simple abstraction is a *disc model* (see [83], [85], [70], etc.) where a detection sensor can detect an event within certain range or *coverage radius*. The coverage problem in this case amounts to providing geometric coverage with discs centered at sensor-locations. In another abstraction, an analytic model is to characterize spatial performance of a sensor. This is referred to as a *sensing performance function* [15]. For example, in [15], a sensing performance function that is inversely proportional to the distance between the sensor and a point is used. The coverage problem formulation in case of such sensors is more involved.

In case of estimation sensors, measurements provided by sensors can be used to reconstruct a field. The quality of estimation depends on the number of sensors, sensor noise and sensors' location. Given the measurement values and their locations, and sensor-noise characterization, estimation theory can be used to estimate the unknown field and find the corresponding estimation error. We think of the coverage problem in case of such sensors as an inverse of the estimation problem. We wish to find an arrangement of sensors such that the estimation error being the coverage metric is minimized.

In this thesis, we address coverage problems for both kinds of sensors with emphasis on mobile sensors. In the next section, we provide classification of mobility of sensors.

2.2.2 Mobility classification

Mobility has become an important aspect of sensor networks owing to advances in robotics, wireless networks and mobile computing. It has lead to a number of challenging problems pertaining to the other aspects of sensors, sensing, communication and computing. We focus on sensing among these.

Networks involving static sensors alone have fixed coverage since nodes' locations are fixed. In some situations, the number of sensors required to provide guaranteed coverage may be very high and may lead to higher costs. For example, in monitoring large domains such as oceans and rivers, the number of static sensors required for monitoring may be very high. In such situations, a few mobile sensors may be necessary and effective. Mobility has the effect of multiplying the number of sensors in the field. Theoretically, a sensor which can move infinitely fast can be at many places at one time instance. A sensor moving at some finite velocity effectively enables that single sensor to act like some finite number of sensors in time-space, enabling what we refer to as *multiplicity*. We categorize sensor mobility into two types, *incidental* and *intentional*. We define incidental mobility as a situation in which a sensor does not have control over its motion. In these situations a sensor moves passively under the influence of the environment (e.g., sensors moving with water currents and nodes mounted on animals). We define intentional mobility as a situation in which a sensor has control over its motion and can actively move to a desired location (e.g., nodes mounted on mobile robots). The advantage of incidental mobility is that neither power nor control is an issue because nodes move under the influence of the external sources. At the same time, coverage depends on the mobility of nodes. On the other hand, intentional mobility provides control over nodes' location and may lead to better coverage but requires effective control strategies and perhaps more power.

In this thesis, we address three coverage problems at the intersection of both mobility types, incidental and intentional and both detection and estimation sensors. We reproduce below Table 1.1 from Chapter 1, which summarizes our categorizations and the coverage problems addressed in this thesis. In what follows, we provide summary of related work on each coverage problem.

Table 2.1: Our categorization of sensors and mobility types and the coverage problems addressed in this thesis

Sensor Types	Mobility Types	
	Incidental	Intentional
Event-detection	Coverage and connectivity of a network of floating sensors in rivers	Reconfiguring a network of cameras to cover pathways
Estimation	Sensor Arrangement Problem	

2.3 Detection Sensors with Disc Coverage Model Floating in Rivers

In the first problem we address in this thesis, we study a network of floating detection-sensors in rivers. We assume that each sensor has the disc model for its coverage. We first present motivation and applications of networks of floating sensors in rivers. Then we present a summary of related work on coverage problems related to sensors with the disc-coverage model. The disc model is also used to model network connectivity. According to this model, two nodes can communicate with each other if the distance between them is less than the communication range. Thus a node is connected to all the nodes within a disc of radius equal to the communication range. Due to similarity of the tools used in the analysis of coverage and connectivity for the disc model, in this thesis we also analyze the connectivity of a network of floating sensors in rivers. We therefore provide a brief literature review on connectivity as well.

2.3.1 Motivation for the river application

70% of the earth's surface is covered with large water bodies – rivers, lakes and oceans. These water bodies stretch over several miles and monitoring at these scales is virtually impossible. However they provide one of the biggest sources of natural mobility in terms of water currents. Floating sensor networks have the potential of providing new levels of automation for monitoring spatio-temporal phenomena in these domains. These include mapping fields of physical quantities such as temper-

ature, salinity, chemical concentrations. This will assist environmental scientists in localizing sources of groundwater seepage in rivers, waste-water spills, pollutants, high nitrogen levels, high vegetation levels, etc. that greatly affect the quality of water [1, 41, 19, 73]. Furthermore there is huge interest in building hydrodynamic models of rivers in order to understand the effects of contaminants propagation in public water intakes [1, 42, 43]. In all these applications the function of anchored buoy sensors is limited in scale and is less capable of collecting sufficient data to detect local events or to model flow patterns [42, 43]. The deployment of a network of floating sensors that move with the flow seems to hold great promise by providing more coverage and flexibility in data collection.

2.3.2 Coverage and connectivity with respect to a disc model

There is a large body of theoretical work in the area of sensor networks that deals with coverage and connectivity analysis corresponding to the disc model (e.g. [39, 56, 9, 85, 70, 53]). With the exception of [53], the other works deal with static sensors that are placed uniformly randomly. In case of static sensors, the coverage requirement is that every point in the region is covered by at least one sensor. The connectivity requirement for static sensors is that a large fraction of nodes form a *connected graph*. In [70], the connectivity model involves another aspect that each nodes is on and off with certain probability at some time instant. This can account for node failures. Other possible connectivity requirements include bounded delay to send information from a node to any other node or *k-connectivity* where each node is connected to at least k nodes at any time [85, 70]. In case of mobile nodes, node position changes over time and it is possible to consider different types of coverage and connectivity requirements. For instance, connectivity requirement could be persistent where all nodes remain connected all the time, or recurrent where nodes connect within bounded delay. Similarly coverage requirements can be persistent or recurrent. In [53], coverage is analyzed for nodes mobility where the node distribution remains uniform and stationary. The analysis is equivalent to the static case. The theoretical ideas in these earlier efforts are rooted in solutions to the *occupancy problems* [57].

2.4 Intentionally-mobile Detection Sensors with Utility based Coverage

The second coverage problem that we address in this thesis involves covering 1D pathways (indoor and outdoor) using a network of intentionally-mobile cameras. Our approach is to model camera as a detection sensor with utility-based coverage. In this section, we provide a detailed summary of related work on coverage problems related to intentionally-mobile detection sensors with coverage modeled as a utility function. First we motivate why such modeling scheme is advantageous over the disc model.

For some detection sensors, the disc model is not an accurate representation of the coverage model. According to the disc model, sensor's *performance* or the guarantee of event detection is same anywhere within the disc and drops to zero beyond the disc. Often, in practice, sensor's performance diminishes gradually. In that sense the disc model may heavily be a conservative estimate of the coverage. In such situations it is often convenient to represent the coverage as a *utility* or a *sensing performance function*. For example, in case of infra-red sensors, the sensing performance function could be the probability of detection. Of course, the disc model is a special case where the sensing performance function has step function like behavior.

Given the coverage model for each sensor as a utility function, it is convenient to think of the overall coverage problem as optimization of some overall utility metric. This problem can be formulated as a locational optimization problem. There is a rich body of literature on locational optimization which has applications for problems such as facility-location [61]. The solution to this problem is based on the generalized Voronoi partitioning and the gradient descent approach starting from the initial configuration. Based on this approach, Cortés *et al.* proposed a distributed control and coordination algorithm to obtain an optimal coverage configuration for mobile sensor networks starting from the initial configuration [13], [15]. Below we briefly present their locational optimization formulation for the coverage problem and their algorithm.

2.4.1 Coverage Problem Formulation

Notation presented in this section is mostly adapted from [15]. Let Q be the convex region that needs to be *covered.* Let $\phi : Q \rightarrow \mathbb{R}^+$ denote the *distribution density function* over the domain. Intuitively this function analytically assigns the importance measure over the domain. Let $P = (p_1, p_2, \cdots, p_n)$ denote the locations of n mobile sensors. Each sensor has the *utility* or the *sensing performance function* that depends on the distance between the location of the sensor and the point at which this function is assessed. Let $f : \mathbb{R}^+ \rightarrow \mathbb{R}^+$ denote the sensing performance function. Thus the sensing performance at point q due to the ith sensor located at point p_i is given by $f(\|q - p_i\|)$. This function is assumed to be non-increasing with the distance. This leads to the *Voronoi partitioning* of domain Q based on the sensor locations where each partition corresponds to the *region of dominance* of the sensor in it. Let $\mathcal{V}(P) = \{V_1, V_2, \cdots, V_n\}$ denote the Voronoi partition of P. Then,

$$V_i = \{q \in Q | \|q - p_i\| \leq \|q - p_j\|, \forall\ j \neq i\}. \tag{2.1}$$

Each sensor has influence over the region corresponding to its Voronoi partition. The *overall utility* can be formulated as the following location optimization function:

$$\mathcal{H}_{\mathcal{V}}(P) = \sum_{i=1}^{n} \int_{V_i} f(\|q - p_i\|)\phi(q)dq. \tag{2.2}$$

The coverage problem is formulated as finding an optimal configuration of the sensors maximizes the overall utility.

$$(p_1^*, p_2^*, \cdots, p_n^*) = \arg \max_{(p_1, p_2, \cdots, p_n)} \mathcal{H}_{\mathcal{V}}(P). \tag{2.3}$$

We use a slightly different convention while defining the sensing performance function above than in [13]. In [13], the sensing performance function is a non-decreasing function of the distance. The coverage problem is defined as minimization of the overall utility function.

2.4.2 Distributed Control and Coordination Algorithm

A gradient descent based iterative approach is proposed in [61] to obtain a solution the above problem. A special case of the sensing performance function is considered in [13], [15], where $f(\|q-p_i\|) = \|q-p_i\|^2$. In this case, the *centroidal Voronoi partition* yields the optimal solution [61], [15]. The centroidal Voronoi partition corresponds to the situation when every sensor is located at the centroid of its Voronoi partition. We will explain this in detail now. Consider the ith node. Assume that the location of its Voronoi neighbors is kept fixed. Suppose that the location of i is varied within its Voronoi partition such that the overall utility is maximized. Then it can be shown that the centroid of the Voronoi partition considering $\phi(q)$ as the mass density function maximizes the overall utility. Now for the case of centroidal Voronoi partition, each sensor is at the centroid of its partition no further improving the overall utility.

Cortés *et al.* translated this idea into a distributed control law [15]. They propose a distributed continuous-time control law for each sensor given by

$$\dot{p}_i = -k(p_i - C_{V_i}), \tag{2.4}$$

where C_{V_i} denotes the centroid of the Voronoi partition of the ith sensor and k denotes the constant gain. The convergence of the algorithm is also proved. The authors also propose the discrete-time asynchronous version of the control law and prove its convergence. This work initiated a number of variations that involved obstacles, communication constraints, etc. The algorithm in [15] requires global knowledge of the distribution density function and in that sense the algorithm is not truly distributed. Schwager *et al.* considered a model in which the distributed density function is a linear combination of a finite set of basis functions. Based on this they proposed a consensus based distributed algorithm that simultaneously learns the density function and obtains a coverage solution [69]. Recently, Lekein *et al.* [51] have considered the case of non-Euclidean distance metrics. Their solution is to map the non-Euclidean metric to a near-Euclidean metric using transformations known as *Cartograms*. They show that convergence of a control algorithm in the transformed Euclidean space

implies convergence in the original non-Euclidean space. The location-dependent sensing model that we use can be thought of as a non-Euclidean distance metric and therefore, in terms of objectives, [51] is closest to our work. The key difference is that in the Cartograms based approach the transformation requires global knowledge of the distance metric and density function.

In all these works with the exception of [51] each sensor is assumed to have identical behavior. In our work we assume that the sensing performance function is *learnt* based on local observations.

2.5 Coverage for Estimation Sensors

In the third coverage problem, we deal with estimation sensors. An estimation sensor provides measurements of physical quantities such as temperature, pressure, humidity, chemical concentration. These quantities can be represented as a spatio-temporal *fields* or *signals*. Although the goal of a sensor network might be to provide a high level inference about related physical phenomenon, the central question is estimating the unknown field. The *quality* of the estimated field depends on the measurements provided by the sensors. In this thesis we focus on sensors that provide measurements at a space-time location at which the sensor is physically located. We refer to these measurements as *point estimates* or *point samples* or simply *samples*. We refer to the set of locations of sensors as a *sensor arrangement*. The quality of the field depends on the geometric arrangement of the samples as well as the sample values. This idea leads to the formulation of some coverage metric and the coverage problem is to find the sensor arrangement that optimizes the coverage metric. We call this problem the *sensor arrangement problem*. We ask when and where to take samples in order to obtain a good estimate of an unknown spatio-temporal field.

Typically sensors provide only approximate measurements of the field. Sources of error include quantization and sensor noise. Assuming that sensors provide accurate measurements of a field, the sensor arrangement problem is still ill-posed. Given an ensemble of samples, there can be infinitely many choices of fields or functions

that conform with the sample values. To avoid this, typically assumptions are made about the space of the field. This involves assuming that the field belongs to a certain class of functions and the goal is to find the *best fit.* The most celebrated result of this type is Shannon's classic result on band-limited signals [71]. In order to support his seminal work in information theory, Shannon needed a way to transform a continuous waveform into a sequence of numbers. In his paper [71], Shannon presented a result that a band-limited signal can be entirely recovered from periodic samples obtained at the rate higher than the *Nyquist rate.* This result is known as Whittaker-Kotel'nikov-Shannon-Nyquist Sampling Theorem or more popularly as Shannon-Nyquist Sampling Theorem. A 1D continuous-time signal $y(t)$ is a band-limited signal if its Fourier Transform $Y(f)$ does not contain any frequencies higher than B, *i.e.*, $Y(f) = 0, \forall f \geq B$. B is referred to as the *bandwidth* of the signal. According to the Sampling Theorem, the function can be completely determined from its sample values at a periodic sequence of points with the period less than or equal to $\frac{1}{2B}$. $2B$ is referred to as the Nyquist rate (twice the highest frequency). Since the establishment of this result, a number of classes of fields have been considered and sampling theories have been developed in the area of signal processing. A detailed account of this is given in the survey paper [79]. An important class of functions is *shift-invariant* functions. A *uniform* or *regular* or *grid* sampling arrangement is the most widely used sampling arrangement in almost every signal processing application. Very few efforts have actually focused on *non-uniform* or *irregular* sampling schemes. In most applications, we actually have control over when and where to take measurements and the regular sampling scheme leads to computationally efficient reconstruction procedure. However, in sensor networks, we seldom have control over deployment of the sensor nodes. Sometimes, in sensing spatio-temporal events, uniform sampling may be impossible for mobile sensors. In such situations non-uniform sampling is inevitable. In the area of sensor networks, the importance of dealing with non-uniform sensor arrangements has been emphasized only recently [28]. We summarize a few research efforts on non-uniform sampling in the area of signal processing below.

Yen proposed an algebraic method to reconstruct a band-limited signal from non-uniform samples when the average sampling density is at least the Nyquist rate [87]. However, this method is numerically unstable meaning that small errors in the samples lead to large errors in the reconstruction. Duffin and Schaeffer first proposed conditions on the sampling pattern under which stable reconstruction of a band-limited signal is possible [20]. Such a sampling pattern is referred to as a *frame*. Frames play an important role in the development of solutions to the sensor arrangement problem addressed in this thesis. Therefore, we provide a brief introduction to frames in Chapter 5. In [34, 35, 37], theoretical and numerical aspects of the reconstruction of a special type of band-limited signal, a *trigonometric polynomial*, from non-uniform samples have been studied. In this case the stable reconstruction is related to 'conditioning' of a certain matrix. In [35], Gröchenig shows that for Δ-dense sampling arrangements, this matrix is well-conditioned and stable reconstruction is possible.

In the area of sensor networks, there have been a few efforts (*e.g.*, [38, 88, 52, 58, 59]) that deal with the sensor arrangement problem. The sensor arrangement problem is closely related to optimal experiment design and is also known as the *sampling design* problem. In [38], the authors consider the near optimal sensor arrangement for Gaussian processes. In [88], Zhang and Sukhatme propose an adaptive sampling approach for a single mobile sensor mounted on a boat in combination with a few static sensors. The approach is based on the optimal experiment design work. In [52], the authors consider elliptical motion paths for mobile underwater vehicles and consider the sensor arrangement problem restricted to these paths. In [58, 59], the authors consider the sensor arrangement problem for trigonometric polynomials in the Bayesian estimation framework. They consider the probabilistically generated sampling arrangements and use the asymptotic analysis techniques to obtain error tolerance values. In addition to the above work, in [73], the authors use active learning methods for mobile sensors for adaptive sampling.

Our choice of Δ-dense arrangements as a class of error tolerant arrangements for trigonometric polynomial fields is inspired from the work in [35, 37].

Part I

Detection Sensors

Chapter 3

Floating Event-Detection Sensors in Rivers

In this part of the thesis, we deal with the event-detection sensors. We focus on the sensors with the disc model in this chapter. We analyze coverage and connectivity of a network of floating sensors moving passively in rivers using simulations and experimental data. As far as we know, this work is one of the first few efforts to understand network properties in the presence of incidental mobility

Organization: In Section 3.1, we examine natural mobility of floating sensors in rivers. In Section 3.2, we discuss the coverage problem we address and in Section 3.3, we provide approximate analysis. Although the focus of this thesis is coverage, because of the same model used to model connectivity as well as coverage, we discuss the connectivity problem and analysis in Sections 3.4 and 3.5. We present results in Section 3.6.

3.1 Natural mobility of sensors in rivers

As a first step towards studying properties of a network of floating sensors in rivers we propose a model for natural mobility of floating nodes in rivers. It is necessary to use a model that captures complexities of the river flow and at the same time allows

for tractable analysis.

Conventionally, hydraulic and environmental engineers study hydrodynamic flow models of water bodies such as rivers, lakes and oceans. They typically study a phenomenon called *dispersion* of *tracers* such as pollutants, chemical and dye in these bodies. Dispersion is defined as spreading of tracer particles in a water body under the combined action of its velocity distribution, and turbulent and molecular diffusion [77, 78, 24, 25]. It is characterized in terms of *dispersion coefficients* along different directions in the flow. These coefficients represent some average metric to capture the *spread* of the tracer along different direction. They can be obtained in terms of the spatio-temporal concentration of the tracer which is given by the *advection-diffusion* equation. The advection-diffusion equation is commonly encountered in the study of transport phenomena and is specified in terms of the mean velocity distribution of the flow and diffusion coefficients in the lateral, longitudinal and vertical directions.

Unlike the case of a tracer, the number of sensors we expect in a river network is small (tens or hundreds of nodes). Our goal is to be able use a mobility model that allows to simulate trajectories of individual sensors as well as network behavior. We use the Lagrangian particle-tracking approach to describe the motion of individual nodes. Based on the geographic scales, river flow is turbulent and it is convenient to describe the motion of fluid elements using random walks. We treat an individual node as a part of the fluid itself. We propose a stochastic random walk model to describe the mobility of a node such that the probability density function corresponding to the walk is the same as the spatio-temporal concentration of a tracer under certain initial conditions.

As a first step we propose a model for the case of a river with ideal channel assumptions. This allows us to analyze network behavior under ideal conditions. Later we propose a model for natural rivers. In both cases we neglect the effects of wind on the velocity distribution of the flow.

3.1.1 Ideal-channel rivers

An ideal-channel river flows through a channel that is straight, and has constant lateral cross-section and constant gravitational descent along the direction of the flow. Figure 3-1 shows the geometry of the channel, the coordinate system we use and the generalized profile of the cross section of a channel. The cross-section is symmetric about the center-line and has a generalized parabolic profile as discussed below. The z and y-axes indicate the vertical and the transverse directions respectively, whereas the x-axis (not shown in the figure) indicates the longitudinal direction of the flow. Hydraulic engineers define a geometric parameter called *hydraulic radius* which is equal to the ratio of the area of the channel and the wetted perimeter of the channel. They specify this parameter even in the case of natural rivers to characterize the flow. A good survey for modeling ideal channel shapes for natural rivers with the equivalent flow is given in [17]. The generalized parabolic profile of the channel in terms of the local flow depth is given in [17] as

$$\frac{h(y)}{H_c} = 1 - \left(\frac{y}{b}\right)^{\beta}, \tag{3.1}$$

where $h(y)$ is the local depth at the corresponding y value, b is half of the surface width B of the channel, H_c is the depth of the channel at the centerline $y = 0$, and β is a parameter which depends on the width-to-depth ratio of the channel.

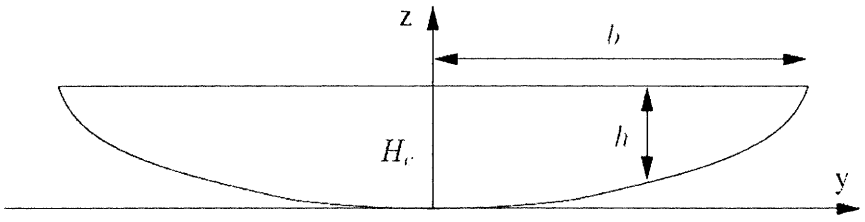

Figure 3-1: Ideal channel coordinate system and profile. The z-axis and y-axis indicate the vertical and transverse directions respectively. The x-axis is not shown in the figure. It comes out of the page and indicates the longitudinal direction of the flow.

As mentioned earlier, our approach to is to propose a stochastic random walk

model for motion of a floating node in a river such that the probability density function of this walk is a solution to the advection-diffusion equation. This requires knowledge of the mean velocity distribution and longitudinal, lateral and vertical diffusion coefficients. Since we are dealing with floating sensors in an ideal-channel river, we make some simplifications. We entirely neglect movements in vertical direction and make 2D flow assumption. We combine the average surface velocity profile and longitudinal and lateral diffusion coefficients to define the natural mobility model as follows:

1. Mean Surface velocity profile: Under ideal channel conditions, the mean surface flow is in the longitudinal direction. The mean velocity flow in the lateral direction is zero. The mean *depth-averaged* velocity profile in the longitudinal direction for ideal channels with width-to-depth ratio > 10 is described in detail by [17]. It is given by,

$$u(y) = \alpha U_c \left(\frac{h(y)}{H_c} \right)^{2/3}, \tag{3.2}$$

where U_c is the centerline depth-averaged velocity and α is a parameter which depends on width-to-depth ratio of the channel. Depth-averaged velocity is typically 0.8 times the surface velocity. Thus, the surface velocity is given by a similar equation with a modified value of α. Note that the velocity profile $u(y)$ also has a generalized parabolic shape. It is the highest along the centerline and decreases towards the side banks of the river.

2. Diffusion coefficients: Turbulent diffusion is a few orders of magnitude larger than molecular diffusion, which can be neglected. We assume that the longitudinal and lateral diffusion coefficients due to turbulence are of the form, $D = kf(y)$, where k is a constant that depends on the *shear velocity* of the flow and $f(y)$ is a function of local depth $h(y)$. It captures reduction in the diffusion coefficients towards banks of the river. Details are available in [25, 17]. For particles that can be treated as fluid elements the value of D varies between 0.1-0.4 m^2/s. For relatively large sensors, these values can be somewhat lower. We denote the longitudinal and lateral diffusion coefficients by D_x and D_y re-

spectively. We assume that $D_x = D_{x0}\frac{h(y)}{H_c}$ and $D_y = D_{y0}\frac{h(y)}{H_c}$, where D_{x0} and D_{y0} are constants.

3. Equations of motion: Given the above expressions for the mean velocity profile and the diffusion coefficients, the advection-diffusion equation for the spatio-temporal floating-tracer concentration is given by [24],

$$\frac{\partial c_t(x,y)}{\partial t} = -u(y)\frac{\partial c_t(x,y)}{\partial x} + \frac{\partial^2(D_x c_t(x,y))}{\partial x^2} + \frac{\partial^2(D_y c_t(x,y))}{\partial y^2}, \tag{3.3}$$

where $c_t(x,y)$ denotes the concentration. We want the probability density function corresponding to the random motion of the nodes to mimic this differential equation. For this reason, we treat the above equation as a Fokker-Planck equation a set of Ito stochastic differential equations that describe motion of a floating sensor [68]. We propose the following mobility model.

$$dx = u(y)dt + \sqrt{2D_x}dW_1 = u(y)dt + \sigma_x dW_1 \text{ and} \tag{3.4}$$

$$dy = \sqrt{2D_y}dW_2 = \sigma_y dW_2, \tag{3.5}$$

where dx and dy indicate the differential increments in x and y coordinates of the current location of a sensor, dt is the differential increment in time, and dW_1 and dW_2 indicate differentials of Gaussian white noise. These equations together provide a simple model for motion of sensors passively moving on the surface of natural rivers. These equations can be numerically simulated to find sample trajectories of particles.

3.1.2 Natural rivers

Flow distribution in natural streams is much more complicated. The channel is not straight and meanders with bends. The cross-section changes everywhere and is highly asymmetric. The channel geometry can be viewed as small-scale variations superimposed on large-scale geometries that change very slowly [24]. The velocity

distribution can then also be viewed as small fluctuations superimposed on the top of mean velocity profile. A few software packages such as EFDC [81] and River2D [60] enable a user to determine an approximate averaged velocity field in rivers and lakes using finite element methods based on the depth information and boundary conditions. These packages also provide averaged solutions to determine dispersion of tracers. We combine the mean velocity profile information with local longitudinal and lateral diffusion coefficient values to propose the following mobility model in natural rivers.

$$dx = u(x,y)dt + \sqrt{2D_x(x,y)}dW_1 = u(x,y)dt + \sigma_x(x,y)dW_1 \text{ and} \tag{3.6}$$

$$dx = v(x,y)dt + \sqrt{2D_y(x,y)}dW_2 = u(x,y)dt + \sigma_y(x,y)dW_2, \tag{3.7}$$

$u(x,y)$ and $v(x,y)$ denote the local mean longitudinal and lateral surface velocity values. $D_x(x,y)$ and $D_y(x,y)$ denote the local longitudinal and lateral diffusion coefficient values. These values can only be observed experimentally. It is virtually impossible to know these values at every location and we rely only on rough approximations.

3.2 Coverage problem

The goal of the coverage problem in rivers is to be able to detect and localize sources of interesting events along the stream. In this work we assume a *disc* model for coverage for the detection sensors, *i.e.*, a sensor is able to detect an event of interest within its *sensing range*. This model holds good in the following three situations.

1. Spatial events of interest are marked by local changes in gradients of physical quantities such as temperature, salinity, pH levels. Depending on the spatial scales of these changes, the disc coverage model is useful for coarse detection and localization of the events.

2. Some detection sensors such as sensors for turbidity and conductivity measure

values over a region and we can approximate this region as a disc. An event of interest in these situations correspond to measurement values above some threshold.

3. Besides detection sensors, we will show in Chapter 6 in the case of estimation sensors under certain conditions, a disc model is a good approximation and leads to mapping of spatial fields of physical quantities such as temperature, concentrations and pressures within tolerable accuracy [18].

In this work, we focus on coverage properties under only natural motion of nodes. Under the natural mobility of a node, its coverage corresponds to the region swept by the coverage disc around the node. The net region covered by all the nodes is the union of all the individual regions swept. The overall coverage depends on four factors: 1) the mobility model, 2) the sensing range, 3) the number of nodes, and 4) the initial distribution of the nodes. A node never moves upstream. This motivates the definition of our coverage metric. We consider a span of the river of certain length between two lateral cross-sections. Our coverage metric corresponds to the net region covered by the sensors as a function of time.

Given the natural mobility model for the river and the sensing range, the choice of the number of nodes and the initial distribution is critical to guarantee to good coverage. We illustrate this with the help of simulations. Figure 3-2 indicates the coverage of 9 nodes that move according to the mobility model for an ideal-channel river with the river width of 200m, the centerline depth of 3m, the centerline velocity of 0.25m/s and constant diffusion coefficient values, $D_x = 0.01m^2/s$ and $D_y = 0.015m^2/s$. The nodes are initially placed uniformly along a cross-section. This suggests that without careful choices of the parameters, the natural mobility even in ideal-channel rivers may lead to *holes* in coverage.

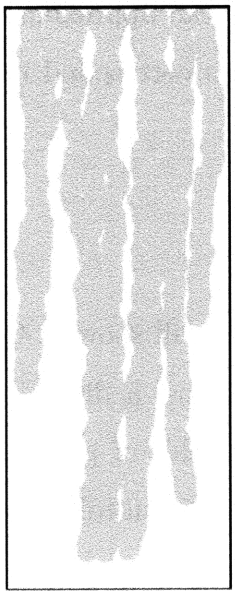

Figure 3-2: Area swept by the coverage-discs of 9 nodes that move according to the mobility model in an ideal-channel river with the simulation parameters described above.

3.3 Coverage analysis for an ideal river mobility

In this section, we present coverage analysis for mobility in an ideal-channel river. Let N denote the number of sensors, each with sensing range r. We consider the span of the river between river cross-sections at $x = 0$ and $x = L$ for some constant L. If B denotes the river width, we analyze coverage of the rectangular region of width B and length L. The y-coordinates for the banks of the river are $\frac{-B}{2}$ and $\frac{+B}{2}$. We let $\rho(t)$ denote our coverage metric which is defined as the fraction of the area covered by the sensors as a function of time for given r, N and L.

In our analysis we make the following assumptions.

1. Initially nodes are deployed uniformly randomly and independent of other nodes along the lateral cross-section, the interval $\left[\frac{-B}{2}, \frac{B}{2}\right]$, at $x = 0$.

2. Each node moves independently of other nodes according to the mobility model in Equations (3.4) and (3.5).

There is a small caveat in this assumption about independent motion: obviously

if two nodes fall at the same location, they would continue to move along the same path. However, we assume that strict separation is maintained between two nodes.

Given these assumptions, we can carry out simulations to characterize $\rho(t)$ for various values of the parameters. We will present simulation results in Section 3.6.3. Here we present analytical results in terms of the parameters and draw insights.

3.3.1 Initial deployment

N nodes are distributed uniformly randomly along the segment of length B between points $\left(0, \frac{-B}{2}\right)$ and $\left(0, \frac{+B}{2}\right)$. As a first step towards guaranteeing coverage, we need to make sure that this segment itself is covered by the sensing discs around the nodes. The projection of each sensing disc on this segment is an interval of length $2r$. This leads to the 1D-coverage question of guaranteeing coverage of a segment of length B with N subsegments, each of length $2r$, placed uniformly randomly. This problem is a simplified version of the extensively studied 2D-coverage problem of covering a unit square with randomly placed discs of radius r [39], [53], [70], [27], [84], [85]. For the sake of completeness, we state and prove the following bound on N for the 1D case based on the results in Lemma 1 of [27] and [57].

Lemma 3.3.1. *If* $N = O\left(\lceil \frac{B}{r} \rceil \log\left(\frac{B}{r}\right)\right)$, *then the lateral cross-section of the ideal-channel river is covered* whp.

Proof. We divide the segment B into at least $m = \lceil \frac{B}{r} \rceil$ subsegments (*bins*), each of length at most r. Note that if we can guarantee that each bin contains at least one node *whp*, then the entire segment is covered *whp*. The probability of a node falling in any one of the bins is $\frac{1}{m}$. Let A_i denote an event that the i-th bin contains at least one node.

$$\mathbb{P}(A_i) = 1 - \mathbb{P}(A_i^c) = 1 - \left(1 - \frac{1}{m}\right)^N.$$

The probability of the event that each bin contains at least one node is given by

$\mathbb{P}(A_1 \cap A_2 \cap \cdots \cap A_m)$. We obtain the following result based on the union bound [57].

$$\begin{aligned}\mathbb{P}(A_1 \cap A_2 \cap \cdots \cap A_m) &= 1 - \mathbb{P}(A_1^c \cup A_2^c \cup \cdots \cup A_m^c) \\ &\geq 1 - \sum_{i=1}^{m} \mathbb{P}(A_i^c) = 1 - m\left(1 - \frac{1}{m}\right)^N.\end{aligned}$$

Based on the fact, $1 - p \leq e^{-p}$ for small p, we obtain,

$$\mathbb{P}(A_1 \cap A_2 \cap \cdots \cap A_m) \geq 1 - me^{-\frac{N}{m}}.$$

Suppose we want the probability of this event to be at least $1 - \delta$ for some small constant δ. This means, $\delta \geq me^{-\frac{N}{m}}$, which implies that $N \geq m \log m + m \log\left(\frac{1}{\delta}\right)$. Thus as long as $N = O(m \log m)$, *whp* each bin contains at least one node. $m = \lceil \frac{B}{r} \rceil$. Therefore, $N \geq \lceil \frac{B}{r} \rceil \log\left(\frac{B}{r}\right)$ guarantees that the river cross-section is covered *whp*. □

Henceforth we assume that N is sufficiently large to guarantee initial coverage. Let u_c denote the mean center-line surface velocity of a node in the river. The nodes close to the bank of the river will have much lower mean velocity than u_c. For relatively smaller values of the sensing radius compared with the river width, u_c can serve as a good estimate to give lower bounds on the coverage. With high probability we can say that

$$\rho(t) \leq \frac{u_c B t}{L}. \tag{3.8}$$

Next we present two approximate models for the natural mobility of nodes in the ideal-channel river to analyze coverage.

3.3.2 An approximation: constant longitudinal velocity walk

This is the first order approximation of the mobility model. In the random walk mobility model, in each time step dt, the longitudinal displacement of the node has contributions from the mean velocity component, $u(y)$ and a random component. The mean velocity component is a function of y. $\bar{U}$, the laterally-averaged mean surface

velocity is given by

$$\bar{U} = \frac{\int_{\frac{-B}{2}}^{\frac{B}{2}} u(y)dy}{B}. \tag{3.9}$$

We make the following two approximations to modify the mobility model.

1. We assume that all the nodes move with the constant longitudinal velocity component equal to $\bar{U}$. We neglect both, the lateral variations in the velocity and the randomness.

2. We neglect variations in the lateral diffusion coefficient D_y and use an average lateral diffusion coefficient $\bar{D}$.

Following these approximations, the new mobility model for each node is given by

$$dx = \bar{U}dt \text{ and} \tag{3.10}$$

$$dy = \sqrt{2\bar{D}}dW_2. \tag{3.11}$$

Although from the networking point of view this approximation is not justified (as we will discuss in Section 3.5), it is reasonable from the coverage point of view. Consider the case when r is relatively very small and all the nodes are initially periodically placed at $x = 0$ to cover the span of the river. In absence of random components in the mobility model, the coverage $\rho(t)$ is approximately $\frac{\bar{U}Bt}{L}$, which is same as the approximate model as we will show below.

In Section 3.6.3, we will present simulation results to compare coverage results for this model with the original model. But the approximate model also allows us to carry out some analysis.

According to the new model, in every time step, the x-coordinate of each node increases by $\bar{U}$ and at the end of i time steps all the nodes are floating on the transverse span of the river at $x = \bar{U}i$. Notice that the y-coordinate of each node changes according to purely diffusive random process (ignoring the boundary effects). In order to simplify the analysis further, we discretize time into unit time steps and discretize the river span from $x = 0$ to $x = L$ into rectangular grid cells, each of size $U \times r$,

where the step U is along the longitudinal direction and step r is along the lateral direction. Thus, in the given rectangular span of $L \times B$, there are $\frac{L}{U} \times \frac{B}{r}$ cells.[1] We approximate the mobility of nodes as a *jump* process, where in every time step a node jumps from one grid cell to another grid cell with some transition probability. The probability values for these transitions can be evaluated by averaging the probability density function of the continuous process. We assign an index pair (i, j) to each grid cell, where i denotes the *longitudinal index* along the x-direction and j denotes the *lateral index* along the y-direction. $i = 1, 2, \cdots, \frac{L}{U}$ and $j = 1, 2, \cdots, \frac{B}{r}$. The set of cells with the same longitudinal index value, say i, corresponds to a lateral *strip* in the channel. Given this discretized approximate model for the mobility of the nodes, we can analyze the number of nodes, N required to guarantee full coverage *whp*.

The motion of N nodes can be viewed as N independent random walks. Let (X_i^n, Y_i^n) denote the index pair of the grid cell of the n-th node in the beginning of the the i-th time step. Note that $X_i^n = i$. Y_i^n is a discrete random variable that changes according to the diffusive process. According to the initial deployment, the nodes are uniformly distributed across the first strip, *i.e.*, $Y_1^1, Y_1^2, \cdots, Y_1^N$ are independent and identically (uniformly) distributed discrete random variables. Each Y_1^i is uniformly chosen from $1, 2, \cdots, \frac{B}{r}$. Note that Y_i^n is a 1D random walk for which the uniform distribution is a *stationary* distribution, *i.e.*, given that Y_1^n is uniformly distributed, Y_i^n for every i is also uniformly distributed. Thus at every time step i $Y_i^1, Y_i^2, \cdots, Y_i^N$ are independent and identically (uniformly) distributed. Now we can analyze coverage for this random walk.

If we can guarantee that every grid cell (i, j) in the river span up to $x = L$ is visited by at least one sensor, then we can guarantee coverage. At the beginning of the ith time step, all the nodes are in the cells in the ith strip. Let A_i denote an event that every cell in the ith strip contains at least one node at the beginning of the ith time step. Guaranteeing high coverage implies that $\mathbb{P}(A_1 \cap A_2 \cap \cdots A_{\frac{L}{U}})$ is sufficiently

[1] We drop ceilings for clean notation.

high. Using union bound, we can show that

$$\mathbb{P}(A_1 \cap A_2 \cap \cdots \cap A_{\frac{L}{\bar{U}}}) \geq 1 - \sum_{i=1}^{\frac{L}{\bar{U}}} \mathbb{P}(A_i^c)$$

Let $m = \frac{B}{r}$. Then based on the proof of Lemma 3.3.1, $\mathbb{P}(A_i^c) \leq e^{-\frac{N}{m}}$. Therefore,

$$\mathbb{P}(A_1 \cap A_2 \cap \cdots \cap A_{\frac{L}{\bar{U}}}) \geq 1 - \frac{L}{\bar{U}} e^{-\frac{Nr}{B}}. \tag{3.12}$$

Based on the analysis similar to Lemma 3.3.1, $N = O\left(\frac{B}{r} \log\left(\frac{L}{\bar{U}}\right)\right)$ guarantees that all the cells are covered with high probability. As long as N is sufficiently large, in every time step, one strip is covered *whp*. The coverage metric $\rho(t)$ then can be approximated as

$$\rho(t) \approx \frac{\bar{U}Bt}{L}. \tag{3.13}$$

3.4 Connectivity problem

Although the focus of this thesis is on coverage problems, we also deal with the connectivity problem (a networking issue) in this chapter because the disc model is also used in literature to model communication. As per this model, two nodes can communicate with each other only if the distance between them is less than the communication range. Owing to the same nature of the model, the same tools are used in the analysis of coverage as well as connectivity. Although the disc model may not hold satisfactorily in real situations, it is a first step towards understanding connectivity to the first order in complex situations such as in mobile nodes in rivers. Also, since we are dealing with the outdoor situation and the line-of-sight is not a concern, the disc abstraction holds better compared with the indoor situations.

Here we assume that nodes communicate with each other using the multi-hop communication, *i.e.*, every node acts as a switch to forward packets from other nodes. We say that two nodes are *connected* if they can communicate directly or via intermediate nodes acting as switches. How often nodes need to remain connected depends on the

application. In some applications, a node is required to be always connected to a part of the network. In this case, we can quantify the network connectivity in different ways, *e.g.*, diameter of the network (maximum number of hops a node encounters in communicating with some nodes in the network), the size of the largest *connected cluster* (LCC) of nodes. However, in some applications nodes need to be connected only within certain tolerable delay. Such networks are *delay-tolerant* networks. In such networks, we can quantify the network connectivity in terms of the maximum delay.

In the context of sensor-networks in rivers, network connectivity is useful in the following situations.

1. Both event-detection and estimation sensors, periodically take measurements in a river to map interesting events. In the wake of the detection of an interesting event, sometime it is essential to take samples at a faster rate and over a larger spatial scale to map the events better. This requires that a fraction of nodes to remain connected in order to be able to quickly diffuse information about the event and trigger *adaptive sampling.*

2. It might be expensive to have a GPS device on every node to obtain location information. Only a few nodes may have GPS devices and others may be using localization techniques to find their locations.

3. In future applications, nodes may have capability to actively navigate along with the passive motion. In this case, nodes will have to react to topology changes, which require network connectivity.

The network connectivity of the floating nodes in rivers depends on: 1) the motion patterns 2) the communication range 3)the number of nodes and 4) the initial distribution of the nodes. Given the natural mobility model and the communication range, the choice of the number of nodes and the initial distribution is critical to guarantee good network connectivity. In this work, we analyze connectivity in ideal-channel rivers in the ad-hoc network setting. We measure the network connectivity in terms of the size of the LCC.

3.4.1 Connectivity challenges

As a first step, we perform simulations for the natural mobility model in the ideal case (Equations 3.4 and 3.5) to observe preliminary results on connectivity.

Figure 3-3 indicates the network connectivity (averaged over 10 simulation runs) versus time for a network of 50 nodes moving in an ideal-channel river according to the natural mobility model in Equations (3.4) and (3.5). The nodes are initially placed uniformly randomly along the transverse cross-section. The communication range of each node is $75m$. The simulation parameters are described in Section 3.6.2. The river width is $500m$, the centerline velocity is $1.1m/s$. The connectivity is measured in terms of the ratio of the size of the LCC and the total number of nodes. We observe that the connectivity reduces with time, sharply in the beginning and more gradually with time. This is because of two reasons. First, the river flow dynamics is such that nodes in the middle portion drift far away compared with the nodes on the sides. Second, the river domain is unbounded and spread of the nodes distribution increases over time. This shows that the natural mobility is amenable to the network connectivity. In the next section, we analyze connectivity in detail to gain insights about the network design to guarantee connectivity.

3.5 Connectivity analysis for an ideal river mobility

The initial distribution of the node is uniformly random along the entire transverse cross-section. We observe that the pdf is the maximum near the center-line and reduces gradually towards the bank with a wide spread along the longitudinal direction. In the connectivity results stated above, the LCC is formed by the nodes close to the center-line. The nodes near the banks loose connectivity quickly. In order to guarantee connectivity over all the nodes, either we need to increase the communication range or for the given communication range, we need to insert large number of nodes. Both the options are disadvantageous in terms of the power consumption and cost.

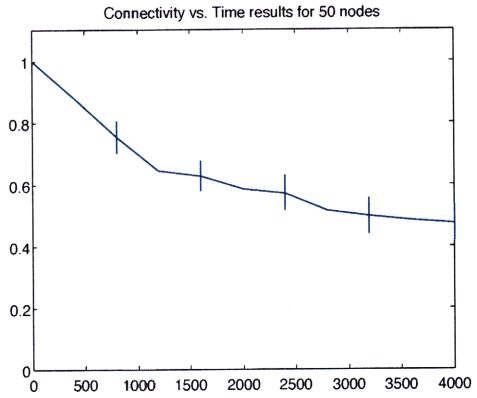

Figure 3-3: Connectivity versus time for 50 nodes deployed uniformly randomly along the transverse cross-section in an ideal-channel river. The communication range of each nodes is $75m$.

Based on this we propose a heuristic. We divide the transverse cross-section into different zones and analyze connectivity in each zone.

Suppose N nodes are placed initially uniformly-randomly and independently along a transverse segment of length b at $x = 0$ as shown in Figure 3-4. Let the random tuple (X_t^i, Y_t^i) denote the x, y location of the ith node. Consider some time instant T. Let $\mathbb{E}[X_T^i] = \mu_x$ and $\mathbb{E}[Y_T^i] = \mu_y$. Also, let $Var[X_T^i] = \Sigma_x$ and $Var[Y_T^i] = \Sigma_y$. Using Chebyshev's inequality [33],

$$\mathbb{P}(|X_T^i - \mu_x| \geq k\Sigma_x) \leq \frac{1}{k^2} \tag{3.14}$$

$$\mathbb{P}(|Y_T^i - \mu_y| \geq k\Sigma_y) \leq \frac{1}{k^2}. \tag{3.15}$$

Thus, with high probability (*whp*), each node falls in the rectangular region shown in Figure 3-4 for some k. Next we analyze how many nodes are necessary to guarantee high level of connectivity among the nodes. We divide the rectangular region of size $2k\Sigma_x k\Sigma_y$ into grid cells, each of size $\frac{R}{2\sqrt{2}} \times \frac{R}{2\sqrt{2}}$. The total number of cells are

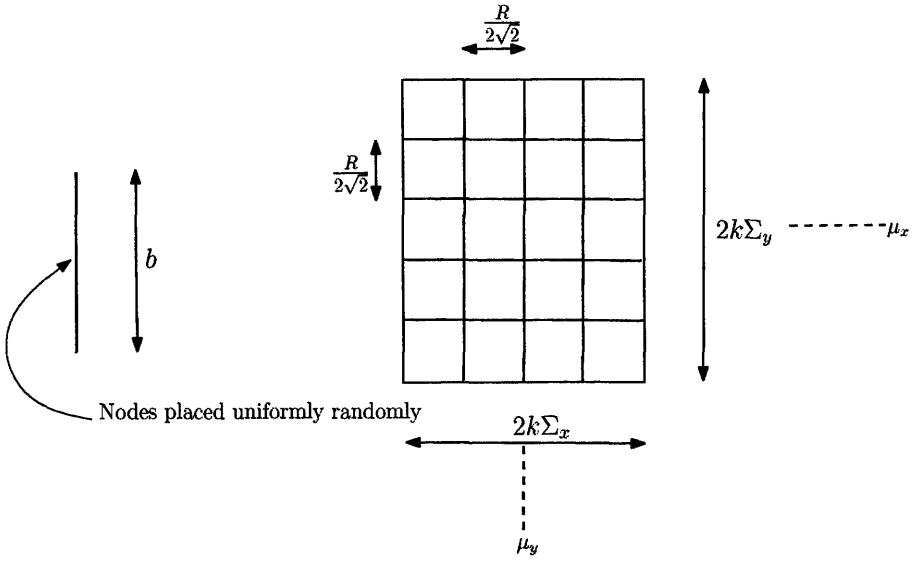

Figure 3-4: Grid arrangement useful in the analysis of connectivity

$\frac{4k\sqrt{2}\Sigma_x}{R} \times \frac{4k\sqrt{2}\Sigma_x}{R}$. The size $\frac{R}{2\sqrt{2}}$ guarantees that if any two adjacent cells contain one node each, then the two nodes can communicate with each other. Suppose we assign an index (i, j) to each cell and let $\mathbb{P}_{ij}$ indicate the probability that a node falls in the cell (i, j). Let $p = \min_{(i,j)\mathbb{P}_{ij}}$. Depending on the distribution p could be a very small number. For now, let us assume that p is not very small. If we make sure that each grid cell contains at least one node *whp*, then the network has high connectivity *whp*. Based on Lemma 3.3.1, $N = O(\frac{1}{p}\log\left(\frac{\Sigma_x\Sigma_y}{R^2}\right))$ nodes are necessary to guarantee connectivity *whp*. Note that $\frac{1}{p}$ is at least equal to the total number of cells. Thus, the number of nodes required to guarantee high connectivity depends on Σ_x and Σ_y. Note that Σ_x depends on σ_x (the contribution from the turbulent diffusion coefficient) as well as the velocity distribution. In fact, it is nothing but the square root of the longitudinal *dispersion coefficient* of the flow. Similarly, Σ_y is also the square root of the lateral *dispersion coefficient* of the flow.

3.6 Experimental Data and Simulation results

We present coverage and connectivity results in two situations. First, we simulate sensor trajectories in an ideal-channel river according to the natural mobility model

which we proposed in Section 3.1.1. Second, we simulate sensor trajectories based on experimental data obtained from another source. In this section, we first describe set-up for experimental data, then we present coverage and connectivity results.

3.6.1 Experimental Data source

Towards the end of the last century, Michigan Department of Environmental Quality (MDEQ) Source Water Assessment Program (SWAP), in cooperation the U.S. Geological Survey (USGS) undertook a project to assess the vulnerability of 13 public water supplies along the St. Clair-Detroit River Waterway [42, 43]. The purpose of this assessment was to identify sources of public water intakes in order to prepare emergency responses during contaminant spills. From 3 to 5 October 2000, The USGS deployed drifting buoys with GPS in St. Clair at 10 reaches to understand flow patterns and turbulent dispersion characteristics. St. Clair River is a connecting channel between Lake Huron and Lake St. Clair that forms part of the international boundary between the United States and Canada [42, 43]. We obtained this data from the USGS.[2] Two kinds of buoys were deployed, spherical and cylindrical.

1. The spherical unit was $16 inch$ in diameter and weighed $45 lbs$. The location data for each unit was captured every $180 s$.

2. The cylindrical unit consisted of two cylinders, one PVC pipe of length $9 inch$ and diameter $3 inch$ mounted on another PVC pipe of length $36 inch$ and diameter $4 inch$. The unit remained in the vertical position such that the smaller cylinder remained above water. The smaller cylinder contained the Garmin GPS unit, the accuracy of which was $49 ft$. The location data for each unit was captured every $45 s$.

Wind affected location of each type of unit; cylindrical unit was less affected than the spherical one.[3] We analyzed the data at different reaches. We present results

[2]The author would like to thank David H. Holtschlag of the USGS for readily providing us with the data.

[3]David H. Holtschlag of the USGS informed the author about wind effects in one of the personal communications.

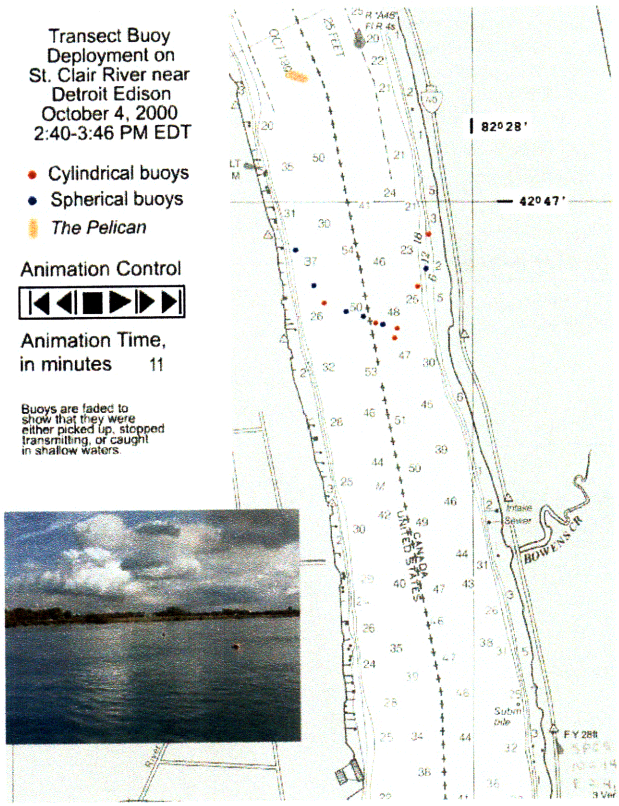

Figure 3-5: St. Clair River near Detroit Edison. The snap-shot of the animation is obtained from the USGS website.

based on the data near two sites, Detroit Edison and Marysville. We describe how data was gathered and how we process the data.

1. **St. Clair River near Detroit Edison:** Figure 3-5 shows a snap-shot of the animated results on the USGS website of the drifting buoy deployments. The numbers in the channel display the depth information at various locations in *feet*. 7 spherical and 6 cylindrical buoys were deployed by a boat across the river cross-section.

2. **St. Clair River near Marysville, Michigan:** Figure 3-6 shows a snap-shot of the animated results on the USGS website of the drifting buoy deployments. The numbers in the channel display the depth information at various locations in *feet*. 7 spherical and 6 cylindrical buoys were deployed by a boat across the river cross-section, although we could not obtain data for one of the cylindrical

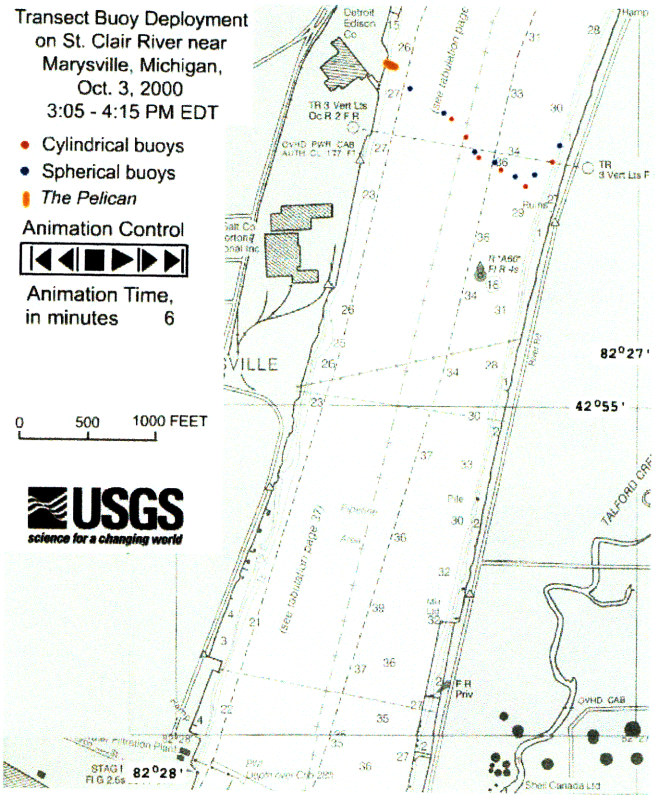

Figure 3-6: St. Clair River near Marysville. The snap-shot of the animation is obtained from the USGS website.

buoys.

3. **Data processing and the mesh model construction:** The data was captured in both the cases for about an hour. We cleaned initial data and analyzed the location data for the first 40 minutes of the deployment. We converted the latitude and longitude readings from the GPS into the Universal Transverse Mercator (UTM) System [21] to obtain the cartesian coordinates. We obtained the coordinates for the river banks using the Google maps. In order to approximately construct the velocity field over the domain, we first approximately calculate the velocity at the GPS location points using the GPS data between the two consecutive samples. We then construct a mesh model using the Delaunay triangulation method, where the velocity at a point is evaluated using the linear interpolation of the velocities at the vertices of the triangle than contains the point. Figure 3-7 and Figure 3-8 show the mesh model near Edison and

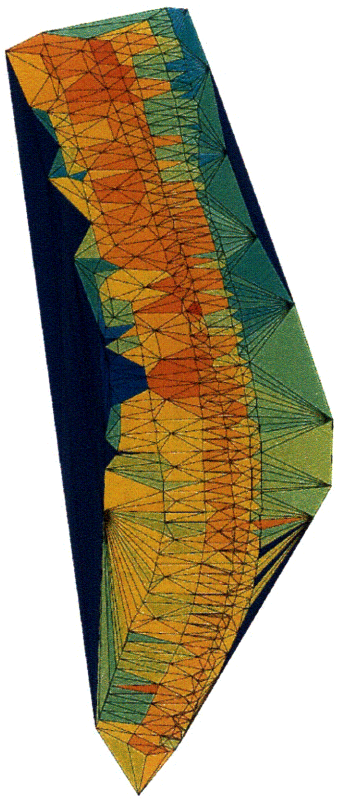

Figure 3-7: The velocity field using the mesh model for Detroit Edison site.

Marysville respectively. The colors represent the magnitude of the velocity at each point. Note that the velocity at the banks of the river is non-zero in some cases as an artifact of the triangulation. We make sure that this does not affect the simulations of the particle trajectories.

4. **Velocity profile:** Figure 3-9 and Figure 3-10 show the surface-velocity profile (magnitude of the velocity) along the transverse cross-section near the initial deployment at both the sites. At both the sites, the river width is nearly $500m$. The average velocity for the case of Detroit Edison site using the mesh model was $\bar{U} = 0.9084m/s$. The maximum velocity was around $1.2m/s$. For the case of Marysville, $\bar{U} = 0.8854m/s$ and the maximum velocity was around $1.07m/s$. In both the cases, we observed that the standard deviation of the velocity of the buoys in the central zone locally varied between 0.04–0.08 m^2/s.

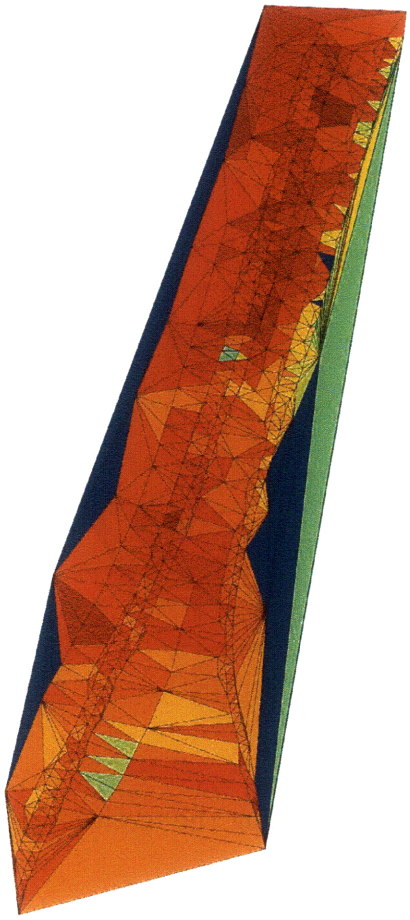

Figure 3-8: The velocity field using the mesh model for Marysville site

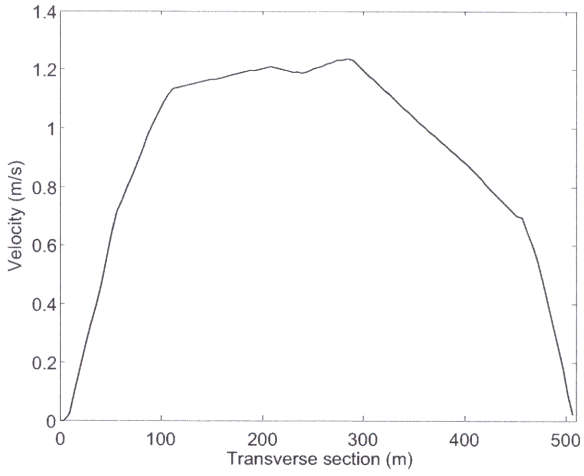

Figure 3-9: Edison velocity profile

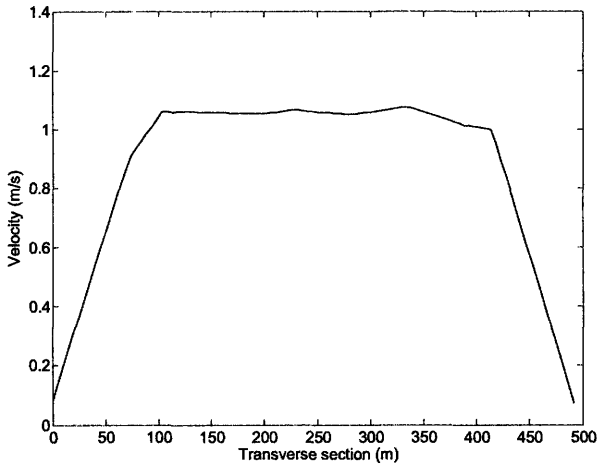

Figure 3-10: Marysville velocity profile

3.6.2 Simulation settings

We also simulate sensor-trajectories in an ideal-channel river to analyze coverage and connectivity. In order to have a fair comparison, we choose parameters of the ideal-channel river closely matching the previous two experimental settings. We choose the river width $B = 500m$, the center-line velocity $U_c = 1.1m/s$, the center-line depth $H = 15m$, the longitudinal turbulent-diffusion coefficient $\sqrt{2D_x} = 0.04m/\sqrt{s}$, the turbulent-diffusion coefficient $\sqrt{2D_y} = 0.04m/\sqrt{s}$. Based on this, we choose $\beta = 3.5$. The average velocity is $\bar{U} = 0.911m/s$. We simulate trajectories for $4000s$.

3.6.3 Coverage results

We measure coverage in terms of the area covered by the discs around the sensors scaled by a constant. In our simulations, we choose the coverage range for each node to be $20m$ and scale the area covered with a constant area of $1200000m^2$ such that the coverage metric is a number between 0 and 1. Figures 3-11, 3-12 and 3-13 show average coverage versus time plots for 20, 30, 40 and 50 nodes initially placed uniformly randomly along the transverse cross-section of the river. Coverage is averaged over 10 simulation runs. The coverage is evaluated every 100s and averaged over 10 simulation runs. The standard deviation is also shown at alternate points. In

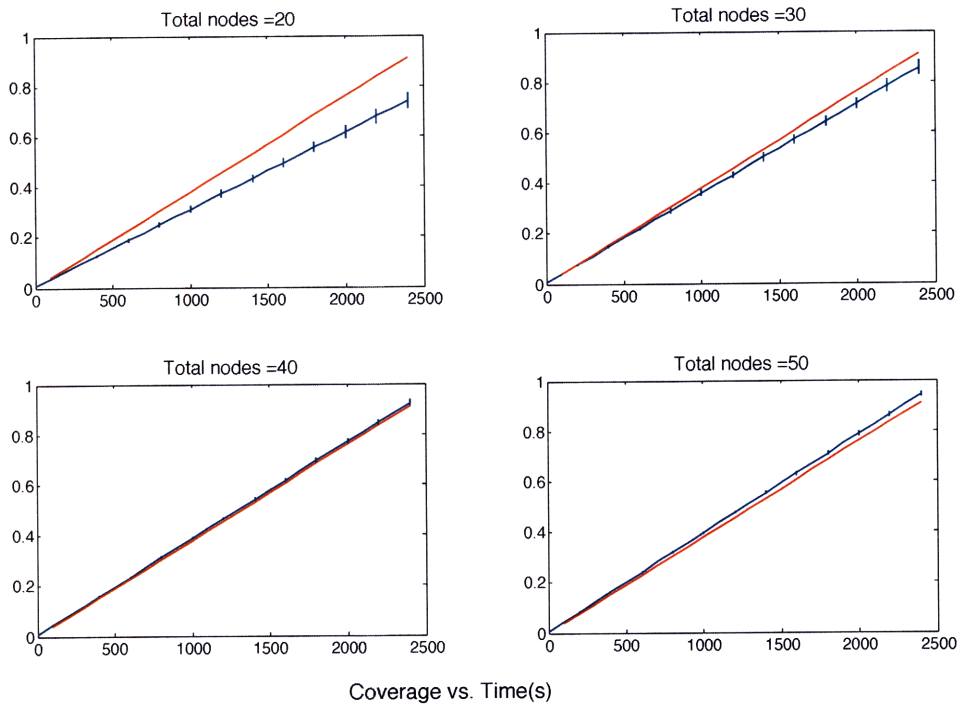

Figure 3-11: Coverage results for the natural mobility in the ideal-channel river for sensors with coverage radius = $20m$

each plot, we also show $\bar{U}Bt$ versus time, *i.e.*, the average coverage corresponding to the approximate model where the longitudinal velocity component is always $\bar{U}$. This coverage curve is shown in red color in all the plots.

We summarize our observations based on these plots as follows:

1. In all the three situations, the coverage of the network increases with the number of nodes at any given instant of time.

2. As the number of nodes increases, the coverage curve approaches the coverage curve corresponding to the average velocity ($\bar{U}Bt$ vs. time). In fact, it is interesting to note that this holds even for the two mesh models based on experimental data. As we see in Figures 3-5 and 3-6, the river has changing width and curvature. Despite these changes, $\bar{U}$ calculated at one cross-section holds as a good measure for quantifying coverage as long as the number of nodes

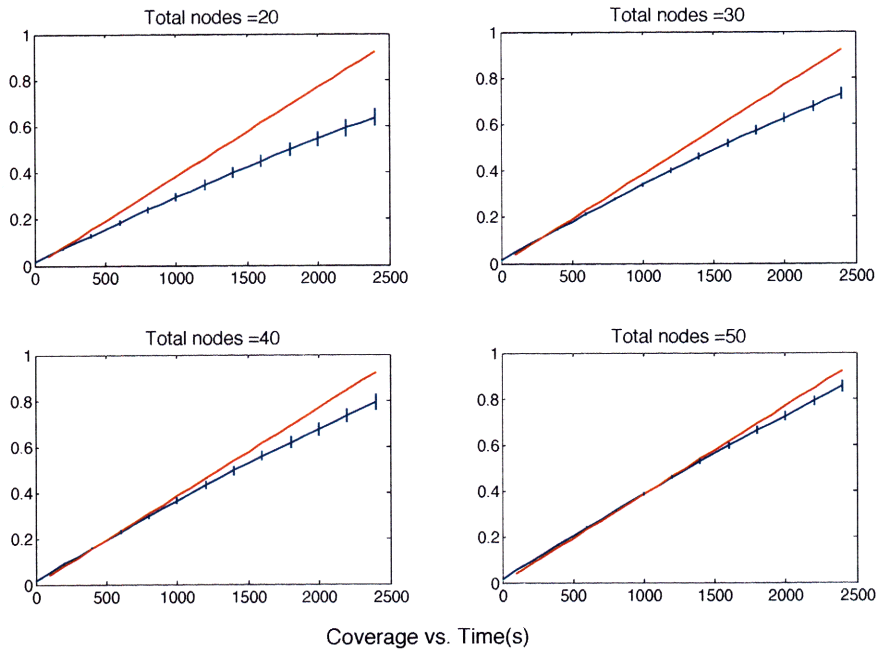

Figure 3-12: Coverage results for the mesh model of St. Clair River at Edison for sensors with coverage radius = $20m$

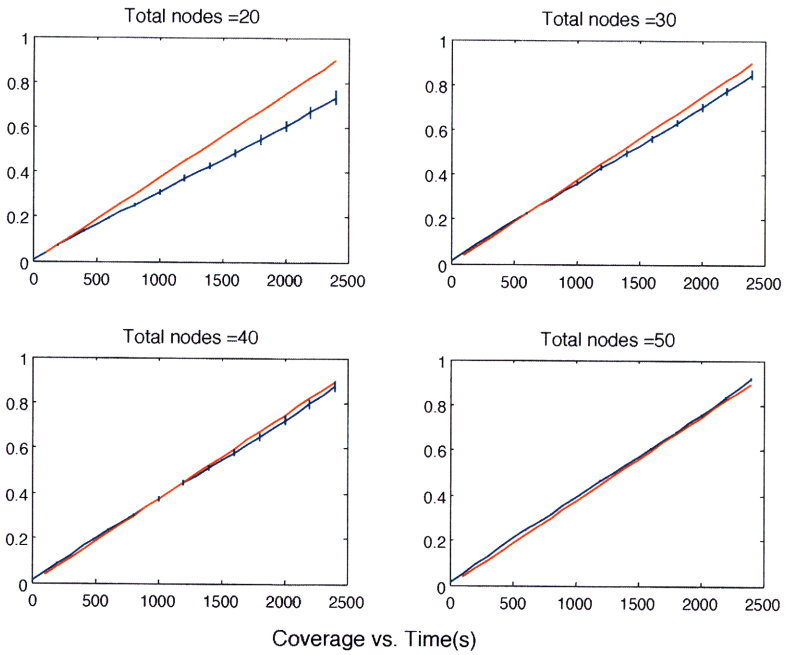

Figure 3-13: Coverage results for the mesh model of St. Clair River at Marysville for sensors with coverage radius = $20m$

are sufficient.

3. The increment in the coverage with the number of nodes is marginal beyond some point, *i.e.*, for given time T, the coverage does not increase beyond $\bar{U}BT$ even if we add additional nodes. For example, in St. Clair River near Marysville, the coverage up to $2000s$ is almost the same for 40 or 50 nodes.

3.6.4 Connectivity results

We present connectivity results in the ad-hoc network setting. In all the results presented here, we assume that the communication range was $75m$. As described earlier, we measure connectivity in terms of the ratio of the size of the largest connected cluster (LCC) and the total number of nodes deployed. We divide the river along the lateral direction into three zones, a central and two side zones and analyze connectivity in each zone by deploying nodes initially uniformly randomly only in one zone. In each case, the river width is about $500m$. We divide the lateral cross-section into three zones each of length $166m$ and deploy nodes uniformly randomly in each zone initially. Below we present the results for each zone. As before we simulate node trajectories for the ideal-channel river with settings described earlier and for the two mesh models. We deploy 10, 15, 20 and 25 nodes in each zone and observe connectivity. In the case of two mesh models, we average results over 5 simulation runs whereas in the ideal river case, we average results over 10 simulation runs. In each case, we show standard deviations on the plots.

1. **Central zone:** Figures 3-14, 3-15 and 3-16 show the connectivity results for the central zone in the ideal river, and St. Clair River near Detroit Edison and Marysville. We observe that connectivity is 100% in most of the cases. Thus, the network is guaranteed to sustain connectivity over a long period.

2. **Side zone 1:** Figures 3-17, 3-18 and 3-19 show the connectivity results for one of the side zones in the ideal river, and St. Clair River near Detroit Edison and Marysville. Unlike the case of central zone, the connectivity reduces significantly

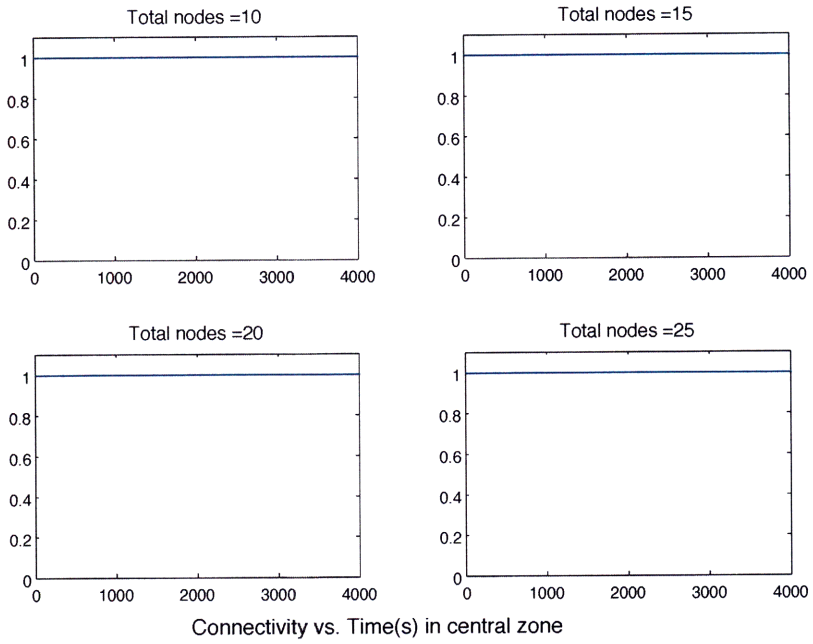

Figure 3-14: Connectivity vs. Time for nodes with communication range $75m$ in the ideal-channel river in the central zone

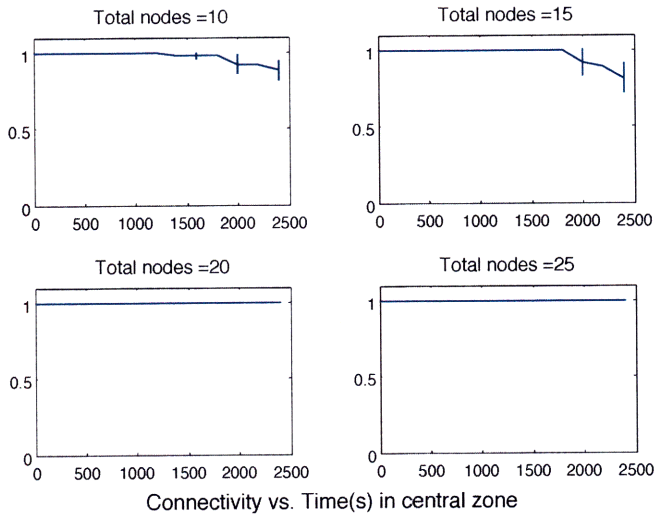

Figure 3-15: Connectivity vs. Time for nodes with communication range $75m$ in St. Clair River near Detroit Edison in the central zone

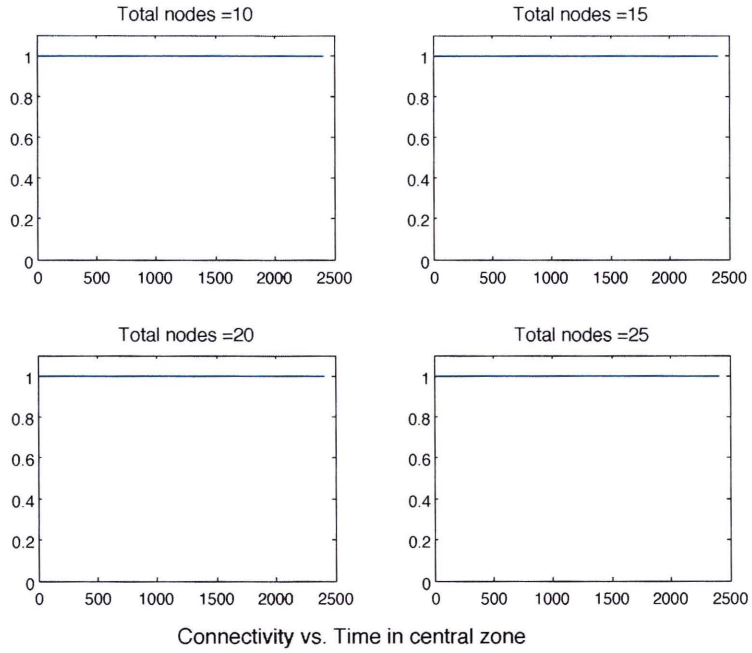

Figure 3-16: Connectivity vs. Time for nodes with communication range $75m$ in St. Clair River near Marysville in the central zone

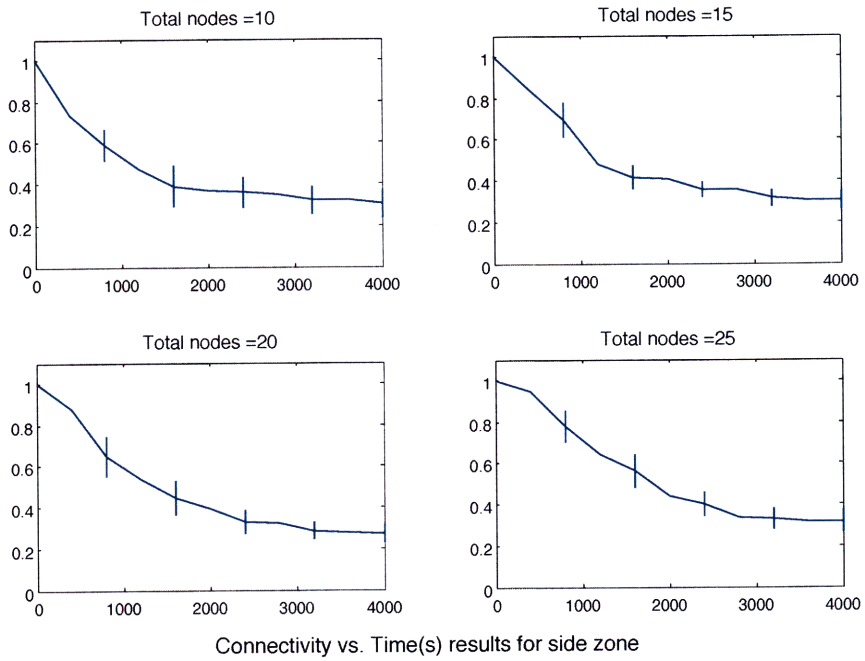

Figure 3-17: Connectivity vs. Time for nodes with communication range $75m$ in the ideal river in the side zone

over time. In fact, after $1500s$ the connectivity drops below 50% in each case. The connectivity, however, improves as the number of nodes increase as observed up to $1000s$ for different number of nodes.

3. **Side zone 2:** Figures 3-20 and 3-21 show the connectivity results for the other side zone in St. Clair River near Detroit Edison and Marysville. Near Detroit Edison, the connectivity trend is same as that for the side zone 1. However, near Marysville, the connectivity is almost like the central zone as the number of nodes increase. This is explained by the velocity profile. Observe that in the mesh model in Figure 3-8, the velocity values are almost the same in one size zone. This is due to the fact that the channel is asymmetric. In Figure 3-6, we notice that on the left hand side of the channel, the depth reduces much gradually whereas on the other side the channel depth reduces sharply. This

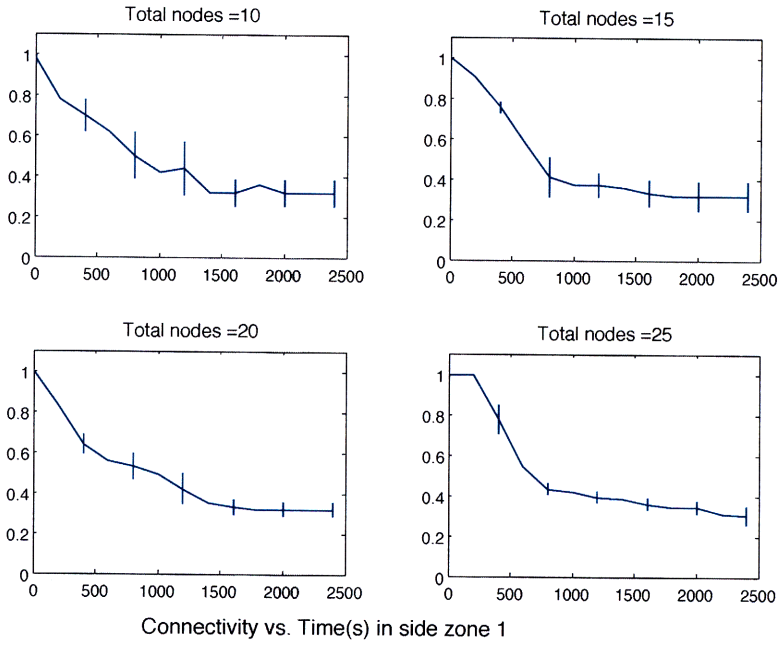

Figure 3-18: Connectivity vs. Time for nodes with communication range $75m$ in St. Clair River near Detroit Edison in one of the side zones

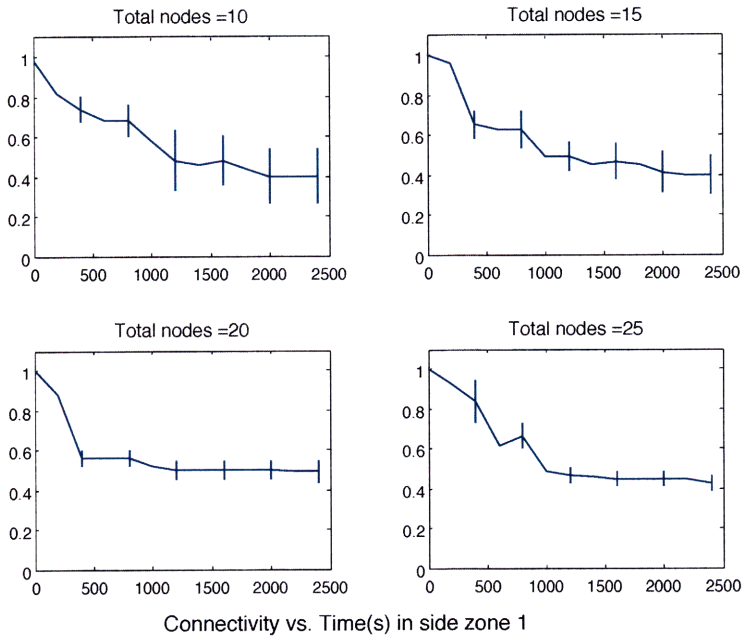

Figure 3-19: Connectivity vs. Time for nodes with communication range $75m$ in St. Clair River near Marysville in one of the side zones

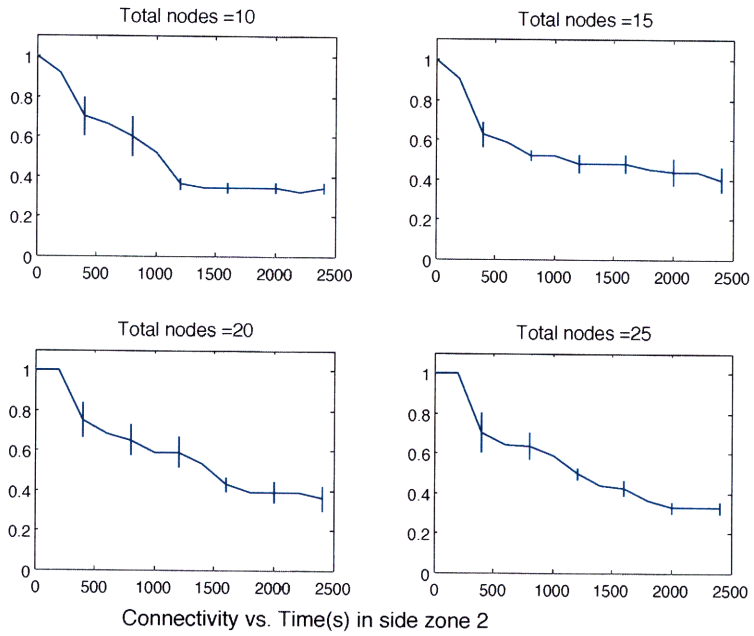

Figure 3-20: Connectivity vs. Time for nodes with communication range $75m$ in St. Clair River near Detroit Edison in the other side zone

example illustrates that the formation of cluster will depend on the velocity field.

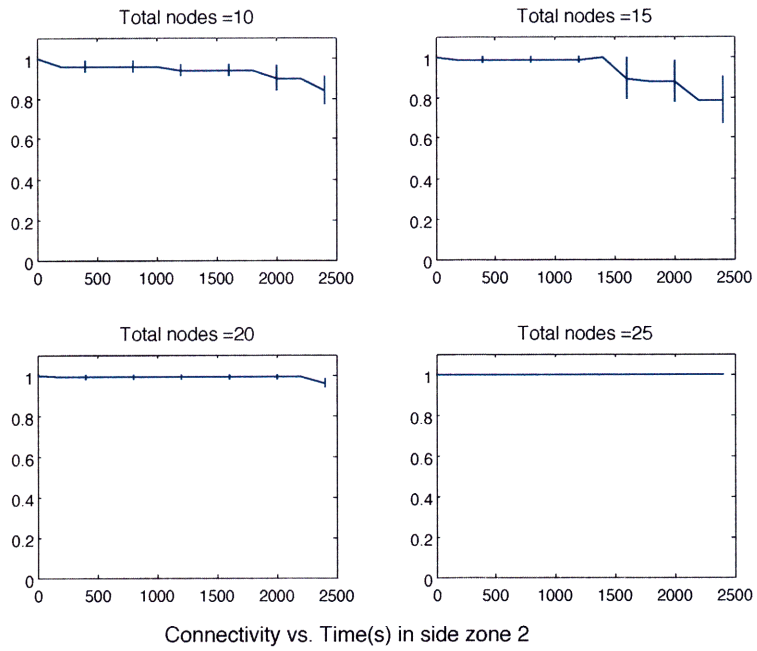

Figure 3-21: Connectivity vs. Time for nodes with communication range $75m$ in St. Clair River near Marysville in the other side zone

Chapter 4

Reconfigurable Camera Sensor Networks

In this chapter, we address the second coverage problem which deals with intentionally mobile detection sensors. We formulate a coverage problem for detection sensors with location-dependent sensing performance function. We propose a distributed coverage algorithm with guaranteed convergence. As an application, we address the problem of covering loopy indoor and outdoor pathways with a network of mobile cameras. Based on our experiments, we propose an empirical sensing performance function to characterize detection behavior of a camera. We present results of our coverage algorithm for indoor and outdoor deployments.

Organization: In Section 4.1, we formulate coverage problem for sensors with location dependent sensing performance function. In Section 4.2, we propose a distributed coverage algorithm and prove its convergence. In Section 4.3, we discuss modeling of a sensing performance function for a camera and present results on indoor and outdoor camera deployments.

4.1 Coverage Problem Formulation

In Section 2.4, we introduced the coverage-problem formulation as in [15] for detection sensors with associated sensing performance function. We build on the notation used in [15] to define our coverage problem. Let Q denote the bounded convex domain in $\mathbb{R}$. We seek to *cover* Q using n mobile sensors. Let $\phi : Q \rightarrow \mathbb{R}$ denote the scalar density function. It captures the importance of covering a particular location. Let $p_1, p_2, \cdots, p_n$ denote the current locations of n sensors. We assume a location-dependent sensing model for each sensor, *i.e.*, the *sensing performance* at point q for the i^{th} sensor not only depends on $||q-p_i||$ but also on the location, p_i itself. Here, $||\cdot||$ denotes the Euclidean norm. We denote the sensing performance function for sensor i at point q by $f(||q-p_i||, p_i)$, where $f : \mathbb{R}^+ \times Q \rightarrow \mathbb{R}$. Note that we explicitly indicate the dependence of the performance function on the sensor location. The performance function naturally induces a *generalized Voronoi partition* of Q. Each sensor has its own *dominance region*, *i.e.*, its Voronoi cell where the sensing performance is better than that for any other sensor. More formally, if W_i denotes the dominance region for the i^{th} sensor, then

$$W_i = \{q \in Q \mid f(||q-p_i||, p_i) \geq f(||q-p_j||, p_j), \ \forall j \neq i\}. \tag{4.1}$$

Now we define our *coverage* metric or *net utility function* as follows:

$$\mathcal{H}(p_1, p_2, \cdots, p_n) = \sum_{i=1}^{n} \int_{W_i} \phi(q) f(||q-p_i||, p_i) dq \tag{4.2}$$

The utility function is the sum of the sensing performance function of each sensor over its dominance region including the weighing density function. We refer to $\int_{W_i} \phi(q) f(||q-p_i||, p_i) dq$ as the *utility* of the i^{th} sensor. We formulate the coverage problem as finding the optimal set of locations of the sensors that maximizes the net utility.

$$(p_1^*, p_2^*, \cdots, p_n^*) = \arg \max_{(p_1, p_2, \cdots, p_n)} \mathcal{H}(P). \tag{4.3}$$

Note that it is possible to formulate other metrics such as maximizing the minimum over the utility functions of all the sensors, as suggested in the literature, *e.g.*, [15]. We would like to note that in the common literature [15] the coverage objective function is known as the *locational optimization function* and the coverage problem is formulated as the minimization problem. In the spirit of the application we consider in this paper, we formulate the problem as the maximization problem.

4.1.1 Partial derivative of the overall utility function

We note that the result about the partial derivative of the net utility function based on the divergence theorem [15] generalizes easily to our case. We use the divergence theorem in the proof of our result [13].

Theorem 4.1.1. *[13] Let $\mathcal{V} = \mathcal{V}(x) \subset Q$ be a region that depends smoothly on real parameter $x \in \mathbb{R}$. $\mathcal{V}$ has a well-defined closed boundary $\partial\mathcal{V}(x)$ for all x. Let $\phi(q)$ be the density function over Q. Then*

$$\frac{d}{dx}\int_{\mathcal{V}(x)} \phi(q) f(||q-y||, y) dq = \int_{\partial\mathcal{V}(x)} \langle \frac{dq}{dx}, n(q) \rangle \phi(q) f(||q-y||, y) dq,$$

where $\langle \cdot, \cdot \rangle$ denotes the dot-product and $n(q)$ denotes the normal vector along $\partial\mathcal{V}(x)$.

We modify the above result for a special case as follows:

Lemma 4.1.2. *Let $\mathcal{V} = \mathcal{V}(x) \subset Q$ be a region that depends smoothly on real parameter $x \in \mathbb{R}$. $\mathcal{V}$ has a well-defined closed boundary $\partial\mathcal{V}(x)$ for all x. Let $\phi(q)$ be the density function over Q. Then*

$$\begin{aligned} \frac{d}{dx}\int_{\mathcal{V}(x)} \phi(q) f(||q-x||, x) dq &= \int_{\mathcal{V}(x)} \phi(q) \frac{\partial f(||q-x||, x)}{\partial x} dq \\ &+ \int_{\partial\mathcal{V}(x)} \langle \frac{dq}{dx}, n(q) \rangle \phi(q) f(||q-x||, x) dq. \end{aligned}$$

Theorem 4.1.3. *The partial derivative of the net utility function with respect to the*

position of the i-th sensor is given by,

$$\frac{\partial \mathcal{H}}{\partial p_i} = \int_{W_i} \phi(q) \frac{\partial f(||q - p_i||, p_i)}{\partial p_i} dq \tag{4.4}$$

Proof. Below we sketch the steps of the proof. We refer readers to [13] for details. Let $p_{j_1}, p_{j_2}, \cdots, p_{j_k}$ be p_1's generalized Voronoi neighbors. Let Δ_{ij_l} be the Voronoi cell boundary between i and neighbor j_l. Note that the following two normal directions are in opposite directions. $n_{ij_l}(q) = -n_{j_l i}(q)$. Then

$$\frac{\partial \mathcal{H}}{\partial p_i} = \frac{\partial}{\partial p_i} \int_{W_i} \phi(q) f(||q - p_i||, p_i) dq + \sum_{l=1}^{k} \int_{\Delta_{j_l i}} \phi(q) f(||q - p_{j_l}||, p_{j_l}) dq.$$

Based on Theorem 4.1.1 and Lemma 4.1.2, and the definition of the generalized Voronoi diagrams, we obtain the desired result.

□

4.2 Distributed coverage control

We propose a distributed coverage control algorithm that is based on iterative local sub-gradient method.

4.2.1 Control Law for each sensor

Let $p_i(n)$ be the position of the i-th sensor after n updates. We state the control law for the position update of the i-th sensor to $p_i(n+1)$. The local control law involves searching for the local optimal solution. During the time the i-th sensor updates its position from, our coverage algorithm does not allow the simultaneous update at the Voronoi neighbors of the i-th sensor. Given that the positions of the Voronoi neighbors are fixed, the net utility $\mathcal{H}$ and the local gradient, $\frac{\partial \mathcal{H}}{\partial p_i}$ are just the functions of p_i. We state the control law as follows.

$$p_i(n+1) = p_i^* \text{ ,where, } p_i^* = \arg\max_{p_i \in W_i} \mathcal{H}(\cdots, p_i, \cdots) \tag{4.5}$$

Essentially, the control law involves local search over the Voronoi partition W_i for the optimal solution p_i^* by solving the constrained optimization problem. If p_i^* does not lie on the boundary of W_i, then it is the root of equation $g(p_i) = 0$ for some function g. Since the search involves finding the optimal location just for one sensor, it is computationally tractable. We state the following lemma about the increase in the net utility after every pose update.

Lemma 4.2.1. *The control law for an individual sensor in Equation 4.5 guarantees that the net utility increases after the position update of the sensor.*

Implementation of the above control law requires the exact knowledge of the sensing performance function $f(||q - p_i||, p_i)$ for each sensor i and the density function $\phi(q)$. Later we show in our case study of camera sensor network that $f(||q - p_i||, p_i)$ can be estimated on the fly using measurements. We also note that [69] shows that the global knowledge of $\phi(q)$ is not required.

4.2.2 Distributed Coverage Algorithm

Below we state the coverage algorithm that runs at each node. We assume discrete time steps, 1, 2, $\cdots$. The algorithm involves the implementation of the local control law that we described in the previous section. A node updates its position only if its Voronoi neighbors are not updating their positions.

Algorithm 1 Coverage algorithm at the i-th sensor: Let p_i denote its position. Let V_i denote the set of its Voronoi neighbors.

t : Update V_i
t+1: Check if any $j \in V_i$ is updating its position
t+2: if yes, wait for random duration of time and repeat the above steps
t+2: if no, schedule position update at t+3 and broadcast over V_i
t+3: start moving to optimal p_i^* as obtained using Equation 4.5
t+k: After the move, wait for random duration before the next update

4.2.3 Convergence

Theorem 4.2.2. *The distributed coverage algorithm at each sensor as described in Algorithm 4.2.2 converges, as the number of position updates tends to infinity.*

The proof follows from the fact that the net coverage utility is bounded and by lemma 4.2.1, it increases monotonically with each iteration of the algorithm.

The algorithm yields a local optimal solution to the coverage problem.

4.3 Deployment of Cyclops camera networks

In this section, we discuss implementation issues and results of our algorithm for the coverage problem using Cyclops camera sensors.[1] The Cyclops camera sensor consists of a CMOS imager with CIF image capability and an internal image processor unit for image interpretation and analysis. It couples with a Mote and periodically captures images (Figure 4-1). Our objective is to *cover* loopy environments such as indoor corridors or outdoor pathways such that an intruder object can be detected. We show that this problem can be mapped into a suitable coverage problem. We first propose a model for the sensing performance function of a camera.

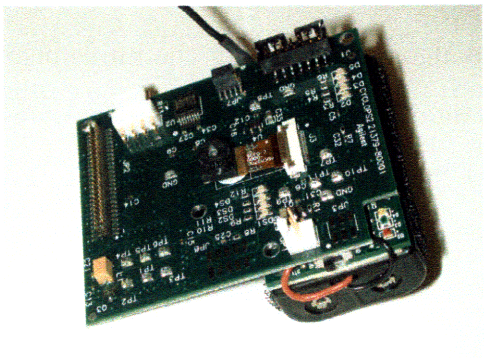

Figure 4-1: Cyclops camera with an attached Mica2 Mote

[1] We do not consider any network related issues here.

4.3.1 Sensing Performance Function

Our choice of the sensing performance function of a camera is related the performance of the object detection algorithm that is based on background subtraction. Foreground object detection using background subtraction has been used extensively in video surveillance applications due to ease of implementation and effectiveness. This method has low resource requirements in terms of memory and computation and is therefore well suited for low complexity camera sensor networks. According to this method, the cyclops camera periodically captures images and maintains a moving average background model of the environment. A foreground model is also constructed as the absolute difference of the instantaneous image and the constructed background. The resulting foreground images are then are passed through a luminance and size filter, which identifies clusters of pixels that have a considerable change in illumination. Figure 4-3(a) shows a cyclops camera set up in a corridor in a building. Figure 4-3(b) and 4-3(c) show the background model and the instantaneous image obtained by placing a white board at some distance. The foreground images as the difference between the two images is shown in Figure 4-3(d). The *detectability* of the object depends on the number of pixels identified after passing the foreground model through the filter – larger the number of pixels, better the detection probability. We therefore use the number of pixels identified as the sensing performance function for each camera sensor. Note that the number of pixels detected is also a function of distance between the camera and the object. The further away the object is, the lower the number of pixels detected will be.

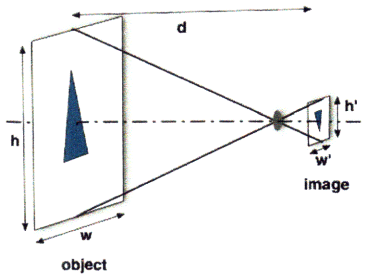

Figure 4-2: Perspective projection model

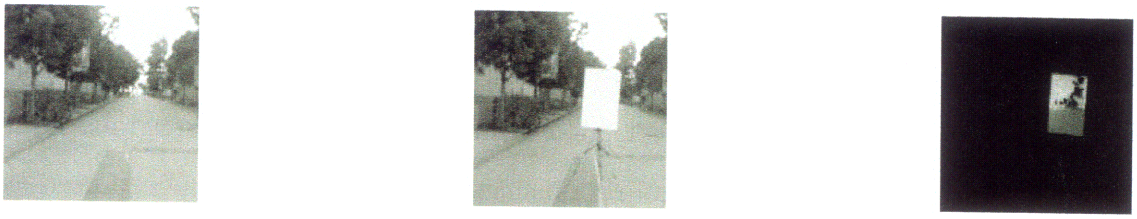

(a) (b) (c)

Figure 4-3: Illustration of pixels on target not detected. (a) background image (b) original image and (c) foreground image. In the foreground image, some of the pixels in the target board are black. These are the pixels that are similar to the background and are therefore not detected by the camera.

Suppose a rectangular object of dimension $h \times w$ placed at a distance d on the camera's central axis exactly facing the camera. Consider an ideal scenario in which every point on the object differs significantly in its illumination characteristics from the background image. Then, according to a perspective projection camera model, the number of pixels, m, detected by the camera is approximately given by:

$$m \simeq \frac{f \cdot h \cdot w}{d^2} \cdot \frac{resolution}{sensor\_area} = k \cdot \frac{h \cdot w}{d^2} \cdot resolution$$

where f is the focal length and k is a constant. Figure 4-2 shows the perspective projection model. Thus, the number of pixels detected is inversely proportional to square of the distance between the camera and the object. We indeed observed this relationship in practice when we experimented with a white board of dimension $3ft \times 2ft$ placed at different distances in front of a cyclops camera that was placed in a well-lit corridor. Figure 4-4.1(a) shows the experimental set-up and Figure 4-4.2(a) shows the number of pixels identified using the background subtraction algorithm as a function of distance between the camera and the white board. We indeed observe the trend that the number of pixels are inversely proportional to the squared distance. However these situations are rare in the environments where the lighting conditions and the object properties are far from the ideal situation. In practice, the number of pixels detected by the camera deviates from this ideal model because some pixels on

the object have the same texture as that of the background and go undetected. This is illustrated in fig 4-3 where the target is a white rectangular board. In the foreground image, the pixels in white are the ones that are detected. Some of the pixels on the board have intensities close to their corresponding pixels in the background.

This indicates that the sensing performance function of a camera depends not only on the distance but also on the location of the camera itself. This very behavior motivates the definition of the coverage problem we address. We restrict ourselves to coverage of narrow pathways reducing the problem to coverage of $1D$ loops. We conducted a series of experiments both indoors and outdoors to extract the sensing performance function of a camera. We placed a white/black rectangular board in front of a camera along its central axis at increments of 5 feet to obtain the number of pixels detected. Based on several data sets we observed that the following empirical model for the sensing performance function best fits the data.

$$f(||x-q||, x) = \frac{k_1(x)}{k_2(x) + ||x-q||^2} \tag{4.6}$$

Here x denotes the location of the camera and q denotes the sensing performance, *i.e.*, the number of pixels detected at location q. Note the dependence on the location of x via functions $k_1(x)$ and $k_2(x)$. Figure 4-4 shows the best fit and the corresponding values of k_1 and k_2 for indoor and an outdoor instances. Note that the sensing performance function is not exact; it corresponds to the best fit with the data.

4.3.2 Coverage Algorithm for 1D loop

In this section, we discuss the coverage problem formulation and algorithm for covering a loopy pathway using the cyclops cameras. We assume that the pathway is narrow enough so that we formulate the problem as a $1D$ coverage problem. We assume that each sensor is a bi-directional camera obtained by combining two cyclops camera modules aligned along the same axis. Thus each sensor can *see* on its *left* and *right* directions on the loop. The sensing performance function along each direction takes the form of Equation 4.6 with possibly different parameter values. For now we

1(a)

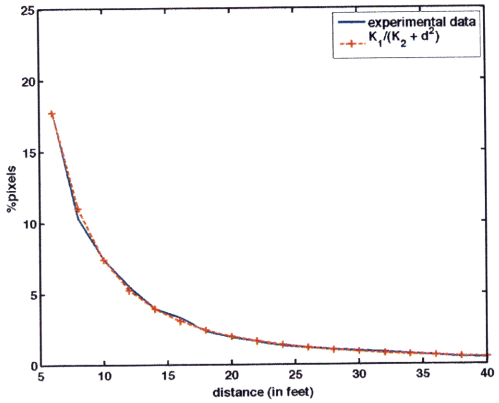

1(b)

2(a)

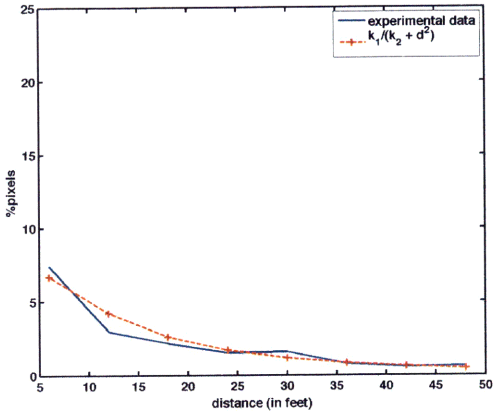

2(b)

3(a)

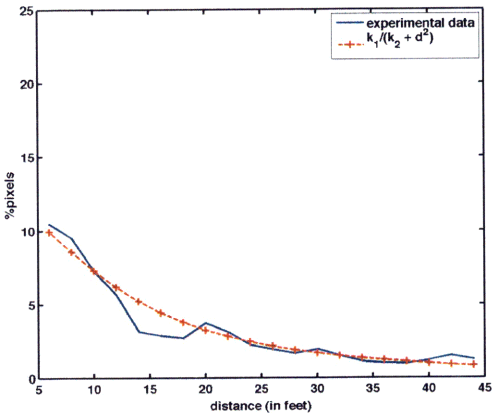

3(b)

Figure 4-4: Validation of the proposed model for pixels detected vs. distance for three different environments. 1(a) is a well-lit corridor and close to an ideal environment. 2(a) is an outdoor pathway with shadows of trees and buildings. 3(a) is inside a lab where the lighting conditions are not uniform. The solid blue line is the number of pixels detected from experiments and the red dashed line is the minimum least squares fit using the model in Equation 4.6

assume that the pathway is a smooth curve that can be parametrized with a single parameter and does not contain any sharp corners, *i.e.*, at any location the curvature of the loop is very large compared with the local *detection range* of the camera assuming that the sensor is always aligned on the loop such that its central axis is always tangential to the loop. Let n be the number of cameras and let $p_1, p_2, \cdots, p_n$ denote their locations on the loop in the order such that p_i is *between* p_{i-1} and p_{i+1}. Further, let $p_{n+1} = p_1$. Let $f_l(||p_i - q||, p_i)$ and $f_r(||p_i - q||, p_i)$ be the left and the right sensing performance functions respectively of the i-th camera located at p_i. We assume that both f_l and f_r have the empirical form described in Equation 4.6:

$$f_l(||p_i - q||, p_i) = \frac{k_{1l}(p_i)}{k_{2l}(p_i) + ||p_i - q||^2} \tag{4.7}$$

$$f_r(||p_i - q||, p_i) = \frac{k_{1r}(p_i)}{k_{2r}(p_i) + ||p_i - q||^2} \tag{4.8}$$

Because the problem is $1D$, the region of dominance of any sensor corresponds to a segment on the loop. We further assume that the region of dominance of the i-sensor strictly belongs to the interval (p_{i-1}, p_{i+1}). In other words, there are no abrupt changes in the sensing behavior over the domain such that each sensor contributes to the net utility function. Let $[l_i, r_i]$ be the dominance range of the i-th sensor. Thus, $l_i \in (p_{i-1}, p_i)$ and $r_i \in (p_i, p_{i+1})$. According to the definition of the dominance region,

$$f_l(||p_i - l_i||, p_i) = f_r(||p_{i-1} - l_i||, p_{i-1}) \text{ and,}$$

$$f_r(||p_i - r_i||, p_i) = f_l(||p_{i+1} - r_i||, p_{i+1}).$$

Using the above notation, the net utility function in 4.2 assuming uniform density function ($\phi(q) = 1$) can be expressed in the following form for the case of $1D$ loop.

$$\mathcal{H}(p_1, p_2, \cdots, p_n) = \sum_{i=1}^{n} \{ \int_{l_i}^{p_i} f_l(||p_i - q||, p_i) dq + \int_{p_i}^{r_i} f_r(||p_i - q||, p_i) \} \tag{4.9}$$

4.4 Simulation Results

4.4.1 Simulation Environment

We ran simulations in MATLAB to test the convergence and resulting coverage of our distributed control law. The path is a $1D$ loop that can have sharp corners and obstacles that cause the sensing performance function to vary abruptly. The sensors start at randomly chosen initial positions and in each iteration of the algorithm, they update their position according to Equation 4.5 using a constrained optimization routine in MATLAB. We assume that sensors are localized and adjacent sensors on the path can communicate with each other. The simulation converges when the no sensor changes its position. We test for different models of $k_1(x)$ and $k_2(x)$, different shapes of the path, and different number of sensors.

4.4.2 Global knowledge of sensor performance function

We first consider the ideal scenario where sensors have perfect knowledge of the sensing performance function. In practice, the sensors will estimate the performance function based on observed data the performance of the coverage algorithm will depend on the accuracy of this estimation. Figure 4-5 shows the performance of the algorithm for three different sensing performance functions. In each case, the sensors start at random initial locations. As expected, for constant parameter values (Figure 4-5.1(a)), the sensors converge to a uniform distribution(Figure 4-5.1(b)). When the parameters have significant variations (Figure 4-5.2(a), 4-5.3(a)), the distribution if non-uniform (Figure 4-5.2(b), 4-5.3(b)). Sensors try to move to positions where the value of k_1 is large and k_2 is small so that their local utility is maximized. Note that in each case the global coverage utility increases monotonically even though the position updates at each sensor are local. This is in agreement with Theorem 4.2. To study the impact of the network size on the algorithm performance, varied the network size from 5 to 100. For each network size, we repeated the simulation 50 times starting with a different random initial position each time. The coverage utility

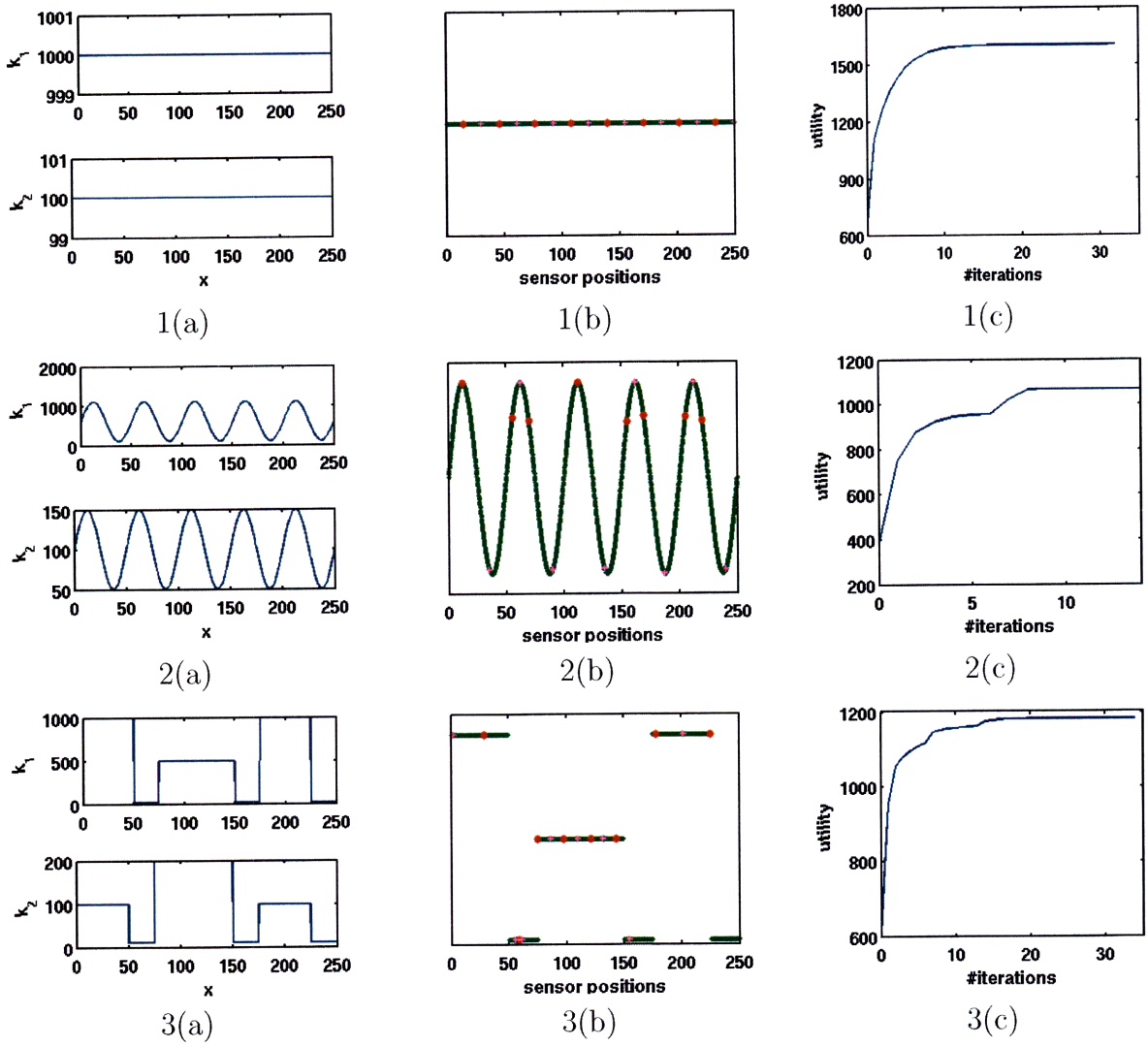

Figure 4-5: Performance of the distributed control law for three types of parameter functions on a $1D$ loop which is a 250 feet long smooth curve. 1(a), 2(a) and 3(a) show the parameter values constant, sine and step. 1(b), 2(b) and 3(b) show the corresponding final positions of sensors (red circles) superimposed on the k_1 function. The crosses show the dominance region boundaries between sensors. 1(c), 2(c) and 3(c) show the variation in the net coverage utility. The utility increases monotonically with each iteration.

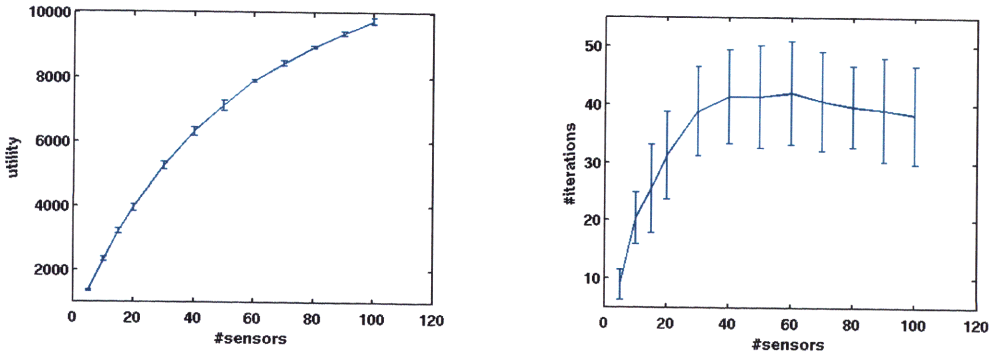

(a) (b)

Figure 4-6: Variation in coverage utility and convergence time for different network sizes averaged over 50 iterations.

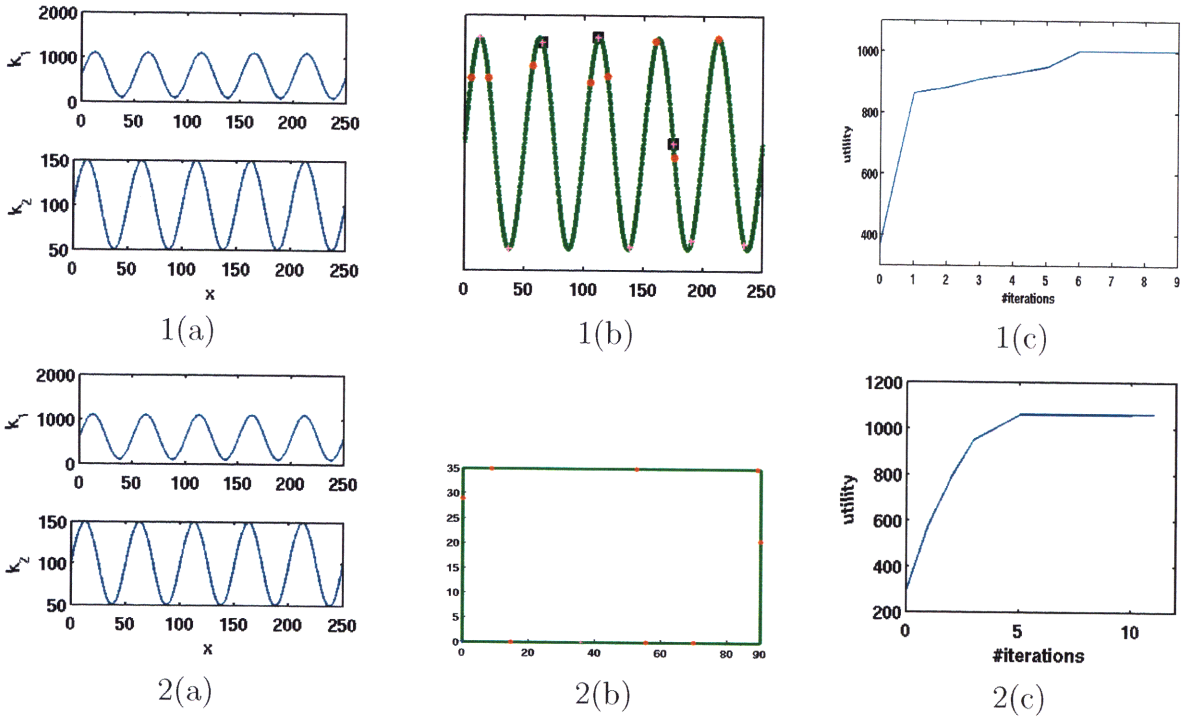

1(a) 1(b) 1(c)

2(a) 2(b) 2(c)

Figure 4-7: Performance of the distributed control law in the presence of occlusions - (1) obstacles and (2) sharp corners.

increases exponentially and eventually saturates (Figure 4-6(a)) since as the number of sensors increases, the marginal utility of each additional sensor decreases and tends to zero. The variation in utility is very small indicating that the initial locations do not impact the final coverage. The convergence time initially increases with the number of sensors and then stops increasing (Figure 4-6(b)) proving that the algorithm is scalable. The large deviations indicate that unlike coverage, the convergence time varies significantly with the initial sensor locations.

4.4.3 Occlusions

Occlusions can occur due to obstacles in the path or sharp corners. Since the camera cannot see through an occlusion, occlusions cause an abrupt drop in the sensing performance function. Equations 4.7, 4.8 can be modified as follows to account for occlusions.

$$f_l(||p_i - q||, p_i) = \begin{cases} \frac{k_{1l}(p_i)}{k_{2l}(p_i)+||p_i-q||^2} & \text{if } q \text{ is not occluded from } p_i \\ 0, & \text{otherwise} \end{cases} \tag{4.10}$$

$$f_r(||p_i - q||, p_i) = \begin{cases} \frac{k_{1r}(p_i)}{k_{2r}(p_i)+||p_i-q||^2} & \text{if } q \text{ is not occluded from } p_i \\ 0, & \text{otherwise} \end{cases} \tag{4.11}$$

Because the sensing function takes on a constant value for points beyond an occlusion, it is possible that the equations $f_l(||p_i - l_i||, p_i) = f_r(||p_{i-1} - l_i||, p_{i-1})$ and, $f_r(||p_i - r_i||, p_i) = f_l(||p_{i+1} - r_i||, p_{i+1})$ that define the dominance region have many solutions. This will happen, for example, when adjacent sensors have two or more obstacles between them. For such cases, we define the dominance region boundary to be the position of its closest occlusion, *i*.e., if the value of the sensing function of a camera is zero at a point q then q is considered *not covered* by the camera and will not belong to its dominance region. Notice that with this definition, the dominance regions may not form a partition of the path and there could be segments of the path that do not belong to any sensor's dominance region. However, since these segments

have zero coverage utility for all the sensors, and the rest of the path is partitioned according to the Voronoi property, this definition of dominance regions is an optimal assignment of points on the path to sensors.

With these new definitions for performance function and dominance regions, we can apply the control law in equation 4.5 and Theorem 4.2 guarantees convergence. However, with this control law, sensors adjacent to occlusions will not cross the occlusions because they only pick new positions within their dominance regions. To further improve the coverage utility, we introduce an additional *switching* step where sensors can cross obstacles if the local utility gained by doing so is more than the utility gain of the optimal location within its dominance region. While computing the switching utility, we account for change in the dominance regions and the utility of the neighboring sensors. Note that the local utility of every other sensor remains unchanged.

Figure 4-7.1 shows the result of the algorithm on a loop of length 250 feet with 3 obstacles. The parameters vary as sine functions. Figure 4-7.1(b) shows the positions of the obstacles (black squares) and final positions of the sensors (red circles). As expected the coverage obtained here is less than Figure 4-5.2(a) where there are no occlusions. Figure 4-7.2 shows an example on a rectangular path with 4 sharp corners that cause occlusions. In both cases, the utility increases monotonically with each iteration and the algorithm converges. We can generalize this approach to deal with more complex pathways with multiple junctions so at a sensor adjacent to a junction reasons about the coverage gain in each of the branches that meet at the junction.

4.4.4 Online estimation of sensor performance function

In the coverage algorithm in the previous section we assumed that each sensor has global knowledge of the sensing performance function $f(||p_i - q||, p_i)$. This permits a sensor to take the best step according to Equation 4.5. However in practice this is not possible. Specifically, in the case of camera sensors, functions $k_1(x)$ and $k_2(x)$ are not globally known. This necessitates modification of the current coverage algorithm. We assume that at every step of the algorithm, a camera *learns* its sensing performance

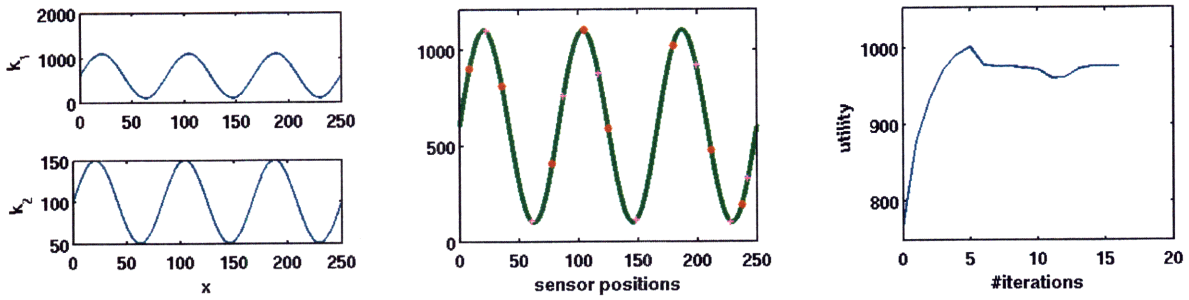

(a) (b) (c)

Figure 4-8: Performance of the distributed control law with partial knowledge of $k_1(x)$ and $k_2(x)$.

function, *i.e.*, the empirical values of k_1 and k_2.

In the simulations shown in Figure 4-8, each sensor builds piecewise linear models of k_1 and k_2 based on data from its neighboring sensors and its current data. To improve the estimation in the first iteration, we assume that sensors share data over multiple hops. We observe that the utility sometimes decreases because of erroneous estimation (Figure 4-8(c)). But even with this very simple estimation, the coverage utility is close to the case when global knowledge was assumed.

(a) indoor (b) outdoor

Figure 4-9: Cyclops setup

4.4.5 Cyclops Experiments and Results

We conducted a series of controlled experiments with cyclops cameras to gather several images in two different environmental settings – indoor and outdoor. We used interpolation techniques on the gathered data to reconstruct the sensing performance functions in these settings and tested the performance of our coverage algorithm for these pseudo-real functions.

1) a rectangular corridor in an building with controlled lighting (figure 4-9(a)) and 2) a rectangular pathway surrounded by trees with uncontrolled lighting (figure 4-9(b)). For each of these settings, we picked sample positions for the camera and for each location, we estimated the sensing performance function (k_1 and k_2) by placing a target at different distances from the camera.

4.4.6 Indoor experiments

Corridors of buildings provide an ideal playground for testing our coverage algorithms with cyclops cameras. We performed experiments under controlled lighting conditions in a rectangular corridor of which the central axis rectangle is of size $90ft \times 30ft$. The corridor is $5ft$ wide and Figure 4-9(a) shows a cyclops camera set up along the length of the corridor. At every $20ft$ along the lengthwise central axis of the corridor, we placed a cyclops camera and captured on both sides the images of the corridor which serve as background models. We also captured images of a white or black board of dimension $3ft \times 2ft$ placed along the central line kept at every $5ft$ from the camera up to $25ft$. These images serve as foreground models. Since the width of the corridor is $30ft$, along the width-wise central axis, we placed a camera at the middle point and captured images on both sides in the similar fashion. We used these images to fit the sensing performance function to obtain the values of k_1 and k_2 at various locations. Along the entire corridor, we obtained 22 pairs of values of k_1 and k_2. We interpolate spline functions through these values of k_1 and k_2 to estimate the *pseudo-real* global sensing performance function. Figure 4-10(a) shows $k_1(x)$ and $k_2(x)$ along the entire length of the corridor. We use this form to test our coverage algorithm.

In our simulations, we placed k sensors initially uniformly randomly. simulations results - comment about number of sensors, utility, global knowledge / vs online estimation, convergence

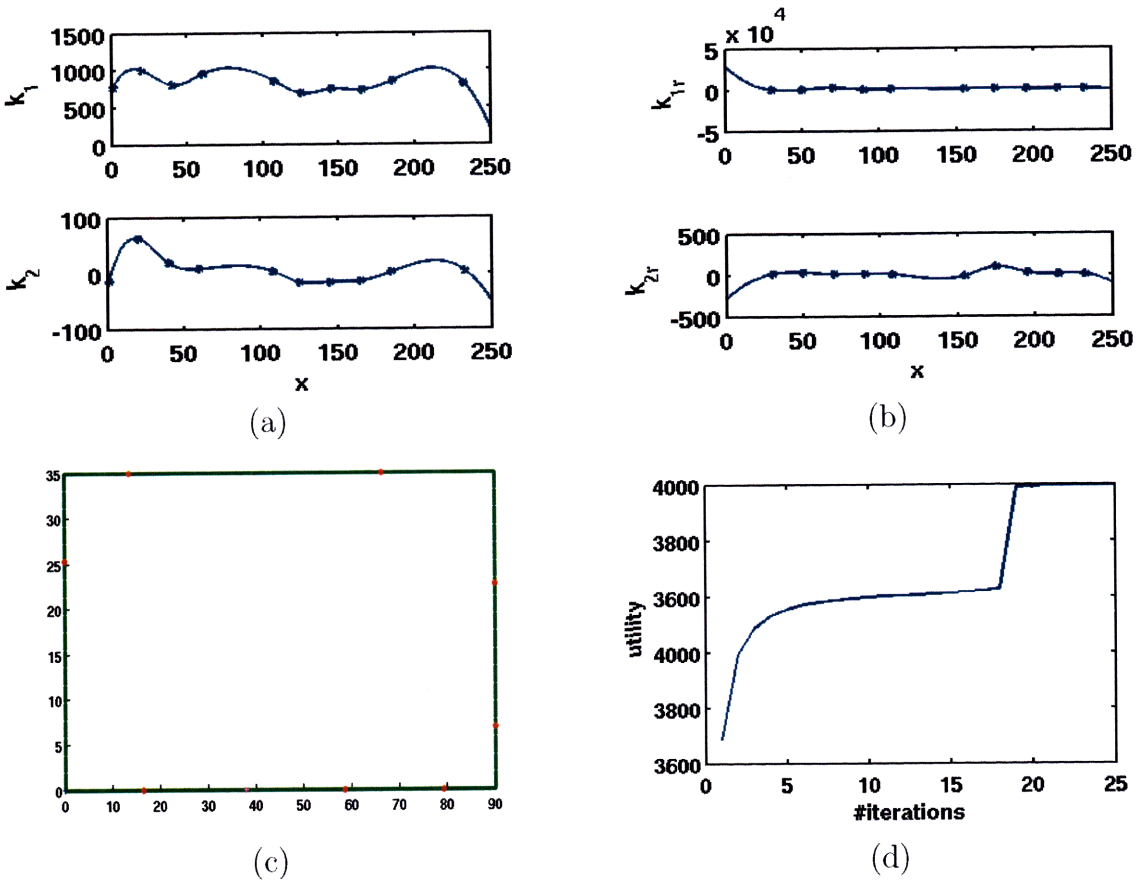

Figure 4-10: Performance of the distributed control law in an indoor rectangular corridor.

4.4.7 Outdoor experiments

We conducted a similar experiment as in the indoor case around an outdoor rectangular pathway surrounded by trees without any control over lighting conditions. The pathway was of size $a \times b$ and Figure 4-9(b) shows a picture of a cyclops camera set up along the pathway. We captured background images and foreground images at n locations around the pathway in both directions. We observed that the lighting conditions in the outdoor setting change rapidly and because of this effect we collected

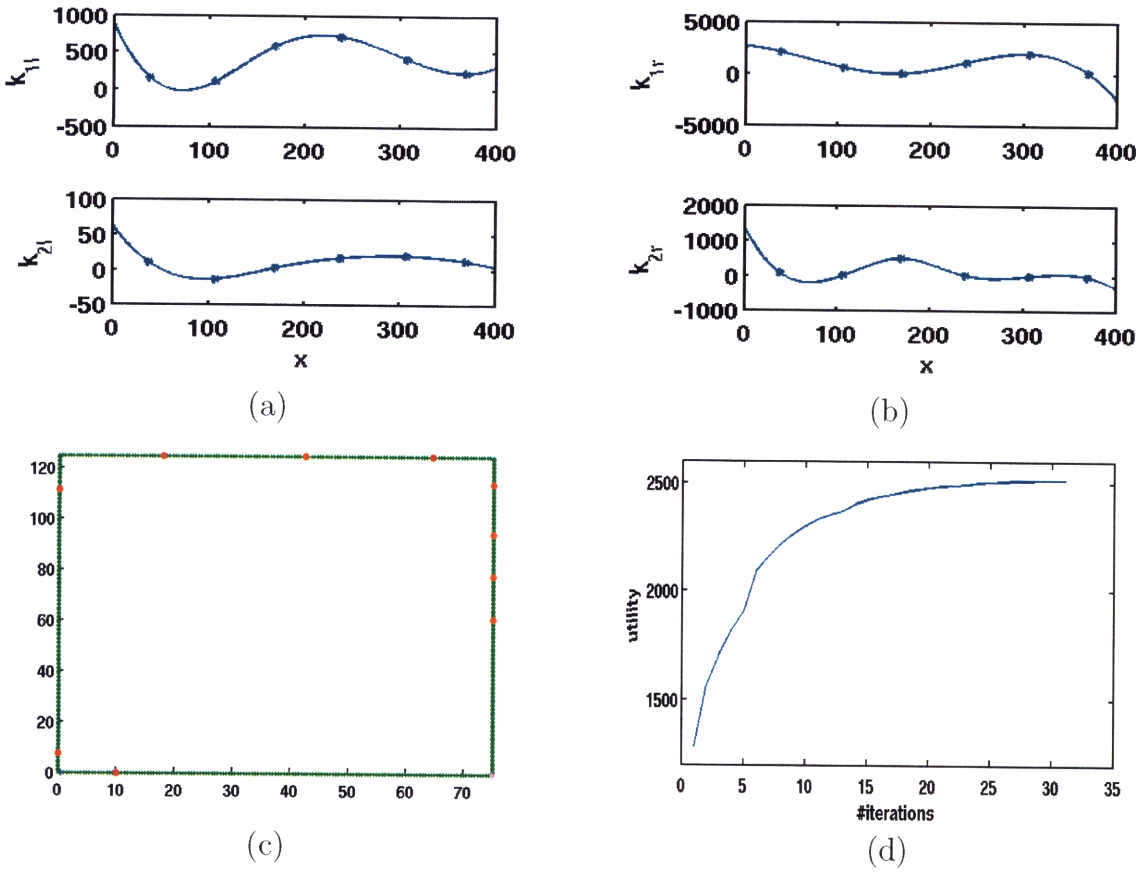

Figure 4-11: Performance of the distributed control law in an outdoor environment.

data at relatively a few spots. Based on these images, we estimated the values of k_1 and k_2 at the sampling points. We interpolate spline functions through these values to obtain the sensing performance function over the domain and Figure 4-11(a) shows this model. We use this model to test our coverage algorithm.

4.4.8 Dynamic Environments

All the experiments we conducted involved manual positioning of the cameras and the test boards and was very time consuming. Unlike the indoor environments, the lighting conditions in outdoor environments change rapidly relative the time scale of collecting all the measurements. However we believe that with some degree of automation, our coverage algorithm can easily implemented in dynamic environments that demand frequent reconfiguration of the sensor positions. In particular, we imagine that the cyclops cameras and the testing board be mounted on mobile platforms that will have localization ability. The images can be processed on board to estimate the sensing performance function at the current location. By means of wireless communication the sensors can implement distributed coverage algorithm. We restricted our work to a simple pixel detection algorithm. It is possible to implement other kinds of algorithms to improve the local sensing performance functions, but our coverage algorithm still holds in this scenario.

Part II

Estimation Sensors

Chapter 5

Frame Theory and Non-uniform Sampling

In this part of the thesis, we deal with the case of estimation sensors. Estimation sensors provide local measurements of a physical quantity such as temperature, pressure, light intensity and chemical concentration. These measurements can be used to estimate the unknown field. The quality of the estimated field depends on the *arrangement* of the sensors. Based on the sampling and the estimation theory, we define and address the coverage problem as the *sensor arrangement problem* in this part of thesis. We ask the question: when and where to place sensors to guarantee that the estimation error is less than the tolerance value. Our approach is to find classes of sensor arrangements that are error tolerant.

The sensor arrangement problem and our approach are closely related to frame theory, and non-uniform sampling theory and function reconstruction. In this chapter, we review relevant results from the literature and in the next chapter, we address the sensor arrangement problem.

Organization: A frame is a generalization of a basis. In Section 5.1, we explain the notion of a basis of a vector space for comparison. In Section 5.2, we introduce frames and their properties, tight frames which form a special subclass of frames and frame algorithms. In Section 5.3, we describe the relationship between a pseudo-inverse of

a frame and linear estimation theory via results proved in [30]. In Section 5.4, we present relevant results from non-uniform sampling theory and show the relationship between frame theory and non-uniform sampling theory via results showed in [3].

5.1 Basis

The notion of a basis of a vector space is fundamental in linear algebra. A basis of a finite-dimensional vector space is defined as follows.

Definition 5.1.1. *Let $\mathcal{V}$ be a finite-dimensional vector space. A sequence $\{\mathbf{e}_k\}_{k=1}^M$ in $\mathcal{V}$ is a* basis *for $\mathcal{V}$ if it satisfied the following two conditions* [10].

1. $\mathcal{V} = span\{\mathbf{e}_k\}_{k=1}^M$ *and*

2. $\{\mathbf{e}_k\}_{k=1}^M$ *is* linearly independent, *i.e., if* $\sum_{k=1}^M c_k\mathbf{e}_k = 0$ *for some scalar* c_k*'s, then* $c_k = 0$ *for all* $k = 1, 2, \cdots, M$.

Thus every element in $\mathcal{V}$ can be represented uniquely as a linear combination of $\mathbf{e}_k$'s. An important class of basis set is an *orthonormal* basis. $\{\mathbf{e}_k\}_{k=1}^M$ is an orthonormal basis if

$$\langle \mathbf{e}_k, \mathbf{e}_j \rangle = \delta_{kj} = \begin{array}{l} 1 \text{ if } k = j \\ 0 \text{ if } k \neq j \end{array}, \tag{5.1}$$

where $\langle \cdot, \cdot \rangle$ stands for the inner product. An element $\mathbf{f} \in \mathcal{V}$ can be represented in terms of the orthonormal basis as

$$\mathbf{f} = \sum_{k=1}^{M} \langle \mathbf{f}, \mathbf{e}_k \rangle \mathbf{e}_k. \tag{5.2}$$

One of the main problems with an orthonormal basis is its lack of flexibility. In analysis, it is often necessary to find an orthonormal basis with desired additional properties. Despite much effort, the problem of finding an orthonormal basis with additional properties is generally difficult [40].

5.2 Frames

A frame is a suitable alternative to an orthonormal basis. The second condition in the definition of a basis is relaxed in frames. In that sense a frame is a basis with additional elements [16], [10]. The notion of frames was first introduced by Duffin and Schaeffer [20] in 1952 in the context of *non-harmonic* Fourier series. Non-harmonic Fourier series involves expansion of periodic functions in complex exponentials of the form $e^{j\lambda_n t}$, where $\lambda_n \neq 2\pi n$. The connection between frames and discretized wavelet functions was first observed in 1985 [16]. In this section we discuss frame fundamentals, *tight frames* which is an important class of frames, and frame algorithms.

5.2.1 Frame Fundamentals

The introduction to frames and the related results presented in this section is adapted from [16] and [30].

Let $\mathcal{H}$ denote a *Hilbert space* with norm $\|\cdot\|$ and inner product $\langle\cdot,\cdot\rangle$.

Definition 5.2.1. [16] *A family of functions $\{\phi_k\}_{k\in J}$ in a Hilbert space $\mathcal{H}$ is called a* frame *if there exists $A > 0$ and $B < \infty$ such that, for all $f \in \mathcal{H}$,*

$$A\|f\|^2 \leq \sum_{k\in J} |\langle f, \phi_k\rangle|^2 \leq B\|f\|^2. \tag{5.3}$$

A and B are referred to as frame bounds.

In this thesis, we will deal with finite dimensional frames in $\mathbb{C}^M$, where $M < \infty$ and $\mathbb{C}$ is the space of complex numbers. Let $\Phi = \{\phi_k\}_{k=1}^N$ be a set of M-dimensional vectors $\phi_k \in \mathbb{C}^M$. Let each ϕ_k be a column vector. Thus, Φ is a *frame* if there exist the frame bounds $A > 0$ and $B < \infty$ such that

$$A\|\mathbf{a}\|^2 \leq \sum_{k=1}^{N} |\langle \mathbf{a}, \phi_k\rangle|^2 \leq B\|\mathbf{a}\|^2, \quad \text{for all } \mathbf{a} \in \mathbb{C}^M. \tag{5.4}$$

In $\mathbb{C}^M$, $\|\cdot\|$ denotes the Euclidean norm and $\langle\cdot,\cdot\rangle$ denotes the usual dot product. The lower bound in Equation (5.4) requires that ϕ_k's span $\mathbb{C}^M$ because otherwise we

will be able to choose a vector in $\mathbb{C}^M$ that is orthogonal to each ϕ_k and this violates the lower-bound inequality in the definition. So a frame will always have $N \geq M$. The ratio $\frac{N}{M}$ is referred to as the *redundancy* of the frame. Note that one can always choose $\sum_{k=1}^{N} \|\phi_k\|^2$ to be the frame upper bound B. Therefore, any finite set of vectors in $\mathbb{C}^M$ that spans $\mathbb{C}^M$ is a frame.

Definition 5.2.2. *A frame is a* uniform *frame if each* $\|\phi_k\| = 1$.

The finite dimensional frame Φ in $\mathbb{C}^M$ can be associated with an operator $\mathbf{F}$ in a matrix form, referred to as a *frame operator*. $\mathbf{F}$ is constructed as,

$$\mathbf{F} = \begin{bmatrix} \phi_1^* \\ \phi_2^* \\ \vdots \\ \phi_N^* \end{bmatrix}. \tag{5.5}$$

Thus $\mathbf{F}$ is an $N \times M$ matrix. It does not matter in what order we stack ϕ_k^*. It is a linear operator because it maps a vector in $\mathbb{C}^M$ to a vector in $\mathbb{C}^N$ as follows:

$$(\mathbf{Fa})_k = \langle \mathbf{a}, \phi_k \rangle, \quad \text{for } k = 1, 2, \cdots, N. \tag{5.6}$$

In terms of the frame operator $\mathbf{F}$, the frame inequalities in 5.4 can be written as

$$\mathbf{a}^* A \mathbf{I}_M \mathbf{a} \leq \mathbf{a}^* \mathbf{F}^* \mathbf{F} \mathbf{a} \leq \mathbf{a}^* B \mathbf{I}_M \mathbf{a}, \quad \text{for all } \mathbf{a} \in \mathbb{C}^M. \tag{5.7}$$

Here $\mathbf{I}_M$ is an identity matrix of size $M \times M$. The above inequality is usually written in the short form as

$$A\mathbf{I}_M \leq \mathbf{F}^* \mathbf{F} \leq B\mathbf{I}_M. \tag{5.8}$$

Frames have an interesting property that is important from the viewpoint of this thesis.

Lemma 5.2.3. *Union of two frames is also a frame.*

Proof. Let Φ and Γ be two frames with the corresponding frame operators $\mathbf{F}$ and $\mathbf{G}$. Let A_1 and B_1 be the frame bounds for frame Φ. Let A_2 and B_2 be the frame bounds for frame Γ. Therefore,

$$A_1\mathbf{I}_M \leq \mathbf{F}^*\mathbf{F} \leq B_1\mathbf{I}_M \qquad \text{and}$$

$$A_2\mathbf{I}_M \leq \mathbf{G}^*\mathbf{G} \leq B_2\mathbf{I}_M.$$

Let Ψ be a frame constructed by union of Φ and Γ. Let $\mathbf{P}$ be the corresponding frame operator obtained as $\mathbf{P} = \begin{bmatrix} F \\ G \end{bmatrix}$. It is easy to verify

$$(A_1 + A_2)\mathbf{I}_M \leq \mathbf{P}^*\mathbf{P} \leq (B_1 + B_2)\mathbf{I}_M.$$

Thus, the union of two frames is also a frame and the frame bounds of the new frame is sum of the frame bounds of the two original frames. □

Note that the redundancy of the frame obtained by the union of two frames is at least 2 [30]. We note an interesting property of the eigenvalues of a frame.

Lemma 5.2.4. *[30] For any frame operator* $\mathbf{F}$ *with the frame bounds* A *and* B*, the eigenvalues of* $\mathbf{F}^*\mathbf{F}$ *lie in the interval* $[A, B]$.

This can be easily observed by considering $\mathbf{a}$ to be an eigenvector of $\mathbf{F}^*\mathbf{F}$ in Equation (5.7). The above lemma implies that $\mathbf{F}^*\mathbf{F}$ is a *positive definite* matrix. Also note that the *condition number* of $\mathbf{F}^*\mathbf{F}$, which is the ratio of the highest and the lowest eigenvalues of $\mathbf{F}^*\mathbf{F}$, is bounded by $\frac{B}{A}$. Because all of its eigenvalues are positive, $\mathbf{F}^*\mathbf{F}$ is invertible. Therefore, the following inequalities hold.

$$B^{-1}\mathbf{I}_M \leq (\mathbf{F}^*\mathbf{F})^{-1} \leq A^{-1}\mathbf{I}_M \tag{5.9}$$

Definition 5.2.5. *For the frame* $\Phi = \{\phi_k\}_{k=1}^N$*, the* dual frame $\tilde{\Phi} = \{\tilde{\phi}_k\}_{k=1}^N$ *is defined as*

$$\tilde{\phi}_k = (\mathbf{F}^*\mathbf{F})^{-1}\phi_k, \qquad \text{for } k = 1, 2, \cdots, N. \tag{5.10}$$

Let $\tilde{\mathbf{F}}$ be the frame operator corresponding to the dual frame $\tilde{\Phi}$. From (5.5),

$$\tilde{\mathbf{F}} = \begin{bmatrix} \tilde{\phi}_1^* \\ \tilde{\phi}_2^* \\ \vdots \\ \tilde{\phi}_N^* \end{bmatrix}. \tag{5.11}$$

Note that $\tilde{\phi}_k = \phi_k^* (\mathbf{F}^*\mathbf{F})^{-1}$. Therefore,

$$\tilde{\mathbf{F}} = \mathbf{F} (\mathbf{F}^*\mathbf{F})^{-1}. \tag{5.12}$$

Furthermore, $\tilde{\mathbf{F}}^*\tilde{\mathbf{F}} = (\mathbf{F}^*\mathbf{F})^{-1}$. Equation (5.9) implies that B^{-1} and A^{-1} are the lower and the upper bounds respectively for the dual frame $\tilde{\Phi}$. We note a useful property of the eigenvalues of a frame.

Lemma 5.2.6. [30] *The sum of the eigenvalues of* $\mathbf{F}^*\mathbf{F}$ *equals the sum of the lengths of the frame vectors. For a uniform frame, this implies that the sum of the eigenvalues is* N.

Proof. The sum of the eigenvalues of $\mathbf{F}^*\mathbf{F}$ is its *trace*. Using the basic properties of the trace and the definition of $\mathbf{F}$ in Equation (5.5),

$$\mathrm{tr}(\mathbf{F}^*\mathbf{F}) = \mathrm{tr}(\mathbf{F}\mathbf{F}^*) = \sum_{k=1}^{N} \phi_k^* \phi_k = \sum_{k=1}^{N} \|\phi_k\|^2.$$

□

5.2.2 Tight Frames

Tight frames constitute an important class of frames. They are of special relevance in this thesis.

Definition 5.2.7. [10] *If the two frame bounds are equal,* $A = B$, *we call the frame a* tight frame.

The definition implies that $\mathbf{F}^*\mathbf{F} = A\mathbf{I}_M = B\mathbf{I}_M$. Note that the frame vectors of a tight frame need not be orthogonal. $\mathbf{F}$ is constructed by stacking row vectors ϕ_k^*. $\mathbf{F}^*\mathbf{F} = A\mathbf{I}_M$ implies that the columns of $\mathbf{F}$ are orthogonal. $\mathbf{F}$ can be thought as made up of the first M columns of an $N \times N$ matrix with orthogonal columns. We note a useful property of the eigenvalues of a tight frame below.

Lemma 5.2.8. *[30] For a tight frame, $\mathbf{F}^*\mathbf{F}$ has eigenvalue A with multiplicity M. If the tight frame is also uniform, $A = \frac{N}{M} = r$.*

Like an orthogonal basis a tight frame allows for weighted linear representation of an unknown vector.

Lemma 5.2.9. [10] *Every element $\mathbf{f} \in \mathbb{C}^M$ can be represented in terms of a tight frame $\Phi = \phi_k{}_{k=1}^N$ as*

$$\mathbf{f} = \frac{1}{A}\sum_{k=1}^{N}\langle \phi_k, \mathbf{f}\rangle \phi_k. \tag{5.13}$$

The above result can be easily verified. Equation (5.13) is similar to Equation (5.2) except the factor $\frac{1}{A}$. However, note that a frame that is tight need not be an orthogonal basis. We present a classic example from [16].

Consider the space $\mathbb{C}^2$. Consider a frame with elements $\phi_1 = \begin{bmatrix} 0 \\ 1 \end{bmatrix}$, $\phi_2 = \begin{bmatrix} -\frac{\sqrt{3}}{2} \\ -\frac{1}{2} \end{bmatrix}$, $\phi_3 = \begin{bmatrix} \frac{\sqrt{3}}{2} \\ -\frac{1}{2} \end{bmatrix}$. Frame operator $\mathbf{F}$ is given by

$$\mathbf{F} = \begin{bmatrix} 0 & 1 \\ -\frac{\sqrt{3}}{2} & -\frac{1}{2} \\ \frac{\sqrt{3}}{2} & -\frac{1}{2} \end{bmatrix}$$

$\mathbf{F}^*\mathbf{F} = \frac{3}{2}\mathbf{I}_2$. But note that ϕ_k's are not orthogonal to each other.

Tight frames have an interesting property that under the geometric transformations such as rigid rotations and reflections of the entire frame, and negations of some of the frame vectors, the new frame is still tight [30]. Consider a tight frame Φ with the frame operator $\mathbf{F}$. The rotation and reflection operations can be represented using

a unitary matrix, say U. The negating of a frame vector can be represented using a scaling factor ± 1. Thus a frame vector ϕ_k gets transformed into

$$\gamma_k = \sigma_k U \phi_k, \qquad \text{for} k = 1, 2, \cdots, N, \tag{5.14}$$

where $\sigma_k = \pm 1$. The new frame operator $\mathbf{G}$ can be represented as

$$\mathbf{G} = \mathbf{\Sigma F U}^*, \qquad \text{where} \Sigma = \text{diag}(\sigma_1, \sigma_2, \cdots, \sigma_N). \tag{5.15}$$

$\mathbf{U}^*\mathbf{U} = \mathbf{I}_M$, $\mathbf{F}^*\mathbf{F} = A\mathbf{I}_M$ and $\mathbf{\Sigma}^*\mathbf{\Sigma} = \mathbf{I}_N$. Now it is easy to verify that

$$\mathbf{G}^*\mathbf{G} = A\mathbf{I}_M. \tag{5.16}$$

A uniform tight frame is bundled with all possible frames obtained through these transformations to form an *equivalence class* in [30]. We refer interested readers to [30] for further properties of the equivalence class.

Lemma 5.2.10. *Union of two tight frames is also a tight frame.*

Proof. The proof is similar to the proof of Lemma 5.2.3. □

The above lemma plays an important role in the next chapter of the thesis. Next we bring this subsection to a closure by stating an important result from [30]. The result is about tightness of randomly chosen frames.

Theorem 5.2.11. [31],[30] *Let $\{\Phi_N\}_{N=M}^{\infty}$ be a sequence of frames in $\mathbb{R}^M$ such that Φ_N is generated by choosing N vectors independently and uniformly randomly on the unit sphere in $\mathbb{R}^M$. Let $\mathbf{F}_N$ be the frame operator corresponding to Φ_N. Then in the mean squared sense,*

$$\frac{1}{N}\mathbf{F}_N^*\mathbf{F}_N \to \frac{1}{M}\mathbf{I}_M \quad \text{elementwise as } N \to \infty.$$

We refer interested readers to the original papers for the proof.

5.2.3 Frame Algorithms

One of the main virtues of frames is that they allow for *overcompleteness*. Many frames have a property that even after deleting a few of their elements, a frame still remains a frame. This is pivotal in communications. In communication applications, an unknown vector can be *encoded* using a frame and transmitted. Encoding simply involves projecting the vector on each element in the frame. The projection coefficients are then transmitted through channels which are noisy and may cause erasures of some of the coefficients. Since frames allow for redundancy, the unknown vector can still be recovered using the remaining coefficients using the corresponding frame elements. This brings us to the question of how to recover a vector from frame projections. One approach is to find a *pseudo-inverse* of the frame operator which we will discuss in the next subsection. This could be computationally expensive for large matrix dimensions. Researchers have come up with iterative numerical algorithms that are computationally effective [10]. One such classical algorithm is the *frame algorithm.*

Theorem 5.2.12. [10] *Let $\Phi = \{\phi_k\}_{k=1}^N$ be a frame in a finite-dimensional space $\mathcal{V}$ with frame bounds A and B. Given $\mathbf{a} \in \mathcal{V}$, define the sequence $\{\gamma_k\}_{k=0}^\infty$ in $\mathcal{V}$ as*

$$\gamma_0 = 0, \quad \gamma_k = \gamma_{k-1} + \frac{2}{A+B}\mathcal{S}\left(\mathbf{a} - \gamma_k\right), \tag{5.17}$$

where operator $\mathcal{S}$ is given by $\mathcal{S}\mathbf{g} = \sum_{j=1}^N \langle \phi_j, \mathbf{g}\rangle \phi_j$. Then

$$\|\mathbf{a} - \gamma_k\| \leq \left(\frac{B-A}{B+A}\right)^k \|\mathbf{a}\|.$$

We refer interested readers [10] for a proof of the above lemma. The ratio $\left(\frac{B-A}{B+A}\right) < 1$ and as $k \to \infty$, $\gamma_k \to \mathbf{a}$. Note that the algorithm depends on the knowledge of the frame bounds. The rate of convergence, $\left(\frac{B-A}{B+A}\right)$ also depends on the frame bounds. If B is much larger than A, then the convergence rate might be slower [10]. Gröchenig proposed two new methods to obtain faster convergence rates, *Chebyshev method* and *conjugate gradient method.* The Chebyshev method requires knowledge of the frame

bounds but guarantees faster convergence rate when B is much larger than A, whereas the conjugate gradient method works without the knowledge of the frame bounds. We refer interested readers to [10] for the details.

5.3 Pseudo-inverse and Linear Estimation

In the previous section we briefly discussed the iterative numerical procedures to recover an unknown vector $\mathbf{a}$ from its projection using a frame. Another approach is to use *pseudo-inverse*. This also known as *Moore-Penrose generalized inverse* [30], [10]. Let $\mathbf{F}$ be a frame operator corresponding to frame $\Phi = \{\phi_k\}_{k=1}^{N}$ in an M-dimensional space $\mathcal{V}$. The pseudo-inverse of $\mathbf{F}$ is given by

$$\mathbf{F}^{\dagger} = (\mathbf{F}^{*}\mathbf{F})^{-1}\mathbf{F}. \tag{5.18}$$

The frame condition ensures that the inverse of $\mathbf{F}^{*}\mathbf{F}$ exists. We can easily verify that $\mathbf{F}^{\dagger}\mathbf{F} = \mathbf{I}_M$. Thus, $\mathbf{F}^{\dagger}(\mathbf{Fa}) = \mathbf{a}$. However the pseudo-inverse is not the only possible inverse of the frame operator. We refer readers to [30] on how to find an inverse matrix using the singular value decomposition. But the pseudo-inverse has a remarkable property over the other inverses. It eliminates the contribution from the errors that are orthogonal to the *range* of the frame operator. Let $\mathbf{a}$ be a vector that is encoded using frame operator $\mathbf{F}$ to $\mathbf{f} = \mathbf{Fa}$. In many applications, $\mathbf{f}$ is not known precisely (*e.g.*, because of quantization, modeling errors, noise) and instead $\hat{\mathbf{f}} = \mathbf{f} + \mathbf{e}$ is known. $\mathbf{e}$ denotes the error. Let $\hat{\mathbf{a}}$ denote the vector that is recovered using noisy projections. $\hat{\mathbf{a}} = \mathbf{F}^{\dagger}\hat{\mathbf{f}}$. Instead of using the pseudo-inverse we can also use any other inverse. However the pseudo-inverse eliminates any influence of $\mathbf{e}$ that is orthogonal to the range of $\mathbf{F}$. $\mathbf{F}^{\dagger}\hat{\mathbf{f}}$ is the orthogonal projection of $\hat{\mathbf{f}}$ onto the range of $\mathbf{F}$ [30]. In that sense the pseudo-inverse is the linear reconstruction method that minimizes the least squared error, $\|\hat{\mathbf{f}} - \mathbf{f}\|^2$ [29].

In the absence of any knowledge of the errors in the projection coefficients, the pseudo-inverse is the *best* one can use in the linear estimation method. It turns out

that this is also true when the errors are stochastic in nature with zero mean and the covariance matrix being a scaled identity matrix. Let $\mathbf{e}$ be such that $\mathrm{E}[\mathbf{e}] = \mathbf{0}$ and $\mathbf{Q} = \mathrm{E}[\mathbf{e}^T\mathbf{e}] = \sigma^2\mathbf{I}_N$. Again, let $\mathbf{a}$ be the vector encoded using the frame operator $\mathbf{F}$. Let $\mathbf{f} = \mathbf{Fa}$. Let $\hat{\mathbf{f}} = \mathbf{f} + \mathbf{e}$ be the noisy measurement. Let $\hat{\mathbf{a}}$ be the decoded vector using the pseudo-inverse of the frame operator and the noisy measurement; $\hat{\mathbf{a}} = \mathbf{F}^\dagger\hat{\mathbf{f}}$. Based on the linear estimation theory [54], [48], the pseudo-inverse yields the solutions that minimizes the *mean squared error* (MSE) over all possible linear reconstruction procedures. We will discuss this in much more detail in the next chapter. The mean squared error for the pseudo-inverse based solution is given by,

$$\mathrm{MSE} = \frac{1}{M}\|\hat{\mathbf{a}} - \mathbf{a}\|^2 = \frac{\sigma^2}{M}\mathrm{trace}\{(\mathbf{F}^*\mathbf{F})^{-1}\} = \frac{\sigma^2}{M}\sum_{k=1}^{M}\frac{1}{\lambda_k}, \tag{5.19}$$

where λ_k's denote the eigenvalues of $\mathbf{F}^*\mathbf{F}$. Consider a set of all uniform frames, each of size N. Recall that for each such uniform frame, each diagonal element of $\mathbf{F}^*\mathbf{F}$ is $\frac{N}{M}$ and the trace value is N. Thus the sum of the eigenvalues is fixed over all such frames. The above characterization of MSE in terms of the inverse of the eigenvalues of $\mathbf{F}^*\mathbf{F}$ leads to the following theorem.

Theorem 5.3.1. *Over all uniform frames, each of size N, the MSE is minimum if and only if the frame is tight.*

We refer interested readers to [30] for further details. The main idea behind the proof is that the sum of the eigenvalues of $\mathbf{F}^*\mathbf{F}$ is fixed for all the uniform frames of size N. The sum of the inverse eigenvalues is minimized if all the eigenvalues are equal. Based on Lemma 5.2.8, this is true if and only if the frame is tight.

Based on Lemma 5.2.4, each eigenvalue lies within the interval $[A, B]$. Hence, for each k, $B^{-1} \leq \frac{1}{\lambda_k} \leq A^{-1}$. The consequences of this are summarized in the following theorem.

Theorem 5.3.2. *[30] For the pseudo-inverse based linear reconstruction with error $\mathbf{e}$ satisfying $\mathrm{E}[\mathbf{e}] = \mathbf{0}$ and $\mathbf{Q} = \mathrm{E}[\mathbf{e}^T\mathbf{e}] = \sigma^2\mathbf{I}_N$, the mean squared error is bounded above and below as*

$$B^{-1}\sigma^2 \;\leq\; \mathrm{MSE} \;\leq\; A^{-1}\sigma^2. \tag{5.20}$$

For a uniform frame, using Theorem 5.3.1,

$$\frac{M\sigma^2}{N} \leq \text{MSE} \leq A^{-1}\sigma^2. \tag{5.21}$$

For a uniform tight frame,

$$\text{MSE} = \frac{M}{N}\sigma^2 = \frac{\sigma^2}{r}. \tag{5.22}$$

The above two theorems have important consequences in the next chapter.

5.4 Non-Uniform Sampling

In this section, we discuss relevant work on function reconstruction from non-uniform samples and its connection with frame theory. The material presented here is inspired from [3] and [37]. Our approach to address the sensor arrangement problem involves finding a set of sensor arrangements, which guarantees that the estimation error for each arrangement is less than certain error tolerance. Such arrangements are often non-uniform. Naturally, the sensor arrangement problem and our approach have a connection with function reconstruction from non-uniform samples.

In their survey-cum-research paper, Aldroubi and Gröchenig address the *sampling problem* which deals with reconstructing an unknown function f from its discrete samples at various locations. Clearly, the problem is not well-defined as given the function values at discrete points, there are infinite possibilities for the choice of such function. Therefore, it is assumed that the unknown function f belongs to a certain class of functions. The first goal of the sampling problem is to find a set of conditions on the sampling set, under which it is possible to reconstruct the function *uniquely* and *stably*. The second goal of the sampling problem is to develop explicit reconstruction schemes. Aldroubi and Gröchenig deal with the sampling problem for a special class of functions known as *shift-invariant spaces*. They present a unified framework for uniform and non-uniform sampling and reconstruction of function in shift-invariant spaces by bringing together other areas such as wavelet theory, frame

theory, *reproducing kernel Hilbert spaces*, approximation theory, *amalgam spaces* and sampling. A detailed discussion is beyond the scope of this thesis. We present a subset of results in this paper modified in the context of our work.

Consider M orthonormal basis functions $\phi_1(x), \phi_2(x), \cdots, \phi_M(x)$ in 1D, where each $\phi_i : \mathbb{D} \rightarrow \mathbb{C}$ and $\mathbb{D}$ is the sampling domain in 1D. We consider the sampling problem over the space of functions that are obtained by a linear combination of these basis functions. We denote this space of functions by $\mathcal{F}$. Thus, an unknown function $f(x)$ can be represented as:

$$f(x) = \sum_{j=1}^{M} a_j \phi_j(x). \tag{5.23}$$

The sampling problem deals with the question of reconstructing $f(x)$ using N discrete samples taken at $x_1, x_2, \cdots, x_N$, where $N \geq M$. Given the set of basis functions, the problem really concerns finding N unknown coefficients, $a_1, a_2, \cdots, a_M$. This problem is actually related to solving a set of linear equations and can be represented in the matrix notation as follows:

$$\begin{bmatrix} f(x_1) \\ f(x_2) \\ \vdots \\ f(x_N) \end{bmatrix} = \begin{bmatrix} \phi_1(x_1) & \phi_2(x_1) & \cdots & \phi_M(x_1) \\ \phi_1(x_2) & \phi_2(x_2) & \cdots & \phi_M(x_2) \\ \vdots & \vdots & \cdots & \vdots \\ \phi_1(x_1) & \phi_2(x_1) & \cdots & \phi_M(x_1) \end{bmatrix} \begin{bmatrix} a_1 \\ a_2 \\ \vdots \\ a_M \end{bmatrix} \quad \text{and} \tag{5.24}$$

$$\mathbf{f} = \mathbf{V}\mathbf{a}. \tag{5.25}$$

In the above compact matrix equation, $\mathbf{f}$ denote the vector of samples values. $\mathbf{a}$ denotes the vector of unknown coefficients. $\mathbf{V}$ is the rectangular matrix consisting of the values of the basis functions at the sample points. In the literature, $\mathbf{V}$ is known as the Vandermonde matrix [37]. Note that it is a rectangular matrix of size $N \times M$. In principle, $f(x)$ can be retrieved using M samples alone. However, in reality, due to finite precision the elements of the Vandermonde matrix as well as the vector of sample values are truncated and we can retrieve $f(x)$ only approximately. This

leads the question of *stable* reconstruction of the function. Aldroubi and Gröchenig address this question in their paper for the space of shift-invariant functions with several generalizations [3]. We discuss the implications of their results for the above class of functions.

Definition 5.4.1. *A set of sampling* $x_1, x_2, \cdots, x_N$ *is* stable *for the space of functions* $\mathcal{F}$ *as defined above, if there exist positive constants* c *and* C *independent of* f *such that the following inequalities hold.*

$$c\|f\|^2 \leq \sum_{i=1}^{N} |f(\mathbf{x}_i)|^2 \leq C\|f\|^2 \tag{5.26}$$

$\|\cdot\|$ *denotes the norm of the function.*

Note that in the original paper [3], the above definition is generalized to *weighted norms*. For the specific case of functions from class $\mathcal{F}$ we consider here, the above inequalities for a stable set of sampling get translated as follows:

$$c\|\mathbf{a}\|^2 \leq \mathbf{a}^*\mathbf{V}^*\mathbf{V}\mathbf{a} \leq C\|\mathbf{a}\|^2 \text{ forevery } \mathbf{a}. \tag{5.27}$$

The above inequalities remind us of the inequalities involving frame bounds c and C as in Equation 5.7. The Vandermonde matrix $\mathbf{V}$ can be seen as a frame operator. We sum up the equivalence of above definition and frames in the following theorem.

Theorem 5.4.2. *The following statements are equivalent.*

1. $x_1, x_2, \cdots, x_N$ *is a stable set of sampling for the space of functions* $\mathcal{F}$ *formed by the linear combinations of the* M *orthonormal basis functions* $\phi_1(x), \phi_2(x), \cdots, \phi_M(x)$ *as discussed above.* $N \geq M$.

2. *There exist positive constants* c *and* C *such that the following inequalities involving these constants, and the Vandermonde matrix* $\mathbf{V}$ *(Equations 5.24 and 5.25) are satisfied for every* $\mathbf{a}$.

$$c\|\mathbf{a}\|^2 \leq \mathbf{a}^*\mathbf{V}^*\mathbf{V}\mathbf{a} \leq C\|\mathbf{a}\|^2 \text{ forevery } \mathbf{a}. \tag{5.28}$$

3. *The Vandermonde matrix* $\mathbf{V}$ *is a frame operator and thus, the columns of* $\mathbf{V}^*$ *form a frame with frame constants* c *and* C.

Again, note that in [3] Aldroubi and Gröchenig show the equivalence of different terminologies such as reproducing kernel Hilbert space, frames and stable sampling sets in non-uniform sampling for a much more generalized classes of functions. We refer interested readers to the original paper [3]. We merely state the specialized result since we will show another equivalence to a terminology in the context of the sensor arrangement problem in the next chapter. The implication of the above result is that the frame algorithms we discussed earlier in Subsection 5.2.3 apply in this case as well. Thus iterative numerical algorithms are readily available for the reconstruction of function from non-uniform stable sampling set. Similarly, the solution based on the pseudo-inverse of the frame operator, the Vandermonde matrix in this case, can also be used.

Chapter 6

Error Tolerant Arrangements of Estimation Sensors

In this chapter, we define and address the *Sensor Arrangement Problem.* As we have seen earlier, it is a type of coverage problem that we have defined for estimation sensors. Estimation sensors provide local measurements of a scalar field such as temperature, pressure, or chemical concentrations, which can be used to estimate the field. The quality of the estimation depends on geometric arrangements of sensors in space and time. This motivates the sensor arrangement problem. We ask the question of when and where to arrange sensors in order to guarantee estimation error less than certain tolerance. The problem of characterizing the space of all such feasible arrangements is hard. Therefore, our approach is to define classes of sensor arrangements and find conditions under which they are error tolerant. In this chapter, we consider fields that are modeled as trigonometric polynomials. We discuss various error tolerant arrangements for these fields. We first motivate and define the sensor arrangement problem.

6.1 Sensor Arrangement Problem

Let us review some basic notions that we already defined in Chapter 2. Estimation sensors provide measurements of physical quantities such as temperature, humidity,

pressure, or chemical concentrations. These quantities are governed by underlying physical phenomena. They can be represented as spatio-temporal *fields* or *signals.* The central question in coordinated sensing is to estimate an unknown field from the measurements before making any inferences. We refer to the field value at a particular space-time coordinate as a *point estimate* or a *point sample* or simply a *sample.* We contrast point sampling sensors with sensors that provide an aggregate measure over the local region, which we do not consider in this thesis. Sample values that sensors provide are approximate due to, among other causes, quantization effects and sensor noise. In this setting, the quality of the estimated field depends on the ensemble of the sample values that are queried. These values depend on the arrangements of the space-time coordinates at which the samples are taken. We refer to this geometric arrangement as a *sensor arrangement.* The quality of the estimated field is a function of the sensor arrangement. This observation motivates the definition of the *Sensor Arrangement Problem* – when and where to take samples in order to guarantee *good* estimate of an unknown field.

The sensor arrangement problem is an inverse problem. The forward problem of estimating a field given the noisy sample values for a given sensor arrangement is widely addressed in many areas of science and engineering. However the inverse problem, *i.e.*, understanding where to take samples, is seldom addressed. We formulate the sensor arrangement problem based on the linear estimation framework. Here is a summary of our approach.

We assume that an unknown field to be estimated is represented as a linear combination of a set of basis functions. We further assume that the sample values which the estimation sensors provide involve random additive noise. In this setting, according to linear estimation theory, [54, 48], the estimation error is a function of the sensor arrangement. Any solution to the sensor arrangement problem belongs to the space of sensor arrangements each of which provides a *good* estimate of the field, *i.e.*, guarantees that the estimation error is less than the error tolerance. However characterizing this space is difficult. Instead, our approach consists of considering different classes of sensor arrangements such that for each class, any of its sensor arrangement

ensures that the estimation error is always less than the error tolerance. We refer to these classes as Error Tolerant Arrangement Classes or ETAC's. We say that each instance of an arrangement from an ETAC is error tolerant. ETAC's are suitably characterized feasible solution spaces to the sensor arrangement problem. They are also convenient when we study mobile sensor networks. We will briefly discuss this issue in the next chapter.

We will now provide formal description of the problem and discuss our approach.

6.1.1 Field Model

Modeling an unknown process (a spatio-temporal field in our case) is at the heart of many engineering problems. There are a number of ways in which an unknown spatio-temporal field can be modeled. Some examples include specifying differential equations, linear representation in terms of a basis functions, Reproducing Kernel Hilbert Spaces (RKHS) in machine learning and stochastic modeling. In this thesis, we represent the field as a linear combination of a finite set of basis functions known *a priori*. This approach is commonly used in the area of signal processing and machine learning, and it is closely linked with the field of *model-order reduction*. The underlying idea is that analytically, any process can be represented as a linear combination of a set of infinitely many basis functions of a particular type. In practice, only finitely many of these functions play a dominant role and need to be used in modeling. This allows for tractable computations.

Let $f(\mathbf{x}) : Q \rightarrow \mathbb{R}$ indicate an unknown spatio-temporal scalar field on a bounded domain $\mathcal{Q}$. Let $Q \subset \mathbb{R}^d$. Let $\Phi = \{\phi_1(\mathbf{x}), \phi_2(\mathbf{x}), \cdots\}$ be a set of linearly independent basis functions where $\phi_k(\mathbf{x}) : Q \rightarrow \mathbb{C}$. Any set of basis functions can be converted into a set of *orthonormal* basis functions using the Gram-Schmidt procedure [54]. Therefore without loss of generality we assume that ϕ_k's form a *complete* set of *orthonormal* basis functions.

Definition 6.1.1. *A set of functions* $\{\phi_1, \phi_2, \cdots, \}$ *is an* orthonormal basis *if*

$$\int_Q \phi_k(\mathbf{x})\phi_l(\mathbf{x})d\mathbf{x} = \delta_{kl}, \quad k, l = 1, 2, \cdots \tag{6.1}$$

where δ_{kl} *indicates the Kronecker Delta function.*

As a consequence of these assumptions, $f(\mathbf{x})$ can be uniquely represented as

$$f(\mathbf{x}) = \sum_{k=1}^{\infty} a_k \phi_k(\mathbf{x}) \tag{6.2}$$

where $a_k's \in \mathbb{C}$ form a set of unknown coefficients. The problem of estimating $f(\mathbf{x})$ reduces to determining possibly infinitely many a_k's, which is computationally intractable. For reasons we have listed before it is practical to limit the analysis to a finite set of basis functions that have a significant contribution. This leads to only an approximate representation of the field. In this work, we assume that the field is represented as

$$\tilde{f}(\mathbf{x}) = \sum_{k=1}^{M} a_k \phi_k(\mathbf{x}). \tag{6.3}$$

Note that $\tilde{f}$ is only an approximation of the real field f. In fact, $\tilde{f}$ is the orthogonal projection of f on to the space spanned by the set of M basis functions, $\{\phi_1(\mathbf{x}), \phi_2(\mathbf{x}), \cdots \phi_2(\mathbf{x})\}$. We assume that ϕ_k's are renumbered so that without loss of generality, *important* M basis functions are considered. The approximation error in the field representation is given by

$$\zeta(\mathbf{x}) = f(\mathbf{x}) - \tilde{f}(\mathbf{x}) = \sum_{k=M+1}^{\infty} a_k \phi_k(\mathbf{x}). \tag{6.4}$$

The L_2 norm of the error over the entire domain is given by

$$\|f - \tilde{f}\|^2 = \sum_{k=M+1}^{\infty} |a_k|^2. \tag{6.5}$$

The above equation indicates that more the number of basis functions incorporated

in the field representation, smaller the norm of the error. But at the same time a greater number of basis functions makes computations more expensive. This leads to a trade-off between accuracy and computation time. In sensing, a larger number of basis functions also demands more samples, which is also expensive.

In the above representation, we assume that ϕ_k's are known *a priori*. The field is determined by unknown a_k's. We assume that a_k's constitute a set of M unknown but *fixed* parameters of the field. There is no *prior* knowledge about them and they can be completely arbitrary. In statistical signal processing, a_k's are assumed to have some known probabilistic *prior*. We would like to emphasize that in this situation also it is possible to proceed with our framework with relevant modifications.

6.1.2 Measurement Model and Matrix Representations

Each sensor takes a sample value at a particular location at any given time. These measurements have several sources of error of which two important ones are quantization and sensor noise. These are particularly important in inexpensive sensors and are hard to quantify. There are two models popular in literature to model the quantization errors for sample values placed at uniform intervals [30].

1. Additive White Gaussian Noise (AWGN): Quantization error at any location is a zero-mean Gaussian random variable with constant variance σ^2.

2. Uniformly random noise: Quantization error at any location is a zero-mean uniformly distributed random variable over interval $[-\frac{\delta}{2}, \frac{\delta}{2}]$. Thus it has variance value equal to $\frac{\delta^2}{12}$.

In addition to quantization effects there could be noise in the measurement due to thermal or radiation effects. We use an additive noise model to capture the effects of both the types of errors.

We assume that measurement $y(\mathbf{x})$ has the following form.

$$y(\mathbf{x}) = f(\mathbf{x}) + \eta(\mathbf{x}) \tag{6.6}$$

where $\eta(\mathbf{x})$ denotes noise. We refer to $\mathbf{x}$ as a *sensor location* or *sampling location.* For the moment we assume that location errors are minimal. We measure field values at N different sampling locations, where $N \geq M$. Let y_i denote the field value at locations $\mathbf{x}_i$, where $i = 1, 2, \cdots, n$. Thus, we have N data pairs $(y_i, \mathbf{x}_i)$. Recall that we used only an approximate model $\tilde{f}$ of f. Thus,

$$y(\mathbf{x}) = \tilde{f}(\mathbf{x}) + \zeta(\mathbf{x}) + \eta(\mathbf{x}) \tag{6.7}$$

where $\zeta(\mathbf{x})$ is the source of modeling error. We combine two errors into $\varepsilon(\mathbf{x}) = \zeta(\mathbf{x}) + \eta(\mathbf{x})$. This leads to the following model.

$$y(\mathbf{x}) = \tilde{f}(\mathbf{x}) + \varepsilon(\mathbf{x}) \tag{6.8}$$

Under these settings, the problem of estimating the unknown field is now reduced to estimating a_k's as a function of N data pairs $(y_i, \mathbf{x}_i)$. We use the following notation:

$$\mathbf{y} = \begin{pmatrix} y_1 \\ y_2 \\ \vdots \\ y_N \end{pmatrix}, \quad \mathbf{e} = \begin{pmatrix} \varepsilon(\mathbf{x}_1) \\ \varepsilon(\mathbf{x}_2) \\ \vdots \\ \varepsilon(\mathbf{x}_N) \end{pmatrix}, \quad \mathbf{z}_k = \begin{pmatrix} \phi_k(\mathbf{x}_1) \\ \phi_k(\mathbf{x}_2) \\ \vdots \\ \phi_k(\mathbf{x}_N) \end{pmatrix},$$

$$\mathbf{v}(\mathbf{x}) = \begin{pmatrix} \phi_1(\mathbf{x}) \\ \phi_2(\mathbf{x}) \\ \vdots \\ \phi_M(\mathbf{x}) \end{pmatrix}, \quad \mathbf{a} = \begin{pmatrix} a_1 \\ a_2 \\ \vdots \\ a_M \end{pmatrix},$$

$$\mathbf{V} = \begin{pmatrix} \mathbf{v}^{\mathbf{T}}(\mathbf{x}_1) \\ \mathbf{v}^{\mathbf{T}}(\mathbf{x}_2) \\ \vdots \\ \mathbf{v}^{\mathbf{T}}(\mathbf{x}_N) \end{pmatrix} = \begin{pmatrix} \mathbf{z}_1 & \mathbf{z}_2 & \cdots & \mathbf{z}_M \end{pmatrix}.$$

Further, let $X = \{\mathbf{x}_1, \mathbf{x}_2, \cdots, \mathbf{x}_n\}$ be the set of N sampling locations. We refer to X as a *sensor arrangement.* $\mathbf{y}$ is referred to as an *observation vector* and $\mathbf{V}$ as an *observation matrix.* Using the above notation, we can express $\tilde{f}(\mathbf{x})$ and the

measurement data as:

$$\tilde{f}(\mathbf{x}) = \mathbf{v}^T(\mathbf{x}) \cdot \mathbf{a} \tag{6.9}$$

$$\mathbf{y} = \mathbf{V}\mathbf{a} + \mathbf{e} \tag{6.10}$$

We assume that the noise vector $\mathbf{e}$ has zero mean, and its covariance matrix $\mathbf{Q} = \mathrm{E}[\mathbf{e}^T\mathbf{e}]$ is known and is positive definite.

6.1.3 Linear Reconstruction

Given the setting in (6.10), the problem of finding a *good* estimate $\hat{\mathbf{a}}$ of $\mathbf{a}$ has been studied extensively in the literature on linear estimation [54],[48]. A variety of error metrics that capture the difference between $\hat{\mathbf{a}}$ and $\mathbf{a}$ and the estimators that minimize these metrics have been discussed. In this paper, we consider the *minimum variance unbiased estimator* (MVUE). MVUE is based on zero bias, *i.e.*, $\mathrm{E}[\hat{\mathbf{a}} - \mathbf{a}] = 0$, and minimizes the Mean Squared Error (MSE).

$$\mathrm{MSE} = \frac{1}{M}\mathrm{E}\left[\|\hat{\mathbf{a}} - \mathbf{a}\|^2\right] = \sum_{k=1}^{m} \mathrm{E}\left[(\hat{a}_k - a_k)^2\right] \tag{6.11}$$

According to the Gauss-Markov theorem [54],[48], the optimal estimate $\hat{\mathbf{a}}$ is given by:

$$\hat{\mathbf{a}} = (\mathbf{V}^*\mathbf{Q}^{-1}\mathbf{V})^{-1}\mathbf{V}^*\mathbf{Q}^{-1}\mathbf{y} \tag{6.12}$$

and the corresponding MSE is given by:

$$\mathrm{MSE} = \frac{1}{M}\mathrm{E}\left[(\hat{\mathbf{a}} - \mathbf{a})(\hat{\mathbf{a}} - \mathbf{a})^T\right] = \frac{1}{M}(\mathbf{V}^*\mathbf{Q}^{-1}\mathbf{V})^{-1} \tag{6.13}$$

Here $\mathbf{V}^*$ denotes the transpose of the complex conjugate of $\mathbf{V}$. Thus, the value of the minimum MSE is given by:

$$\min \frac{1}{M}\mathrm{E}\left[\|\hat{\mathbf{a}} - \mathbf{a}\|^2\right] = \frac{1}{M}\mathrm{trace}(\mathbf{V}^*\mathbf{Q}^{-1}\mathbf{V})^{-1} \tag{6.14}$$

Given X and $\mathbf{y}$ in this setting, the expression in Equation (6.14) is the minimum

MSE one can achieve [48].

6.1.4 Sensor Arrangement Problem

The error covariance and the optimal MSE corresponding to the MVUE as in (6.13) and (6.14) are functions of the sensor arrangement X alone and are independent of the observation vector. Through the rest of the chapter, we denote the MSE corresponding to the MVUE as $\mathrm{Err}(X)$ to capture its dependence on the sensor arrangement X. Thus,

$$\mathrm{Err}(X) = \frac{1}{M}\mathrm{trace}(\mathbf{V}^*\mathbf{Q}^{-1}\mathbf{V})^{-1} \tag{6.15}$$

We refer to $\mathrm{Err}(X)$ as the *error metric*. We say that the field estimate $\hat{\mathbf{a}}$ is *good* if the error metric $\mathrm{Err}(X)$ is less than a certain error tolerance value.

Definition 6.1.2. *We formally define the* sensor arrangement problem *as follows:*

$$\text{Find } X \text{ s.t. } \mathrm{Err}(X) \leq \Theta \tag{6.16}$$

where Θ denotes a certain tolerance value and we refer to it as error tolerance.

Thus, the sensor arrangement problem involves finding a sensor arrangement that guarantees that the error metric is less than the error tolerance. Such an arrangement is referred to as an *error tolerant arrangement* with respect to the given error tolerance. Note that the solution to the sensor arrangement problem need not be unique. It is also possible to define the optimal sensor arrangement problem as finding the sensor arrangement that yields the optimal value of the error metric for a given number of samples. The sensor arrangement problem can be defined in a similar way for other settings that involve different types of fields, measurement models and the corresponding estimators.

6.1.5 Relevance to non-uniform sampling and frame theory

In Chapter 5, we discussed how a *set of sampling* is related to a *frame*. In this subsection, we show how the notion of an error tolerant arrangement is equivalent to

these two notions in one special case when the noise covariance $\mathbf{Q}$ is equal to $\sigma^2\mathbf{I}$.

Theorem 6.1.3. *The following three statements are equivalent.*

1. $X = \{\mathbf{x}_1, \mathbf{x}_2, \cdots, \mathbf{x}_n\}$ *is a set of sampling with lower bound* A *and upper bound* B.

2. $\Phi = \{\mathbf{v}(\mathbf{x}_1), \mathbf{v}(\mathbf{x}_2), \cdots, \mathbf{v}(\mathbf{x}_N)\}$ *is a frame with lower bound* A *and upper bound* B.

3. *If the noise covariance* $\mathbf{Q} = \sigma^2\mathbf{I}$, *then* X *is an error tolerant arrangement with respect to error tolerance* $\frac{\sigma^2}{A}$.

Proof. The equivalence of the first two statements was already shown in Theorem 5.4.2. If $\mathbf{Q} = \sigma^2\mathbf{I}$, then $\mathrm{Err}(X) = \mathrm{MSE} = \frac{\sigma^2}{M}\mathrm{trace}(\mathbf{V}^*\mathbf{V})^{-1}$. In Chapter 5, in Theorem 5.3.2 [30], we showed that the MSE can be bounded in terms of the frame bounds as

$$B^{-1}\sigma^2 \;\leq\; \mathrm{MSE} \;\leq\; A^{-1}\sigma^2. \tag{6.17}$$

Thus, $\mathrm{Err}(X)$ is guaranteed to be bounded above by $\frac{\sigma^2}{A}$. Hence X is an error tolerant arrangement with respect to error tolerance $\frac{\sigma^2}{A}$. □

Thus, the frame bounds A and B translate into the following bounds on the error metric for the special case of $\mathbf{Q} = \sigma^2\mathbf{I}$.

$$\frac{\sigma^2}{B} \leq \mathrm{Err}(X) \leq \frac{\sigma^2}{A}. \tag{6.18}$$

A relatively loose lower bound (A) of a frame only guarantees a higher error tolerance value for the corresponding error tolerant arrangement. In the perspective of frame theory described in Chapter 5, weak frame bounds are sufficient because iterative frame algorithms exist to recover an unknown vector from frame projections at relatively quick convergence rates even for weak bounds. However from the perspective of the sensor arrangement problem, better knowledge of the frame bound

will guarantee an arrangement with lower error tolerance. In other words, our application demands tighter bounds than are necessary in the areas where frame theory is typically invoked.

6.2 Our Approach: Error Tolerant Arrangement Classes (ETAC's)

Suppose $S(\Theta)$ denotes the set of all feasible solutions to the sensor arrangement problem in (6.16). Ideally we would like to characterize the space $S(\Theta)$, which would allow us to formulate an optimization problem over the space $S(\Theta)$. For instance, in case of intentionally mobile sensors, we can imagine a motion planning problem that involves *touring* sampling locations corresponding to a sensor arrangement in $S(\Theta)$ such that the energy spent in motion is minimal. On the other hand, in the incidental motion of sensors, we can pose a problem to verify whether a particular mobility model guarantees motion paths that conform with a solution in $S(\Theta)$. Unfortunately characterizing $S(\Theta)$ is complicated by the highly non-linear nature of the error metric. In order to deal with this problem, we follow a reverse approach. We define so called the *Error Tolerant Arrangement Classes* (ETAC's) for sampling. We say that a class of sensor arrangements where each arrangement satisfies certain properties is an ETAC if every sensor arrangement in that class guarantees that the corresponding error metric value is less than the error tolerance. More formally,

Definition 6.2.1. *Let $\mathbb{X}_{\mathcal{A}}$ denote a set of sensor arrangements characterized by certain properties $\mathcal{A}$. We say that $\mathbb{X}_{\mathcal{A}}$ is an* Error Tolerant Arrangement Class *or an ETAC if $\forall\ X \in \mathbb{X}_{\mathcal{A}}$, $\mathrm{Err}(X) \leq \Theta$, where Θ is a certain error tolerance.*

Note that it is likely to be easier to analyze a motion planning problem over the ETAC space because it is more explicitly defined than $S(\Theta)$. This approach is fairly general because it allows us to deal with different kinds of classes. For instance, in the case of intentionally mobile sensors, it is easier to plan motion that is characterized by certain properties. This will allow us to define an appropriate $\mathbb{X}_{\mathcal{A}}$ and identify

conditions under which it is an ETAC. Similarly, incidental motion itself may lead to a certain $\mathbb{X}_{\mathcal{A}}$ and we can analyze conditions under which it is an ETAC.

6.3 ETAC's for Trigonometric Polynomials

Numerous choices such as splines, wavelets, sinc functions and radial basis functions exist to model a spatio-temporal field. Here we limit our analysis to fields that are modeled as trigonometric polynomials. A trigonometric polynomial is simply a truncation of the Fourier series representation up to a certain finite number of terms. It serves as a good approximation for most smoothly varying physical processes. The trigonometric polynomial is a popular choice of basis functions while solving partial differential equations for various physical phenomena. We first formally define the sensor arrangement for trigonometric polynomial fields, and then follow with a discussion on different types of ETAC's. We mostly restrict our discussion to 1D and 2D fields, though the analysis directly extends to higher dimensional fields.

6.3.1 Trigonometric polynomials

First will discuss a 1D trigonometric polynomial. Let $f : [0,1] \rightarrow \mathbb{R}$ be a scalar field in 1D. We assume that the domain is scaled to $[0,1]$. $f(x)$ is represented as a trigonometric polynomial with complex exponential basis functions as follows:

$$f(x) = \sum_{k=-M}^{+M} a(k) \frac{e^{2\pi jkx}}{\sqrt{2M+1}}. \tag{6.19}$$

Each basis function is of the form $\frac{e^{2\pi jkx}}{\sqrt{2M+1}}$ and there are $2M+1$ basis function in total. $a(k)$'s correspond to the unknown complex coefficients. Note that the basis functions form an orthogonal set, *i.e.*,

$$\int_0^1 \frac{e^{2\pi jkx}}{\sqrt{2M+1}} \cdot \frac{e^{2\pi jlx}}{\sqrt{2M+1}} dx = \frac{\delta_{kl}}{2M+1} \tag{6.20}$$

where δ_{kl} denotes the Kronecker delta.

A 2D scalar field $f(x,y)$ is defined in a similar fashion: $f : [0,1] \times [0,1] \rightarrow \mathbb{R}$. $f(x,y)$ is represented as a trigonometric polynomial as follows:

$$f(x,y) = \sum_{k=-M}^{+M} \sum_{l=-M}^{+M} a(k,l) \frac{e^{2\pi j(kx+ly)}}{2M+1}. \tag{6.21}$$

Each basis function is of the form $\frac{e^{2\pi j(kx+ly)}}{2M+1}$. In total there are $(2M+1)^2$ complex exponential basis functions and $(2M+1)^2$ unknown complex coefficients, $a(k,l)$. Again, the basis functions form an orthogonal set, *i.e.*,

$$\int_0^1 \int_0^1 \frac{e^{2\pi j(kx+ly)}}{2M+1} \cdot \frac{e^{2\pi j(mx+ny)}}{2M+1} dxdy = \frac{\delta_{(k,l)(m,n)}}{(2M+1)^2} \tag{6.22}$$

where $\delta_{(k,l)(m,n)}$ is the Kronecker delta is defined as:

$$\begin{aligned} \delta_{(k,l)(m,n)} &= 1 \quad \text{iff } k = m \text{ and } l = n \\ &= 0 \quad \text{otherwise.} \end{aligned}$$

As discussed in the previous section, we assume that the measurement model involves additive random noise. In this work, we exclusively deal with additive zero-mean random noise with noise covariance of the form $\sigma^2\mathbf{I}$. Thus our measurement model is:

$$z(x,y) = f(x,y) + \varepsilon_{(x,y)} \tag{6.23}$$

where $z(x,y)$ is a field measurement value at location (x,y), and $\varepsilon_{(x,y)}$ is random noise with $E[\varepsilon_{(x,y)}] = 0$ and $E[\varepsilon^2_{(x,y)}] = \sigma^2$. We further assume that noise values at any two locations are independent and identically distributed random variables. We will briefly discuss the validity of this assumption later.

Suppose we take N samples at points $(x_1,y_1),(x_2,y_2),\cdots,(x_N,y_N)$. Let X denote the sensor arrangement of these sampling locations. We denote field values at the corresponding locations by $z_1, z_2, \cdots, z_N$ and we denote the observation vector by $\mathbf{z}$. We arrange unknown coefficients $a(k,l)$'s as a vector $\mathbf{a}$. Using the vector and matrix

notation that we defined earlier, we can represent N samples in terms of the following system of linear equations.

$$\mathbf{z} = \mathbf{V}\mathbf{a} + \mathbf{e} \tag{6.24}$$

Note that each column of $\mathbf{V}$ can be indexed by the pair (k, l) corresponding to the unknown coefficient $a(k, l)$. Let $\mathbf{V}_{(k,l)}$ denote this column. Thus,

$$\mathbf{V}_{(k,l)} = \frac{1}{(2M+1)^2} \begin{pmatrix} e^{2\pi j(kx_1+ly_1)} \\ e^{2\pi j(kx_2+ly_2)} \\ \vdots \\ e^{2\pi j(kx_N+ly_N)} \end{pmatrix} \tag{6.25}$$

Based on our assumption, $E[\mathbf{e}] = 0$ and $E[\mathbf{e}\mathbf{e}^T] = \sigma^2\mathbf{I}$, where $\mathbf{I}$ is the $N \times N$ identity matrix. Let $\hat{\mathbf{a}}$ indicate the estimate of $\mathbf{a}$ obtained using the MVUE. The Gauss-Markov theorem implies the following:

$$\hat{\mathbf{a}} = (\mathbf{V}^*\mathbf{V})^{-1}\mathbf{V}^*\mathbf{z} \tag{6.26}$$

$$\mathrm{E}\left[(\hat{\mathbf{a}} - \mathbf{a})(\hat{\mathbf{a}} - \mathbf{a})^T\right] = \sigma^2(\mathbf{V}^*\mathbf{V})^{-1} \tag{6.27}$$

$$\mathrm{Err}(X) = \mathrm{MSE} = \frac{1}{(2M+1)^2}\mathrm{E}\left[\|\hat{\mathbf{a}} - \mathbf{a}\|^2\right] = \frac{\sigma^2}{(2M+1)^2}\mathrm{trace}\{(\mathbf{V}^*\mathbf{V})^{-1}\}. \tag{6.28}$$

Let $\mathbf{T} = \mathbf{V}^*\mathbf{V}$. Thus,

$$\mathrm{Err}(X) = \frac{\sigma^2}{(2M+1)^2}\mathrm{trace}\{\mathbf{T}^{-1}\} \tag{6.29}$$

$\mathbf{T}$ is a matrix of size $(2M+1)^2 \times (2M+1)^2$. Each element of $\mathbf{T}$ is given by the dot product of two columns of $\mathbf{V}$ and can be indexed by the indices of those two columns. Thus,

$$\mathbf{T}_{kl,mn} = \mathbf{V}^*_{(k,l)} \cdot \mathbf{V}_{(m,n)} = \frac{\sigma^2}{(2M+1)^2} \sum_{i=1}^{N} e^{-2\pi j[(k-m)x_i + (l-n)y_i]}$$
$$\text{where } k, l, m, n = -M, -M+1, \cdots, 0, 1, \cdots, +M \tag{6.30}$$

Note that $\mathbf{T}$ has a special structure. Each element of $\mathbf{T}$ just depends on k, l, m, n. Such a matrix is called a *block Toeplitz* matrix.

Lemma 6.3.1. *The error metric in (6.28) is invariant to the translation of the sensor arrangement. Suppose we translate each point in X by $s = (\Delta x, \Delta y)$ along the x and y axes and let $X + s$ denote the new arrangement after mapping all the points to $[0,1] \times [0,1]$. Note that a trigonometric polynomial $f(x,y)$ is a periodic function and the sampling domain $[0,1] \times [0,1]$ corresponds to one period. Thus for any point (x,y) outside this domain, it is always possible to find an equivalent point in $[0,1] \times [0,1]$. Then,*

$$\mathrm{Err}(X + s) = \mathrm{Err}(X) \tag{6.31}$$

This invariance of the error metric to the translation of a sensor arrangement allows us to rearrange the sensor arrangement such that one of the sampling locations is always at $(0,0)$. In the remaining subsections, we discuss different classes of error tolerant arrangements for trigonometric polynomials under the *i.i.d.* noise assumption.

6.4 Regular Sensor Arrangements

Regular sampling is undoubtedly the simplest sensor arrangement to specify and analyze. The only information that we need to specify a regular arrangement is the period or the spacing between neighboring samples. In this subsection, we discuss 2D arrangements and bring out non-trivial features not observed in 1D. First we consider the case when the sampling period is the same along x as well as the y-direction. Next we discuss the case when the sampling periods along x and y direction are different. Finally we will consider a special form of regular sampling – *line-regular sampling*. In each case, we will show that the error metric value is inversely proportional to the number of samples as long as regularity of distribution is maintained.

6.4.1 Regular arrangement with the same period along each axis

Suppose we take samples at points of an $N \times N$ 2D Cartesian grid with grid spacing $\frac{1}{N}$. Figure 6-1(a) shows an example where 16 samples are arranged along 4×4 grid points. We assume that the origin of the lattice is at $(0, 0)$ because the error metric is translation invariant. We can easily evaluate the error metric value for this sampling scheme.

Lemma 6.4.1. *Let $f(x, y)$ be a 2D trigonometric polynomial as in (6.21). We have the regular sampling arrangement X_{reg} of $N \times N$ samples with the sampling period $\frac{1}{N}$ along each direction. Let the measurement model be as in (6.23), which gives a system of linear equations (6.24). Let $N^2 \geq (2M+1)^2$. Then,*

$$\mathrm{Err}(X_{reg}) = \sigma^2 \frac{(2M+1)^2}{N^2}. \tag{6.32}$$

Proof. The (x, y) coordinates of the sampling locations are given by $(\frac{i_1}{N}, \frac{i_2}{N})$, where $i_1, i_2 = 0, 1, \cdots, N-1$. Let $\mathbf{T}^{reg}$ be the corresponding block Toeplitz matrix. Note that each diagonal element of $\mathbf{T}^{reg}$ is simply $\frac{N^2}{(2M+1)^2}$. A non-diagonal element of $\mathbf{T}^{reg}$ is given by,

$$\begin{aligned}
\mathbf{T}^{reg}_{kl,mn} &= \frac{1}{(2M+1)^2} \sum_{i_1=0}^{N-1} \sum_{i_2=0}^{N-1} e^{-2\pi j[(k-m)\frac{i_1}{N} + (l-n)\frac{i_2}{N}]}, \ k \neq m, l \neq n \\
&= \frac{1}{(2M+1)^2} \sum_{i_1=0}^{N-1} e^{-2\pi j(k-m)\frac{i_1}{N}} \cdot \sum_{i_2=0}^{N-1} e^{-2\pi j(l-n)\frac{i_2}{N}}.
\end{aligned}$$

Using the geometric series summation formula for each of the above expressions, we can show:

$$\mathbf{T}^{reg}_{kl,mn} = 0, \ k \neq m, l \neq n$$

Thus, $\mathbf{T}^{reg} = \frac{N^2}{(2M+1)^2}\mathbf{I}$, where $\mathbf{I}$ is the identity matrix of size $(2M+1)^2 \times (2M+1)^2$.

Therefore,

$$\mathrm{Err}(X_{reg}) = \frac{\sigma^2}{(2M+1)^2}\mathrm{trace}((\mathbf{T}^{reg})^{-1}) = \sigma^2\frac{(2M+1)^2}{N^2}.$$

□

We now prove that this regular arrangement yields the optimal value of the error metric for a given number of samples. First we prove a lower bound on the error metric for any sensor arrangement.

Theorem 6.4.2. *Let $f(x,y)$ be a 2D trigonometric polynomial as in (6.21). Let the measurement model be as in (6.23), which gives a system of linear equations (6.24). For any sensing arrangement X with K sampling locations, the error metric is lower bounded as follows:*

$$\mathrm{Err}(X) \geq \frac{\sigma^2(2M+1)^2}{K}. \tag{6.33}$$

Proof. We provide two alternate proofs for this result.

Proof 1: Note that each diagonal element of $\mathbf{T}$ is just $\frac{K}{(2M+1)^2}$.

$$\mathbf{T}_{kl,kl} = \mathbf{V}^*_{(k,l)}\mathbf{V}_{(k,l)} = \frac{K}{(2M+1)^2}.$$

$\mathbf{T}$ is a Hermitian matrix. Hence all its eigenvalues are real [29]. In addition, $\mathbf{T}$ is a block Toeplitz matrix and hence it is positive definite [37]. Let $\lambda_1, \lambda_2, \cdots, \lambda_{(2M+1)^2}$ denote the eigenvalues of $\mathbf{T}$. Note that λ_i>0. We have the following relations.

$$\mathrm{trace}(\mathbf{T}) = \sum_{i=1}^{(2M+1)^2} \lambda_i = K$$

$$\mathrm{Err}(X) = \frac{\sigma^2}{(2M+1)^2}\mathrm{trace}(\mathbf{T}^{-1}) = \frac{\sigma^2}{(2M+1)^2}\sum_{i=1}^{(2M+1)^2}\frac{1}{\lambda_i}$$

Since all λ_i's are positive, we use the Arithmetic Mean - Harmonic Mean inequality

to obtain the following result:

$$\frac{\sum_{i=1}^{(2M+1)^2} \lambda_i}{(2M+1)^2} \geq \frac{(2M+1)^2}{\sum_{i=1}^{(2M+1)^2} \frac{1}{\lambda_i}}$$

Using the above inequality and the previous two equations,

$$\sum_{i=1}^{(2M+1)^2} \frac{1}{\lambda_i} \geq \frac{(2M+1)^4}{K}$$
$$\mathrm{Err}(X) \geq \sigma^2 \frac{(2M+1)^2}{K}$$

Thus we have a lower bound on the value of error metric for any sensor arrangement X of size K.

Proof 2: This proof directly follows from the statement of Theorem 5.3.2 in the previous chapter. In our representation of a trigonometric polynomial, basis functions are scaled such that each column of $\mathbf{V}^*$ form a uniform frame. According to Theorem 5.3.2, MSE $\geq \sigma^2 \frac{(2M+1)^2}{K}$. Hence the bound on the error metric follows. □

From Lemma 6.4.1 and the above theorem, we see that the regular sampling arrangement yields the error metric value that is a lower bound for any sampling arrangement with the same number of samples. We summarize this observation as the following key theorem.

Theorem 6.4.3. *Let $f(x,y)$ be a 2D trigonometric polynomial as in (6.21). We have the regular sampling arrangement X_{reg} of $N \times N$ samples with the sampling period $\frac{1}{N}$ along each direction. Let the measurement model be as in (6.23), which gives a system of linear equations (6.24). Let $N^2 \geq (2M+1)^2$. Then the regular sampling arrangement yields the optimal value of the error metric over all possible sensor arrangements consisting of $N \times N$ sampling locations.*

$$\min_X \ \mathrm{Err}(X) = \sigma^2 \frac{(2M+1)^2}{N^2} \tag{6.34}$$

An alternative line of reasoning comes from Theorem 5.3.2 in the previous chapter. Note that the regular sensor arrangement leads to a uniform tight frame and hence, yields the optimal error.

With the above result, it is easy to find conditions under which the class of regular sensor arrangements is an ETAC. Let Θ denote the error tolerance. We know that $\mathrm{Err}(X_{reg}) = \frac{\sigma^2(2M+1)^2}{N^2}$. We find the smallest N_o such that the inequality $\frac{\sigma^2(2M+1)^2}{N_o^2} \leq \Theta$ holds. Then, for any $N > N_o$, the error is always less that Θ. Thus, for any given Θ we can find conditions under which the regular arrangements form an ETAC.

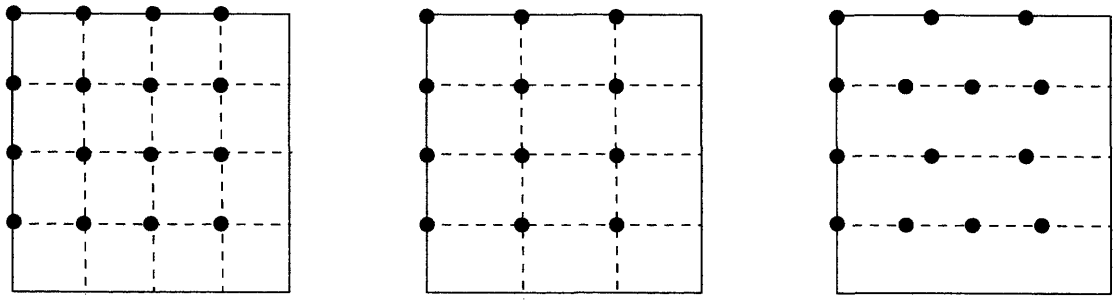

Figure 6-1: (a) Regular sampling with the same period along both axes (b) Regular sampling with different periods along each axis (c) Line-regular sampling

6.4.2 Regular sensor arrangement with different sampling periods along each direction

In this section the second case of 2D regular sampling arrangement in which samples are place regularly with different periods along each direction. We assume that $N_1 \times N_2$ samples are regularly placed with the periods $\frac{1}{N_1}$ along the x-axis and $\frac{1}{N_2}$ along the y-axis. Figure 6-1(b) shows an example of this type of arrangement where 12 samples are arranged with different periods, $\frac{1}{3}$ and $\frac{1}{4}$, along x and y-axis. We assume that $N_1 \geq 2M+1$ and $N_2 \geq 2M+1$. In this case also, we show that over all possible sampling arrangements of $N_1 \times N_2$ samples this regular arrangement yields the minimum estimation error.

Theorem 6.4.4. *Let $f(x,y)$ be a 2D trigonometric polynomial as in (6.21). We have the regular sampling arrangement X_{reg} of $N_1 \times N_2$ samples with the sampling*

periods $\frac{1}{N_1}$ *along the x-axis and* $\frac{1}{N_2}$ *along the y-axis. Let the measurement model be as in (6.23), which gives a system of linear equations (6.24). Let* $N_1 \geq 2M+1$ *and* $N_2 \geq 2M+1$. *Then the regular sampling arrangement yields the optimal value of the error metric over all possible sensor arrangements consisting of* $N_1 \times N_2$ *sampling locations.*

$$\min_X \ \mathrm{Err}(X) = \sigma^2 \frac{(2M+1)^2}{N_1 \times N_2} \tag{6.35}$$

Proof. According to Theorem 6.4.2, over all possible arrangements of $N_1 \times N_2$ sampling locations, the minimum estimation error that is possible to achieve is $\sigma^2 \frac{(2M+1)^2}{N_1 \times N_2}$. Along the lines of the proof of Lemma 6.4.1, it is possible to show using simple calculations that the regular sampling arrangement considered in this theorem indeed yields this estimation error. In fact, this regular sampling arrangement also leads to a uniform tight frame. Thus, by Theorem 5.3.2 in the previous chapter, the regular arrangement yields the optimal estimation error. □

With the above theorem, it is easy to find conditions under which this class of regular sensor arrangements is an ETAC. Let Θ denote the error tolerance. It is possible to achieve the estimation error of $\frac{\sigma^2(2M+1)^2}{N_1 \times N_2}$ using a regular arrangement of $N_1 \times N_2$ samples, where $N_1 \geq 2M+1$ and $N_2 \geq 2M+1$. We can find the smallest $N_1 \times N_2$ such that the inequality $\frac{\sigma^2(2M+1)^2}{N_1 \times N_2} \leq \Theta$ holds. Then, for any regular sampling arrangement of size $N_3 \times N_4$, where $N_3 \geq N_1$ and $N_4 \geq N_2$, the estimation error is always less that Θ. Thus, for any given Θ we can find conditions under which this class of regular arrangements form an ETAC. Note that in the previous subsection we considered the number of samples that is strictly a squared number. In this case, that is not necessary, hence providing us more flexibility in order to meet the error-tolerance condition.

6.4.3 Line-regular sensor arrangement

In this section, we consider another class of regular arrangements. The two classes we discussed earlier are commonplace. But in both the cases, the number of samples had to be a special type of number, a perfect square greater than $(2M+1)^2$ as in

the first case, or a product of two integers (each greater than or equal to $2M+1$) as in the second case. But what if the choice of the number of samples is neither of these types? Does there exist a regular sampling arrangement that still achieves the lower bound on the estimation error as seen in Theorem 6.4.2? The answer is yes. In this section, we discuss a special type of regular arrangement, which we call as a *line-regular* sensor arrangement, precisely achieves this.

We now describe a procedure for constructing a line-regular sensor arrangement. In the square domain $[0,1] \times [0,1]$, we place N lines parallel to x-axis periodically with period $\frac{1}{N}$. We assume that $N \geq 2M+1$. Along each horizontal line we place a few samples regularly. Let K_i denote the number of samples placed uniformly with period $\frac{1}{K_i}$ along the ith horizontal line which has $y = \frac{i-1}{N}$, where $i = 1, 2, \cdots, N$. We assume that each $K_i \geq 2M+1$. Thus, the total number of samples is $K = \sum_{i=1}^{N} K_i$. Note that $K \geq (2M+1)^2$. Figure 6-1(c) shows an example of a line-regular sampling arrangement of 14 samples. In the following lemma, we evaluate the estimation error corresponding to the line-regular sensor arrangement.

Lemma 6.4.5. *Let $f(x,y)$ be a 2D trigonometric polynomial as in (6.21). We have a line-regular sampling arrangement $X_{line-reg}$ of K samples constructed according to the procedure described above. Let the measurement model be as in (6.23), which gives a system of linear equations (6.24). Then,*

$$\mathrm{Err}(X_{line-reg}) = \sigma^2 \frac{(2M+1)^2}{K}. \tag{6.36}$$

Proof. Let (x_{mn}, y_{mn}) be the coordinate of the nth sampling location along the mth horizontal line, where $m = 1, 2, \cdots, N$ and $n = 1, 2, \cdots, K_m$. According to our placement strategy, $x_{mn} = \frac{n-1}{K_m}$ and $y_{ij} = \frac{m-1}{N}$. Let $\mathbf{T}^{line-reg}$ be the corresponding block Toeplitz matrix for this sampling arrangement. An element $\mathbf{T}^{line-reg}_{kl,st}$ of $\mathbf{T}^{line-reg}$

is given by,

$$\begin{aligned}\mathbf{T}^{line-reg}_{kl,st} &= \frac{1}{(2M+1)^2}\sum_{m=1}^{N}\sum_{n=1}^{K_m} e^{-2\pi j[(k-s)\frac{n-1}{K_m}+(l-t)\frac{m-1}{N}]} \\ &= \frac{1}{(2M+1)^2}\sum_{m=1}^{N} e^{-2\pi j(l-t)\frac{m-1}{N}}\sum_{n=1}^{K_m} e^{-2\pi j(k-s)\frac{n-1}{K_m}}.\end{aligned}$$

Using the geometric series summation formula for each of the above expressions, we can show that $\mathbf{T}^{line-reg} = \frac{K}{(2M+1)^2}\mathbf{I}$, where $\mathbf{I}$ is the identity matrix of size $(2M+1)^2 \times (2M+1)^2$. Therefore,

$$\mathrm{Err}(X_{line-reg}) = \frac{\sigma^2}{(2M+1)^2}\mathrm{trace}((\mathbf{T}^{line-reg})^{-1}) = \sigma^2\frac{(2M+1)^2}{K}.$$

□

Based on the above lemma and Theorem 6.4.2, we see that the line-regular sampling achieves the minimal estimation error.

Theorem 6.4.6. *Let $f(x,y)$ be a 2D trigonometric polynomial as in (6.21). We have a line-regular sampling arrangement $X_{line-reg}$ of K samples constructed according to the procedure described above. Let the measurement model be as in (6.23), which gives a system of linear equations (6.24). Let $N_1 \geq 2M+1$ and $N_2 \geq 2M+1$. Then the line-regular sampling arrangement yields the optimal value of the error metric over all possible sensor arrangements consisting of K sampling locations.*

$$\min_X \ \mathrm{Err}(X) = \sigma^2\frac{(2M+1)^2}{K} \tag{6.37}$$

With the above theorem, it is easy to find conditions under which a class of line-regular sensor arrangements is an ETAC. Let Θ denote the error tolerance. We can find the smallest K such that the inequality $\frac{\sigma^2(2M+1)^2}{K} \leq \Theta$ holds. Then, for any line-regular sensor arrangement of size K according to the construction procedure above, the estimation error is always less that Θ. Thus, for any given Θ we can find conditions under which this class of regular arrangements form an ETAC. In comparison with

the two types of regular sensor arrangements discussed earlier, line-regular sampling arrangements do not impose any conditions on how the number of samples should be and provide maximum flexibility in terms of the choice of the number of samples for the given error tolerance.

6.5 Δ-dense Sensor Arrangement

Δ-dense sensor arrangements have been studied in the context of the stable reconstruction of band limited signals using non-uniform sampling in the context of the numerical issues involved there [35], [37].

Definition 6.5.1. *Let X denote a sensor arrangement in $[0,1] \times [0,1]$. We say that X is* Δ-dense *if for any point $(x,y) \in [0,1] \times [0,1]$, there exists some $(x_i, y_i) \in X$ such that $\max\{|x - x_i|, |y - y_i|\} \leq \Delta$,* i.e., *the L_∞ distance between (x,y) and (x_i, y_i) is at most Δ. Intuitively, within a square of size 2Δ,* i.e., *an L_∞-disc of radius Δ, placed anywhere in $[0,1] \times [0,1]$, there is at least one sampling location. We refer to a collection of all Δ-dense sensor arrangements as the class of Δ-dense sensor arrangements.*

It can be observed that if X is Δ-dense, then it is also Δ'-dense for any $\Delta' > \Delta$. However a Δ'-dense arrangement need not be Δ-dense. Furthermore, the L_∞ distance between any two nearest neighbor sampling locations from a Δ-dense sensor arrangement is at most 2Δ. Intuitively, a Δ-dense arrangement does not contain a square *hole* of size larger than 2Δ. Based on this geometric interpretation, we can conclude that any Δ-dense arrangement contains at least $\frac{1}{(2\Delta)^2}$ sampling points.

We find the conditions on Δ under which the Δ-dense arrangements form an ETAC. Let Θ be the error tolerance. In the previous section, we found the conditions under which uniform arrangements form an ETAC. Suppose we place $N \times N$ samples uniformly to form the sensor arrangement X_{reg} as in the previous section. Let N be the smallest integer such that $\mathrm{Err}(X_{reg}) \leq \Theta$. Note that X_U is in fact $\frac{1}{2N}$-dense and $\mathrm{Err}(X_{reg}) = \frac{\sigma^2(2M+1)^2}{N^2}$. Loosely speaking, X_{reg} is the *tightest* among all the $\frac{1}{2N}$-dense arrangements since it needs the smallest number of samples than any other

arrangement in this class. Based on several simulation runs, we make the following conjecture.

Conjecture 6.5.2. *Let X be a $\frac{1}{2N}$-dense sensor arrangement, where N is the smallest integer such that $\frac{\sigma^2(2M+1)^2}{N^2} \leq \Theta$. Then $\mathrm{Err}(X) \leq \Theta$. Thus, the class of $\frac{1}{2N}$-dense sensor arrangements is an ETAC with respect to the error tolerance Θ.*

$$N' = \lceil \frac{1}{(2\Delta)^2} \rceil \tag{6.38}$$

$$\mathrm{Err}(X) \leq \frac{\sigma^2(2M+1)^2}{N'} \tag{6.39}$$

$$\frac{\sigma^2(2M+1)^2}{N} \leq \mathrm{Err}(X) \leq \frac{\sigma^2(2M+1)^2}{N'} \tag{6.40}$$

Thus, the uniform arrangement with $N \times N$ samples is also the *tightest* in terms of the error because it represents the upper bound on the estimation error for any $\frac{1}{2N}$-dense arrangement. We observed this over several simulation runs though we have not been able to prove the claim.

The class of Δ-dense sensor arrangements has a connection with the geometric *coverage problem* of covering the domain with L_∞-discs (square discs) of radius Δ. Note that any Δ-dense sensor arrangement is a valid solution to the *coverage* problem because if we locate a square of size 2Δ centered at each sampling location of a Δ-dense arrangement, then by the definition the entire domain $[0,1] \times [0,1]$ is guaranteed to be *covered* by these L_∞ discs. Furthermore, if we imagine a few mobile square shaped robots of size 2Δ *tour* through the sites of a Δ-dense arrangement, then the entire domain is *swept* by these robots. Note that the tour involves only translational motion of the robots (no rotations) according to the definition of a Δ-dense arrangement.

6.6 Incrementally Constructed Sensor Arrangements

Independent of the previous two ETAC's, we propose an approach to construct an error-tolerant arrangement from a given initial arrangement. This approach is inspired from an *active learning* method in the machine learning literature [46]. As the name suggests we incrementally add chosen sampling sites to the already existing sensor arrangement one by one such that the estimation error is reduced at every step until the error is less than the error tolerance value. At this point the sensor arrangement is error tolerant. We propose a heuristic to construct such an arrangement. In this sense, this approach does not exactly lead to an ETAC, but it given a way to construct an error-tolerant arrangement from a given initial arrangement. A set of arrangements obtained from various initial sensor arrangements is particularly useful for the case of intentionally mobile sensors. Suppose $(2M+1)^2$ points are already chosen in the sensor arrangement. These might be obtained by placing a few static sensors or measurements available from a few mobile sensors. Suppose we need to make a few additional measurements to guarantee that the error metric is within the error tolerance. In this case, the class of incrementally constructed sensor arrangements allows us to find a set of additional measurements.

Let X_n denote a sensor arrangement of n points. Suppose we wish to add a sampling location to X_n such that the estimation error is further reduced. Let $\mathbf{T}_n$ denote a Toeplitz matrix corresponding to X_n. $\mathbf{T}_n = \mathbf{V}_n^* \mathbf{V}_n$. Suppose we add the sampling location (x_{n+1}, y_{n+1}) to obtain X_{n+1} and let $\mathbf{T}_{n+1}$ be the new Toeplitz matrix. We add a new observation to the already existing system of linear equations as in (6.24), we add a new row to $\mathbf{V}_n$. Let $\mathbf{v}$ denote the column vector corresponding to all the basis function values at (x_{n+1}, y_{n+1}). Thus,

$$\mathbf{T}_{n+1} = \mathbf{T}_n + \bar{\mathbf{v}}\mathbf{v}^T \tag{6.41}$$

where $\bar{\mathbf{v}}$ denotes the complex conjugate of $\mathbf{v}$. $\mathbf{T}_{n+1}^{-1}$ can be expressed in the closed

form as follows [46]:

$$\mathbf{T}_{n+1}^{-1} = \mathbf{T}_n^{-1} - \frac{1}{1 + \mathbf{v}^T \mathbf{T}_n^{-1} \bar{\mathbf{v}}} \{\mathbf{T}_n^{-1}\} \bar{\mathbf{v}} \mathbf{v}^T \{\mathbf{T}_n^{-1}\} \tag{6.42}$$

Hence,

$$\text{trace}(\mathbf{T}_{n+1}^{-1}) = \text{trace}(\mathbf{T}_n^{-1}) - \frac{\mathbf{v}^T \mathbf{T}_n^{-1} \mathbf{T}_n^{-1} \bar{\mathbf{v}}}{1 + \mathbf{v}^T \mathbf{T}_n^{-1} \bar{\mathbf{v}}} \tag{6.43}$$

Therefore,

$$\text{Err}(X_{n+1}) = \text{Err}(X_n) - \frac{\mathbf{v}^T \mathbf{T}_n^{-1} \mathbf{T}_n^{-1} \bar{\mathbf{v}}}{1 + \mathbf{v}^T \mathbf{T}_n^{-1} \bar{\mathbf{v}}} \tag{6.44}$$

Since $\mathbf{T}_n$ is positive definite and Hermitian, the second term in the above equation is always positive and this shows that any extra sample reduces the estimation error. We consider the following optimization problem of finding the (x_{n+1}, y_{n+1}) that reduces the estimation error the most.

$$\begin{aligned} (x_{n+1}^*, y_{n+1}^*) = \arg \max_{(x_{n+1}, y_{n+1})} & \frac{\mathbf{v}^T \mathbf{T}_n^{-1} \mathbf{T}_n^{-1} \bar{\mathbf{v}}}{1 + \mathbf{v}^T \mathbf{T}_n^{-1} \bar{\mathbf{v}}} \\ \text{s.t.} \quad & (x_{n+1}, y_{n+1}) \in [0,1] \times [0,1] \end{aligned} \tag{6.45}$$

The constrained optimization problem above is highly nonlinear and has many local maxima. Figure 6-2 shows a regular arrangement of 8×8 points except one missing sample in the center. Clearly, if we add the missing sample, we achieve the global optimum. We evaluated the value of $\text{Err}(X)$ numerically as a function of location that is added to the current arrangement. Figure 6-3 shows $\text{Err}(X)$ as a function of (x, y). Note that there are many local optima. Moreover, the reduction in the estimation error for the missing sample location from the uniform arrangement is significantly higher than that for any other location. In our numerical simulations, we observed that different initial choices lead to different local optima when we solve the above constrained optimization problem. Thus the choice of initial guess to the optimization solver is crucial.

In order to get around these local effects, we propose an approach to calculate initial guesses to the optimization solver using a heuristic based on Voronoi diagrams of sampling locations. Figure 6-4 shows the Voronoi diagram for a set of randomly

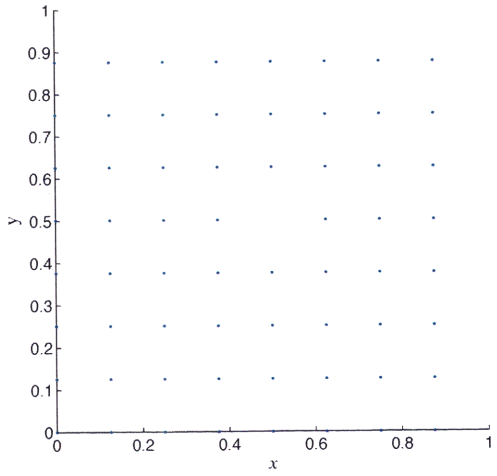

Figure 6-2: $M = 3$, $\sigma^2 = 1$; samples are uniformly placed at points of a regular 8×8 grid, except one sample is missing.

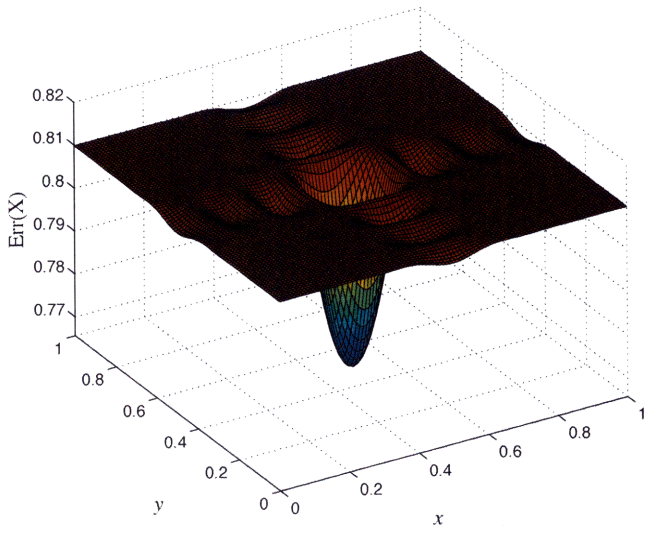

Figure 6-3: For the arrangement shown in Figure 6-2, $\mathrm{Err}(X)$ is shown as a function of (x, y) where (x, y) is added to the already existing arrangement of samples. There are many local optima. The estimation error is reduced the most when the sample is placed at the missing sample site.

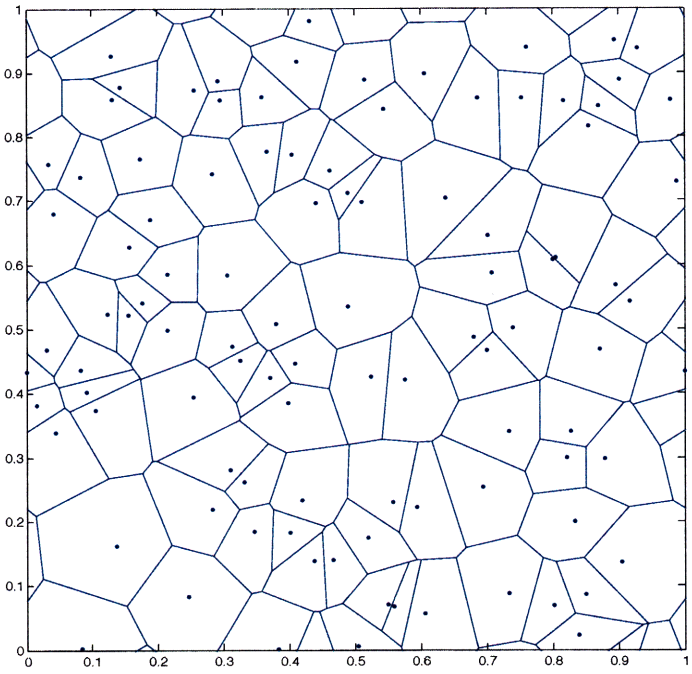

Figure 6-4: Voronoi diagram for a set of points randomly placed in 2D domain. This Voronoi diagram conforms with the toroidal nature of the sampling domain.

placed sampling locations in 2D generated using MATLAB. Note that the Voronoi diagram conforms with the toroidal assumption of the domain. The underlying idea of our heuristic is that we find the Voronoi cell that has the maximum area and choose the farthest vertex of that cell from the source point as the initial solution. This is inspired by the insights from regular and Δ-dense sampling which indicate that large holes are best avoided. Intuitively a large Voronoi cell indicates a large hole between sensor locations. As mentioned before, we assume toroidal topology of the domain $[0,1] \times [0,1]$. Hence we consider Voronoi diagrams on a torus rather than on a plane. We summarize our approach in the form of an algorithm as follows.

Algorithm 2 A heuristic based on Voronoi diagrams to find an initial guess for the optimization problem in (6.45)

1: **Input:** X, a sensor arrangement
2: **Output:** Initial guess (x_o, y_o)
3: Draw Voronoi diagram of points in X
4: Find the Voronoi cell P of the maximum area and its source (x, y)
5: Choose the vertex of P which is farthest from (x, y) as (x_o, y_o)

Once we determine an initial guess at any step, we find the next sample and add it to the existing arrangement. At each step the estimation error is reduced and we continue until it is less than the tolerance error. At this point the arrangement is error tolerant. It is worth noting that this procedure yields results that depend very much on the initial set.

Numerical example: Let $M = 3$ and $\sigma^2 = 1$. We chose 64 sampling sites randomly. They are shown in Figure 6-5. We use the nonlinear constrained optimization module of MATLAB to solve the optimization problem at each stage. We compare three schemes of adaptive sampling by adding 10 samples to the arrangement in each case. In the first scheme, we follow the brute force search method to find the global optima that yields the lowest estimation error. In the second scheme, we use our heuristic in Algorithm 2 to find an initial guess at each stage. In the third scheme, we choose initial guess randomly. In Figure 6-6, we show how $\mathrm{Err}(X)$ behaves as a function of any point (x, y) in the domain. We observe that for the first extra sample, our heuristic gives global optima. The figure also indicates that there are many local

optima and usually the larger reduction in the estimation error occurs when a new sample is placed in the region of large gaps. In Figure 6-7, we compare the estimation error for 10 additional samples for these different schemes. The brute force search method yields the lowest estimation error at each stage. However it is extremely time consuming. Our heuristic approach yielded the estimation error always less than the random guess at each stage. Moreover it is easy to implement and the error is close to the brute force search method.

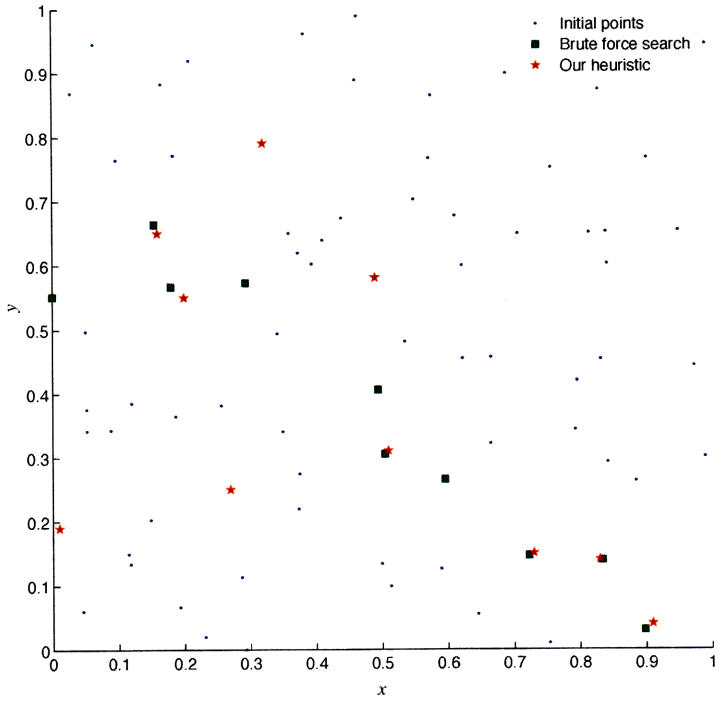

Figure 6-5: 64 sample sites are randomly chosen. 10 additional sample points obtained using the brute force search method and our heuristic are shown along with the initial randomly chosen sites.

6.7 Random Sensor Arrangements

So far we discussed sensor arrangements that can be described in deterministic terms. In this section, we discuss random sensor arrangements where sampling locations are

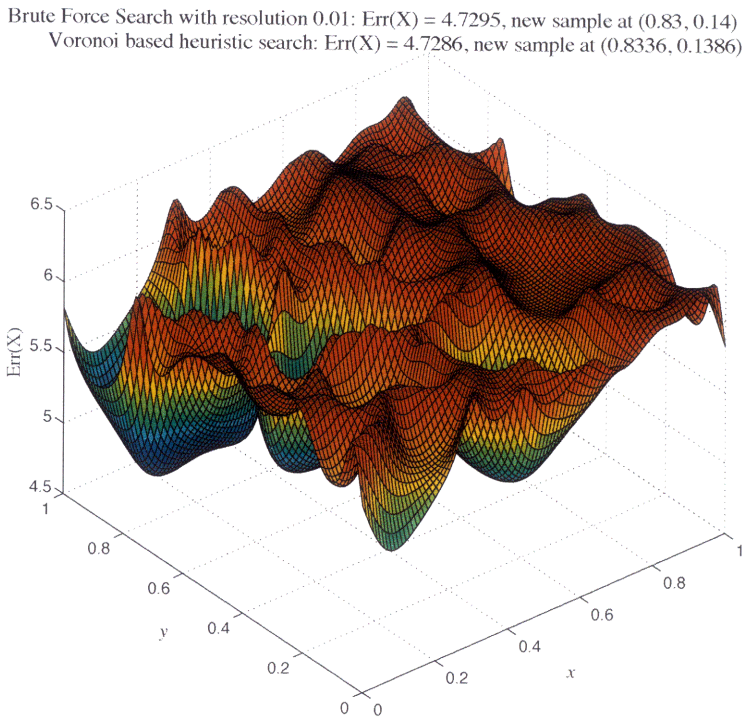

Figure 6-6: For the arrangement shown in Figure 6-5, $\mathrm{Err}(X)$ is shown as a function of (x, y) where (x, y) is added to the already existing sensor arrangement. The resolution between consecutive points is 0.01. There are many local optima.

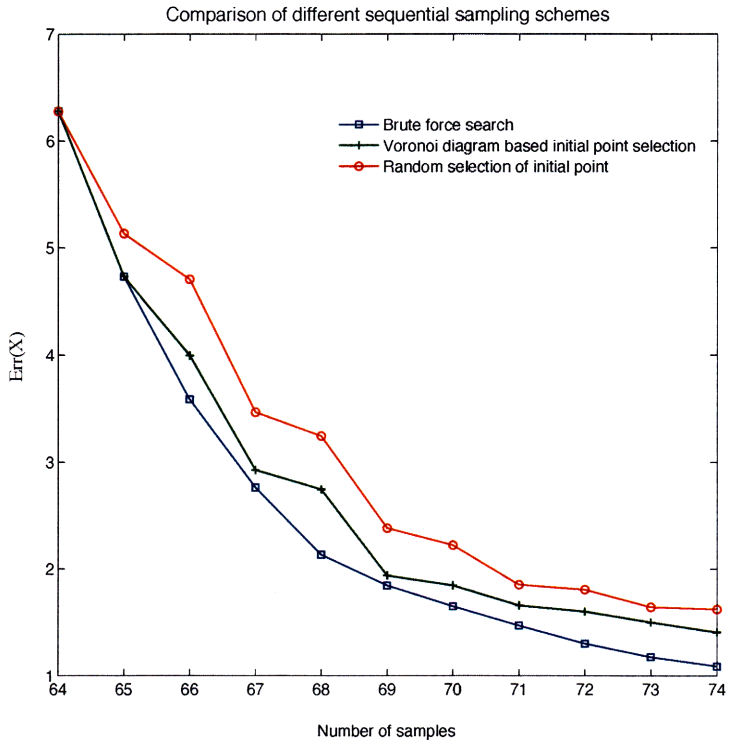

Figure 6-7: Comparison of the estimation error values for three different schemes of incremental sampling: (1) the brute force search method for global minima at each step carried at resolution of 0.01 (2) our heuristic based on Voronoi diagrams to choose initial point for optimum search at each step (3) random selection of an initial point for optimum search at each step.

selected according to some random distribution. Randomness leads to only *probabilistic* guarantees on the estimation error. We describe classes of random sensor arrangements that are error tolerant *with high probability.*

Random sensor arrangements have some advantages over deterministic sensor arrangements. First, analyzing *optimal* error tolerance values or the *worst-case error estimate* for a class of deterministic sensor arrangement is sometimes hard (as observed in the Δ-dense case above). In contrast, probabilistic estimates are usually easier to derive as we will see. Second, the probabilistic approach adapts to fields consisting of basis functions of different types like splines, radial, *etc.* Third, random sensor arrangements are important from the perspective of incidental as well as intentional motion. Sometime incidental motion can be easily described in terms of random walks of nodes and this leads to instances of sensor arrangements according to some probability distribution. In the case of intentionally mobile sensors, it might be easy to program nodes to take samples at random sampling locations. In both these situations it is important to identify conditions under which the arrangements are error tolerant with high probability. Finally, probabilistic methods can be applied to situations where the exact location of the sensor is not known. It is often infeasible to instrument a sensors, *e.g.* in a river, with GPS-like location devices because of cost and technical issues. Our approach is inspired by recent work [4], [36] on learning of trigonometric polynomials from random samples. This work analyzes issues related to numerical analysis using probabilistic techniques; it primarily discusses guarantees on the condition number for random sampling schemes. We use their results and their techniques to analyze error tolerance guarantees for two types of random sensor arrangements.

6.7.1 Sensor arrangement with one randomly placed sample per grid cell

Among all possible random sensor arrangement, the simplest is uniformly random arrangement where sampling locations are placed uniform randomly over the entire

domain. We indeed discuss this in the next subsection. Uniformly random sensor arrangement sometimes leads to a case when samples form isolated clusters leaving large holes in the domain. The particular sensor arrangement we study in this subsection prohibits formation of such clusters and evenly spreads samples across the space. In this arrangement, we divide the sampling domain into grid cells and impose a constraint that in every grid cell a sampling location is chosen uniformly randomly. For example, consider the case of 1D trigonometric polynomial with domain $[0, 1]$ and suppose there are N sampling locations. Then in our sensor arrangement we divide $[0, 1]$ into N equal intervals, each of length $\frac{1}{N}$ and in each interval we place a sampling location uniformly randomly. This enforces a condition that two neighboring samples are at most $\frac{2}{N}$ distance apart. This fact implies that the sensor arrangement thus obtained is $\frac{2}{N}$-dense and allows for direct comparison with the Δ-dense error tolerant arrangements we discussed earlier. below shows this sensor arrangement pictorially. Now we analyze the error metric for this arrangement. We restrict our discussion to 1D field, however the analysis can easily be extended to higher dimensions.

Suppose we take N samples in $[0, 1]$ according to the random sampling scheme we described to get a sensor arrangement $X = \{x_1, x_2, \cdots, x_N\}$. Without loss of generality let us assume that x_i's are arranged in increasing order. Further, let us assume that x_i is chosen uniformly randomly in the interval $[\frac{i}{N} - \frac{1}{2N}, \frac{i}{N} + \frac{1}{2N}]$, where $i = 1, 2, \cdots, N$. Note that the length of each interval is $\frac{1}{N}$. Thus, the probability density function of x_i is a constant equal to N, and $\mathbb{E}[x_i] = \frac{i}{N}$ and $Var[X^i_{kl}] = \frac{1}{12N^2}$. Further, note that

$$\max_{i=1,2,\cdots,N} |x_{i+1} - x_i| \leq \frac{2}{N}. \tag{6.46}$$

Thus X is a $\frac{2}{N}$-dense arrangement as described above. Owing to our sampling scheme, the block Toeplitz matrix $\mathbf{T}$ is a random matrix. Let T_{kl} denote an element in the kth row and lth column. Let $X^i_{kl} = \frac{e^{2\pi j(l-k)x_i}}{2M+1}$. Thus,

$$T_{kl} = \sum_{i=1}^{N} \frac{e^{2\pi j(l-k)x_i}}{2M+1} = \sum_{i=1}^{N} X^i_{kl}. \tag{6.47}$$

X_{kl}^i's are *independent* complex random variables. X_{kl}^i has the following mean and variance.

$$\mathbb{E}[X_{kl}^i] = \int_{\frac{i}{N}-\frac{1}{2N}}^{\frac{i}{N}+\frac{1}{2N}} \frac{e^{2\pi j(l-k)x}}{2M+1} N dx \tag{6.48}$$

$$= \frac{e^{2\pi j(l-k)\frac{i}{N}}}{2M+1} \frac{\sin(\frac{\pi(l-k)}{N})}{\frac{\pi(l-k)}{N}} \tag{6.49}$$

$$= \frac{e^{2\pi j(l-k)\frac{i}{N}}}{2M+1} \text{sinc}\left(\frac{\pi(l-k)}{N}\right). \tag{6.50}$$

$$\mathbb{E}[Re\left(X_{kl}^i\right)] = \frac{\cos(2\pi j(l-k)\frac{i}{N})}{2M+1} \text{sinc}\left(\frac{\pi(l-k)}{N}\right), \text{and} \tag{6.51}$$

$$\mathbb{E}[Im\left(X_{kl}^i\right)] = \frac{\sin(2\pi j(l-k)\frac{i}{N})}{2M+1} \text{sinc}\left(\frac{\pi(l-k)}{N}\right), \text{and} \tag{6.52}$$

where Re and Im denote real and imaginary parts of a complex number.

$$Var[X_{kl}^i] = \mathbb{E}[(\overline{X_{kl}^i - \mathbb{E}[X_{kl}^i]})(X_{kl}^i - \mathbb{E}[X_{kl}^i])] \tag{6.53}$$

$$= \mathbb{E}[\overline{X_{kl}^i} X_{kl}^i] - \mathbb{E}[\overline{X_{kl}^i}]\mathbb{E}[X_{kl}^i] \tag{6.54}$$

$$= \frac{1}{(2M+1)^2}\left[1 - \text{sinc}^2\left(\frac{\pi(l-k)}{N}\right)\right]. \tag{6.55}$$

Note that the variance of X_{kl}^i is independent of i.

T_{kl} has the following mean and variance.

$$\mathbb{E}[T_{kl}] = \sum_{i=1}^{N} \mathbb{E}[X_{kl}^i] = \sum_{i=1}^{N} \frac{e^{2\pi j(l-k)\frac{i}{N}}}{2M+1} \text{sinc}\left(\frac{\pi(l-k)}{N}\right) = \frac{N}{2M+1}\delta_{kl}. \tag{6.56}$$

$$Var[T_{kl}] = \sum_{i=1}^{N} Var[X_{kl}^i] = \frac{N}{(2M+1)^2}\left[1 - \text{sinc}^2\left(\frac{\pi(l-k)}{N}\right)\right]. \tag{6.57}$$

Therefore,

$$\mathbb{E}[\mathbf{T}] = \frac{N}{2M+1}\mathbf{I}. \tag{6.58}$$

Let $\|\mathbf{C}\|$ denote the largest eigenvalue of a positive definite square matrix $\mathbf{C}$. Then

[29],

$$\|\mathbf{C}\| = \max_{\mathbf{x}} \|\frac{\mathbf{x}\mathbf{C}^T\mathbf{x}}{\mathbf{x}^T\mathbf{x}}\|. \tag{6.59}$$

First we analyze $\|\mathbf{T} - \frac{N}{2M+1}\mathbf{I}\|$ for the random sensor arrangement X. The techniques used below are borrowed from the ones in [36], Theorem 3.6. A more general result is proved in [36], Theorem 3.6 for general random sensor arrangements. We produce the result specifically for our sampling scheme. Note that our proof involves initial steps different than the proof of [36], Theorem 3.6 improving the constants. We specifically highlight these steps in the proof.

Before plunging into the analysis of $\|\mathbf{T} - \frac{N}{2M+1}\mathbf{I}\|$, we state the following useful lemmas.

Lemma 6.7.1. **(Bernstein's inequality** [7]) *Let $y_1, y_2, \cdots, y_n$ be n independent real random variables with zero mean and $Var[y_i] = \sigma_i^2$. Each random variable is bounded so that $|y_i| \leq M_i$. Let, $M = \max M_i$ and $\sigma^2 = \sum_{i=1}^n \sigma_i^2$. Then,*

$$\mathbb{P}\left(\left|\sum_{i=1}^n y_i\right| \geq \epsilon\right) \leq 2\exp\left(-\frac{\epsilon^2}{2\sigma^2 + \frac{2}{3}M\epsilon}\right). \tag{6.60}$$

Lemma 6.7.2. *Let $y_1, y_2, \cdots, y_n$ be n random variables. Then,*

$$\mathbb{P}\left(\sum_{i=1}^n y_i \geq c\right) \leq \sum_{i=1}^n \mathbb{P}\left(y_i \geq \frac{c}{n}\right).$$

Proof. Let A denote an event that $\sum_{i=1}^n y_i \geq c$. Let A_i denote an event that $y_i \geq \frac{c}{n}$. Then $A \subseteq A_1 \cup A_2 \cup \cdots \cup A_n$. Then by union bound [57], $\mathbb{P}(A) \leq \sum_{i=1}^n \mathbb{P}(A_i)$. Hence the result follows. □

Lemma 6.7.3. *The following bounds hold.*

$$\left|Re\left(X_{kl}^i\right) - \mathbb{E}[Re\left(X_{kl}^i\right)]\right| \leq \frac{2}{2M+1} \tag{6.61}$$

$$\left|Im\left(X_{kl}^i\right) - \mathbb{E}[Im\left(X_{kl}^i\right)]\right| \leq \frac{2}{2M+1} \tag{6.62}$$

Proof. We prove the first bound. The second bound follows similarly.

$$\begin{aligned}
\left|Re\left(X_{kl}^{i}\right) - \mathbb{E}[Re\left(X_{kl}^{i}\right)]\right| &= \left|\frac{\cos(2\pi j(l-k)x)}{2M+1} - \frac{\cos(2\pi j(l-k)\frac{i}{N})}{2M+1}\text{sinc}\left(\frac{\pi(l-k)}{N}\right)\right| \\
&\leq \left|\frac{\cos(2\pi j(l-k)x)}{2M+1}\right| + \left|\frac{\cos(2\pi j(l-k)\frac{i}{N})}{2M+1}\text{sinc}\left(\frac{\pi(l-k)}{N}\right)\right| \\
&\leq \frac{1}{2M+1} + \frac{1}{2M+1} = \frac{2}{2M+1}.
\end{aligned}$$

□

We state the following equalities without showing the calculations.

$$\sum_{i=1}^{N} Var[Re(X_{kl}^{i})] = \frac{N}{2(2M+1)^2}\left[1 - \text{sinc}^2\left(\frac{\pi(l-k)}{N}\right)\right]. \tag{6.63}$$

$$\sum_{i=1}^{N} Var[Im(X_{kl}^{i})] = \frac{N}{2(2M+1)^2}\left[1 - \text{sinc}^2\left(\frac{\pi(l-k)}{N}\right)\right]. \tag{6.64}$$

Note that each variance above is half the variance of T_{kl} as shown in (6.57).

Theorem 6.7.4. Gershgorin Circle Theorem [29] *Let* $\mathbf{A}$ *be a complex square matrix of size* $N \times N$. *If* $\mathbf{X}^{-1}\mathbf{A}\mathbf{X} = \mathbf{D} + \mathbf{F}$, *where* $\mathbf{D}$ *is a diagonal matrix with diagonal entries* $d_1, d_2, \cdots, d_N$ *and* $\mathbf{F}$ *has zero diagonal entries, then*

$$\lambda(\mathbf{A}) \subseteq \cup_{i=1}^{N} D_i, \tag{6.65}$$

where $D_i = \{z \in \mathbb{C} : |z - d_i| \leq \sum_{j=1}^{N} |f_{ij}|\}$.

The above theorem is useful in matrix perturbation theory [29]. Each D_i is a disc of radius $\sum_{j=1}^{N} |f_{ij}|$ centered at d_i. The theorem says that each eigenvalue of $\mathbf{A}$ lies in at least some D_i.

$\mathbf{T}$ is a Toeplitz matrix. $T_{kl} = \sum_{i=1}^{N} \frac{e^{2\pi j(l-k)x_i}}{2M+1}$. T_{kl} essentially depends on $(l-k)$. Let us denote T_{kl} by simply $T_{(l-k)}$ just for the following discussion in this subsection. We prove the following bound.

Lemma 6.7.5.

$$\max_k \sum_{l,l\neq k} |T_{kl}| \leq 2\sum_{m=1}^{M} |T_m| + \sum_{m=M+1}^{2M} |T_m|. \tag{6.66}$$

Proof. $\mathbf{T}$ has the following structure.

$$\mathbf{T} = \begin{pmatrix} T_0 & T_1 & T_2 & \cdots & T_{2M} \\ T_{-1} & T_0 & T_1 & \cdots & T_{2M-1} \\ T_{-2} & T_{-1} & T_0 & \cdots & T_{2M-2} \\ \vdots & \vdots & \vdots & \vdots & \vdots \\ T_{-2M} & T_{-2M+1} & \cdots & T_{-1} & T_0 \end{pmatrix}$$

Note that the first row and the last row of the matrix together contain all the elements of $\mathbf{T}$. Also note that $|T_{kl}| = |T_{(l-k)}| = |T_{(k-l)}| = |T_{lk}|$. Based on these observations, the result of the lemma follows. □

Now we prove the following theorem about $\|\mathbf{T} - \frac{N}{2M+1}\mathbf{I}\|$ for our random sensor arrangement.

Theorem 6.7.6. *Consider a 1D trigonometric polynomial field. Let $X = \{x_1, x_2, \cdots, x_N\}$ be a sensor arrangement in $[0,1]$ such that x_i's are arranged in increasing order and each x_i is chosen uniformly randomly in the interval $[\frac{i}{N} - \frac{1}{2N}, \frac{i}{N} + \frac{1}{2N}]$, where $i = 1, 2, \cdots, N$. $N \geq (2M+1)$. Let $\mathbf{T}$ be the corresponding block Toeplitz matrix. Then,*

$$\mathbb{P}\left(\|\mathbf{T} - \frac{N}{2M+1}\mathbf{I}\| \leq \frac{N}{2M+1}\epsilon\right) \geq 1 - \psi, \tag{6.67}$$

where,

$$\psi = 4(2M+1)\exp\left(-\frac{N\epsilon^2}{\frac{9}{2}(2M+1)^2\left[1 - \operatorname{sinc}^2\left(\frac{\pi(2M+1)}{N}\right)\right] + 2\sqrt{2}(2M+1)\epsilon}\right). \tag{6.68}$$

Proof. Consider the event $\|\mathbf{T} - \frac{N}{2M+1}\mathbf{I}\| \geq \frac{N}{2M+1}\epsilon$. We will show that the probability of this event is exponentially small. The diagonal elements of matrix $\mathbf{T} - \frac{N}{2M+1}\mathbf{I}$ are

zero. Gershgorin Circle Theorem implies the following.

$$\|\mathbf{T} - \frac{N}{2M+1}\mathbf{I}\| \leq \max_k \sum_{l,l\neq k} |T_{kl}|.$$

$$\begin{aligned}
\mathbb{P}\left(\|\mathbf{T} - \frac{N}{2M+1}\mathbf{I}\| \geq \frac{N}{2M+1}\epsilon\right) &\leq \mathbb{P}\left(\max_k \sum_{l,l\neq k} |T_{kl}| \geq \frac{N}{2M+1}\epsilon\right) \\
&\leq \mathbb{P}\left(2\sum_{m=1}^{M} |T_m| + \sum_{m=M+1}^{2M} |T_m| \geq \frac{N}{2M+1}\epsilon\right) \text{ (Lemma 6.7.5)} \\
&\leq \sum_{m=1}^{M} \mathbb{P}\left(|T_m| \geq \frac{N}{\frac{3}{2}(2M+1)^2}\epsilon\right) + \\
&\quad \sum_{m=M+1}^{2M} \mathbb{P}\left(|T_m| \geq \frac{N}{\frac{3}{2}(2M+1)^2}\epsilon\right) \text{ (Lemma 6.7.2)} \\
&\leq \sum_{m=1}^{2M} \mathbb{P}\left(|T_m| \geq \frac{N}{\frac{3}{2}(2M+1)^2}\epsilon\right).
\end{aligned}$$

Note that $|T_m|^2 = Re^2(T_m) + Im^2(T_m)$. Therefore, $|T_m| \geq d$ implies either $|Re(T_m)| \geq \frac{d}{\sqrt{2}}$ or $|Im(T_m)| \geq \frac{d}{\sqrt{2}}$. Therefore,

$$\begin{aligned}
\mathbb{P}\left(\|\mathbf{T} - \frac{N}{2M+1}\mathbf{I}\| \geq \frac{N}{2M+1}\epsilon\right) &\leq \sum_{m=1}^{2M} \mathbb{P}\left(|Re(T_m)| \geq \frac{N}{\frac{3\sqrt{2}}{2}(2M+1)^2}\epsilon\right) + \\
&\quad \sum_{m=1}^{2M} \mathbb{P}\left(|Im(T_m)| \geq \frac{N}{\frac{3\sqrt{2}}{2}(2M+1)^2}\epsilon\right)
\end{aligned}$$

$$\begin{aligned}
\mathbb{P}\left(|Re(T_{kl})| \geq \frac{N}{\frac{3\sqrt{2}}{2}(2M+1)^2}\epsilon\right) &= \mathbb{P}\left(|\sum_{i=1}^{N} Re(X_{kl}^i)| \geq \frac{N}{\frac{3\sqrt{2}}{2}(2M+1)^2}\epsilon\right) \\
&= \mathbb{P}\left(|\sum_{i=1}^{N} \left(Re(X_{kl}^i) - \mathbb{E}[Re(X_{kl}^i)]\right)| \geq \frac{N}{\frac{3\sqrt{2}}{2}(2M+1)^2}\epsilon\right) \\
&\quad \text{(From Equation 6.56)}
\end{aligned}$$

Applying Lemma 6.7.1, Lemma 6.7.3 and Equation (6.63),

$$\begin{aligned}
\mathbb{P}\left(|Re(T_m)| \geq \frac{N}{\frac{3\sqrt{2}}{2}(2M+1)^2}\epsilon\right) &\leq \\
&2\exp\left(-\frac{\left(\frac{N}{\frac{3\sqrt{2}}{2}(2M+1)^2}\epsilon\right)^2}{\frac{2N}{2(2M+1)^2}\left[1-\operatorname{sinc}^2\left(\frac{\pi m}{N}\right)\right]+\frac{2}{3}\cdot\frac{2}{2M+1}\cdot\frac{N}{\frac{3\sqrt{2}}{2}(2M+1)^2}\epsilon}\right) \\
&= 2\exp\left(-\frac{N\epsilon^2}{\frac{9}{2}(2M+1)^2\left[1-\operatorname{sinc}^2\left(\frac{\pi m}{N}\right)\right]+2\sqrt{2}(2M+1)\epsilon}\right) \\
&\leq 2\exp\left(-\frac{N\epsilon^2}{\frac{9}{2}(2M+1)^2\left[1-\operatorname{sinc}^2\left(\frac{\pi(2M+1)}{N}\right)\right]+2\sqrt{2}(2M+1)\epsilon}\right)
\end{aligned}$$

A similar result follows for the imaginary part. This implies,

$$\mathbb{P}\left(\|\mathbf{T}-\frac{N}{2M+1}\mathbf{I}\| \geq \frac{N}{2M+1}\epsilon\right) \leq \psi,$$

where

$$\psi = 4(2M+1)\exp\left(-\frac{N\epsilon^2}{\frac{9}{2}(2M+1)^2\left[1-\operatorname{sinc}^2\left(\frac{\pi(2M+1)}{N}\right)\right]+2\sqrt{2}(2M+1)\epsilon}\right).$$

This leads to the final result. □

Thus, the probability of the largest eigenvalue of $\mathbf{T}-\frac{N}{2M+1}\mathbf{I}$ being too large is exponentially small for sufficiently large values of N. Let us analyze conditions on N under which the probability is sufficiently small. Let δ be this small fixed probability and let $\delta \geq 4(2M+1)\exp\left(-\frac{N\epsilon^2}{\frac{9}{2}(2M+1)^2\left[1-\operatorname{sinc}^2\left(\frac{\pi(2M+1)}{N}\right)\right]+2\sqrt{2}(2M+1)\epsilon}\right)$. Then,

$$N \geq \frac{2}{\epsilon^2}\log\left(\frac{2M+1}{\delta}\right)\left[\frac{9}{2}(2M+1)^2\left[1-\operatorname{sinc}^2\left(\frac{\pi(2M+1)}{N}\right)\right]+2\sqrt{2}(2M+1)\epsilon\right].$$

This implies,

$$N \geq \max\{\frac{9}{\epsilon^2}(2M+1)^2 \log\left(\frac{2M+1}{\delta}\right)\left[1-\text{sinc}^2\left(\frac{\pi(2M+1)}{N}\right)\right], 2\sqrt{2}\frac{(2M+1)}{\epsilon}\log\left(\frac{2M+1}{\delta}\right)\}. \tag{6.69}$$

Typically, for constant values of ϵ and δ, the first term dominates and the number of samples required is,

$$N \geq C(2M+1)^2 \log(2M+1) \tag{6.70}$$

where C is a constant that depends on δ and ϵ.

Now we prove results about error tolerance of this arrangement. The above theorem about a bound on $\|\mathbf{T} - \frac{N}{2M+1}\mathbf{I}\|$ implies the following theorem.

Theorem 6.7.7. *Consider a 1D trigonometric polynomial field. Let $X = \{x_1, x_2, \cdots, x_N\}$ be a sensor arrangement in $[0,1]$ such that x_i's are arranged in increasing order and each x_i is chosen uniformly randomly in the interval $[\frac{i}{N} - \frac{1}{2N}, \frac{i}{N} + \frac{1}{2N}]$, where $i = 1, 2, \cdots, N$. $N \geq (2M+1)$. Let $\mathbf{T}$ be the corresponding block Toeplitz matrix. Then with probability at least $1 - \psi$,*

$$\frac{N}{2M+1}(1-\epsilon) \leq \lambda_i(\mathbf{T}) \leq \frac{N}{2M+1}(1+\epsilon) \text{for} i = 1, 2, \cdots, 2M+1, \tag{6.71}$$

where psi is given by Equation (6.68) and $\lambda_i(\mathbf{T})$ denotes the ith eigenvalue of $\mathbf{T}$.

Proof. The result follows from the previous theorem and Theorem 8.1.5 in [29]. □

The bounds on the individual eigenvalues allows to calculate bounds on the error metric value given by the sensor arrangement.

Theorem 6.7.8. *Consider 1D trigonometric polynomial field. Let $X = \{x_1, x_2, \cdots, x_N\}$ be a sensor arrangement in $[0,1]$ such that x_i's are arranged in increasing order and each x_i is chosen uniformly randomly in the interval $[\frac{i}{N} - \frac{1}{2N}, \frac{i}{N} + \frac{1}{2N}]$, where $i = 1, 2, \cdots, N$. $N \geq (2M+1)$. Then with probability at least $1 - \psi$,*

$$\sigma^2 \frac{2M+1}{N(1+\epsilon)} \leq \text{Err}(X) \leq \sigma^2 \frac{2M+1}{N(1-\epsilon)} \tag{6.72}$$

where ψ is given by Equation (6.68). Since there are N samples, the lower bound can be improved based on Theorem 6.4.3.

$$\sigma^2 \frac{2M+1}{N} \leq \mathrm{Err}(X) \leq \sigma^2 \frac{2M+1}{N(1-\epsilon)}. \tag{6.73}$$

The above theorem allows us to compare the bounds with Δ-dense sensor arrangements. Recall that the random sensor arrangement of N samples we study in this subsection is in fact a $\frac{2}{N}$-dense arrangement. Let Y be a $\frac{2}{N}$-dense arrangement with N samples. Based on Theorem 6.4.3 and Conjecture 6.5.2, we obtain the following bounds for a $\mathrm{Err}(Y)$.

$$\sigma^2 \frac{2M+1}{N} \leq \mathrm{Err}(X) \leq 2\sigma^2 \frac{2M+1}{N}. \tag{6.74}$$

The random sensor arrangement guarantees tighter error tolerance value, albeit probabilistically.

6.7.2 Uniformly random sensor arrangement

Uniformly random sensor arrangement is the simplest type of random sensor arrangements. Again, we deal with 1D trigonometric polynomials as in the previous section. We assume that N samples are placed uniformly randomly over the domain $[0, 1]$. As in the previous section, we can carry out moment analysis to get similar error bounds in this case as well. In the previous section, we noted that $N = O((2M+1)^2 \log(2M+1))$ samples are required to achieve error bounds *whp*. However, in [36], the authors proved a better bound, $N = O((2M+1)\log(2M+1))$ using techniques in *compressed sensing*. The sensor arrangement in the previous section definitely seems superior over the uniform sensor arrangement because it leads evenly-spread samples. However, so far we have not been able to prove a better bound on the number of samples and are currently working on it. In this section, we reproduce the result in [36] on the uniformly random sensor arrangement.

Lemma 6.7.9. *[36] Consider a 1D trigonometric polynomial field. Let $X = \{x_1, x_2, \cdots, x_N\}$*

be a sensor arrangement in $[0,1]$ *such that* x_i*'s are chosen uniformly randomly in the interval* $[0,1]$*, where* $i = 1, 2, \cdots, N$*.* $N \geq (2M+1)$*. Let* $\mathbf{T}$ *be the corresponding block Toeplitz matrix. Choose* $0 < \epsilon < 1$*,* $0 < \alpha < \epsilon^2$*, and* $\psi > 0$*. If*

$$\left\lfloor \frac{\alpha N}{3(2M+1)} \right\rfloor \geq \left[\ln\left(\frac{\epsilon^2}{\alpha}\right) \right]^{-1} \ln\left(\frac{2M+1}{\psi(1-\alpha)}\right), \tag{6.75}$$

then with probability at least $1 - \psi$*,*

$$\frac{N}{2M+1}(1-\epsilon) \leq \lambda_{min}(\mathbf{T}) \leq \lambda_{max}(\mathbf{T}) \leq \frac{N}{2M+1}(1+\epsilon). \tag{6.76}$$

If we choose, $\alpha = \frac{\epsilon^2}{e}$,

$$N \geq \frac{3(2M+1)e}{\epsilon^2} \left[\ln\left(\frac{2M+1}{\psi}\right) + 2 - \ln(e-1) \right]. \tag{6.77}$$

We translate above result into a theorem pertinent to error-tolerant arrangements.

Theorem 6.7.10. *[36] Consider a 1D trigonometric polynomial field. Let* $X = \{x_1, x_2, \cdots, x_N\}$ *be a sensor arrangement in* $[0,1]$ *such that* x_i*'s are chosen uniformly randomly in the interval* $[0,1]$*, where* $i = 1, 2, \cdots, N$*.* $N \geq (2M+1)$*. Let* $\mathbf{T}$ *be the corresponding block Toeplitz matrix. Choose* $0 < \epsilon < 1$*,* $0 < \alpha < \epsilon^2$*, and* $\psi > 0$*. If*

$$\left\lfloor \frac{\alpha N}{3(2M+1)} \right\rfloor \geq \left[\ln\left(\frac{\epsilon^2}{\alpha}\right) \right]^{-1} \ln\left(\frac{2M+1}{\psi(1-\alpha)}\right),$$

then with probability at least $1 - \psi$*,*

$$\sigma^2 \frac{2M+1}{N(1+\epsilon)} \leq \mathrm{Err}(X) \leq \sigma^2 \frac{2M+1}{N(1-\epsilon)}. \tag{6.78}$$

Since there are N *samples, the lower bound can be improved based on Theorem 6.4.3.*

$$\sigma^2 \frac{2M+1}{N} \leq \mathrm{Err}(X) \leq \sigma^2 \frac{2M+1}{N(1-\epsilon)}. \tag{6.79}$$

In comparison with Theorem 6.7.8, the above theorem suggests that for $N = O((2M+1)\log(2M+1))$ it is possible to achieve similar bounds on the error metric

whp. This indeed is a tighter bound on the number of samples required. We are currently working on using proof techniques used in [36] to improve the results in the previous subsection.

6.8 On the i.i.d. noise assumption

Throughout our treatment of trigonometric polynomials, we assumed that measurement noise at any location is an independent and identically distributed random variable. In this section, we touch upon this topic. We discuss implications and validity of this assumption.

Recall that we used $\mathbf{e}$ to denote the vector of measurement noise. We assumed, regardless of the locations of measurement, that $E[\mathbf{e}] = 0$ and $E[\mathbf{e}^T\mathbf{e}] = \sigma^2\mathbf{I}$. Consider the problem of sampling a trigonometric polynomial in 1D over the domain $[0, 1]$ using N samples. The i.i.d. noise assumption leads to the following formulation for the error metric for a given arrangement X.

$$\text{Err}(X) = \frac{\sigma^2}{(2M+1)}\text{trace}\{\mathbf{T}^{-1}\} \tag{6.80}$$

where,

$$\mathbf{T}_{k,l} = \frac{1}{(2M+1)}\sum_{i=1}^{N} e^{-2\pi j(k-l)x_i}$$
$$\text{where } k, l = -M, -M+1, \cdots, 0, 1, \cdots, +M$$

Now consider a situation in which we take samples only over the domain $[0, \delta]$. Moreover assume that we follow regular sampling strategy over this interval. Thus,

$$\mathbf{T}_{k,l} = \frac{1}{(2M+1)}\sum_{i=1}^{N} e^{-2\pi j(k-l)\frac{(i-1)\delta}{N}}. \tag{6.81}$$

Suppose we keep δ fixed and let the number of samples increase to a large number. In that case we will be able to approximate the above summation using the following

integral.

$$\mathbf{T}_{k,l} = \frac{1}{(2M+1)} \sum_{i=1}^{N} \frac{e^{-2\pi j(k-l)\frac{(i-1)\delta}{N}}}{N} \approx \frac{N}{(2M+1)} \int_0^{\delta} e^{-2\pi j(k-l)x} dx \tag{6.82}$$

The integral in the above equation evaluates a value which is a function of δ. Thus,

$$\mathbf{T} \approx \frac{N}{(2M+1)} \mathbf{C}(\delta) \tag{6.83}$$

where $\mathbf{C}(\delta)$ is a constant matrix of size $(2M+1) \times (2M+1)$ and a function of δ. Thus, the error metric will approximate to the following:

$$\text{Err}(X) \approx \frac{\sigma^2}{N} \text{trace}\{\mathbf{C}^{-1}(\delta)\}. \tag{6.84}$$

For a given δ and M, the quantity trace$\{\mathbf{C}^{-1}(\delta)$ is fixed. Thus, the error metric is inversely proportional to N. By arbitrarily increasing N, we can make the error arbitrarily small. This will have deep implications on the sampling problem, and in turn on the mobile sampling problem. If we make δ very small but constant, and increase the number of samples to a very large value, the error metric will still be very small. In other words, by sampling over a tiny interval itself, we will be able to reconstruct the entire function. For the mobile sampling problem, this will mean that the mobile node will have to travel over a very small distance and spend less energy in motion. This seems too good to be true in reality. There is a caveat in the above argument. Measurement error is not a pure i.i.d. random variable! We assumed that the measurement error stems from two sources, quantization and sensor noise. Even if we assume that sensor noise is i.i.d., quantization will introduce correlations between measurement errors at two nearby locations. In fact, even sensor noise could be correlated at nearby locations. Correlations will prevent us from making the error metric arbitrarily small by mere over-sampling. At the first place, we not be able to use Equation 6.29. We will have to resort to Equation 6.15 to calculate the error metric with the knowledge of the noise correlation matrix. It is very hard to characterize quantization and sensor noise effects. The i.i.d. assumption

for quantization error allows for much more tractable analysis [30]. It is also shown to be a good approximation at high resolution for uniform sampling of smooth functions. We refer interested readers to [32] for an extensive survey on quantization. Based on this, we can perhaps impose a constraint on the minimum distance between two neighboring samples is not too small. Currently we are working on simulations to evaluate the validity of the i.i.d. assumption for quantization errors for different sampling schemes. Note that, we have not discussed anything about the modeling errors, *i.e.* errors introduced due to band-limited assumption. Some of the above discuss applies for this case and it is a topic of our future research.

Chapter 7

On Mobility of Point Estimation Sensors

In this chapter, we discuss a couple of problems that are related to motion planning over the classes of error-tolerant arrangements to minimize energy costs in motion.

In the previous chapter we introduced the sensor arrangement problem for estimation sensors, where our goal is to decide when and where to take samples such that the error in function estimation is less than a certain error tolerance level. We noted that characterizing the space all such arrangements is hard. Instead we defined the notion of an ETAC (class of error-tolerant arrangements) where every arrangement is error-tolerant and satisfies a set of properties that defines the class. We discussed a few types of deterministic as well as random ETACs for trigonometric polynomials. For instance, we discussed regular sensor arrangements and discussed conditions under which a subset of these form an ETAC. Similarly, we discussed Δ-dense sensor arrangements and discussed conditions on Δ such that a Δ-dense arrangement is an ETAC. In case of random sensor arrangements, we discussed arrangements that are error-tolerant with high probability. When we discussed the notion of an ETAC, we mentioned that we will be able to overlay motion-related problems over ETACs. In this thesis, we emphasized on two types of mobility, incidental (where nodes move under the influence of the environment) and intentional (where nodes have control over where they move). In this chapter, we argue that motion-planning problems

for either type of mobile sensors can be overlay-ed on ETACs. We discuss this via a few example problems. Our intent here is not to discuss a detailed solution to any particular type of motion-related problem but highlight that there is a rich class of problems that can be addressed through the notion of ETACs.

7.1 A few motion-related problems overlay-ed on ETACs

In this section, we discuss a few problems related to intentional as well as incidental mobility of sensors overlay-ed on the space of error-tolerant arrangements. First we deal with Δ-dense arrangements and later with random sensor arrangements.

7.1.1 Δ-dense sensor arrangements

In the previous chapter we defined Δ-dense arrangement as the one where any L_∞-disc with Δ radius placed anywhere in the domain contains at least one sample. In other words, L_∞-discs of radius Δ centered at all the sampling sites should overlap the entire domain. Another interpretation is that there should not be a *large* hole in the sampling domain. In the previous chapter, based on our conjecture 6.5.2, we discussed conditions under which a Δ-dense arrangement is error-tolerant. In this section, we discuss problems related to mobility of the nodes that can be overlay-ed on the space of error-tolerant Δ-dense arrangements. We deal with fields that are *stationary* with respect to time or changing very slowly with time. In other words, the field is only spatial and does not change with time. We can easily extend the problems below along the temporal dimension. But the solutions to the problems involving temporal dimension need to account for the fact that time always moves forward! Below we discuss problems related to intentional as well as incidental mobility overlay-ed on the space of Δ-dense distributions. In each of these problems, we assume a trigonometric polynomial model for the unknown field as described in the previous chapter. We further assume that we can characterize errors due to modeling, quantization and

sensor noise as additive independent and identically distributed Gaussian random variables. Based on the required error-tolerance, we can find the value of Δ.

Problem 1: The first problem concerns intentionally mobile sensors. Consider a scenario in which we want to map an unknown field using sensors mounted on intentionally mobile nodes. There maybe a few static sensor nodes already deployed in the domain. A possible objective of this sensor network could be to reconstruct the unknown field with tolerable estimation error using the static as well as the mobile sensors with minimum energy spent by the mobile nodes. A possible example of this scenario is discussed in [88]. In this paper, the authors consider the problem of sampling temperature and chlorophyll concentration fields in lakes using a network of a few static sensors and one sensor mounted on a mobile robotic boat capable of intentional motion.

Our approach to deal with the above problem is to overlay the mobility problem on the space of Δ-dense arrangements. Energy spent by a mobile node will have different characterizations depending on the application. A simple metric can be the distance traveled by a mobile node. A more detailed characterization could be in terms of the velocities, accelerations, decelerations, etc. of a mobile node. A special case of this problem is related to the *traveling salesman problem* [12]. In this problem a network of cities is given with distances connecting them. The goal of a salesman is to find a minimum-distance tour starting from a particular city such that he visits every city in the network and returns to the starting city [12]. Consider a scenario in which we have just one mobile node and no static sensors. Suppose we consider only Δ-dense sensor arrangements. For a given Δ-dense arrangement, the minimum-energy tour of the mobile node is the traveling salesman tour. The solution to the original sampling problem involves finding a Δ-dense arrangement for the given error-tolerance, which leads to the shortest tour. Unfortunately, the traveling salesman problem and its variations have been shown to be *NP-hard* and one can hope for only an approximate solution. The other versions of the sampling problem including multiple mobile nodes in combination with static sensors is even more complicated.

Problem 2: This problem concerns intentionally mobile sensors with a limited ability to move.[1] Consider a sensor network implementation in which each sensor, although intentionally mobile, has a limited ability to move and remains static for the most part. Assume that the number of sensors deployed is sufficiently large. Consider a situation in which the distribution of the sensors does not meet the necessary conditions to form a Δ-dense arrangement and perhaps is not error-tolerant. This situation could very well occur in practice when the sensors are randomly deployed initially. Also, in some situations sensors may slowly drift under the influence of external effects (*e.g.* wind currents, water currents) during their operation. In these cases, sensors need to reconfigure themselves to form a Δ-dense arrangement. The question we pose is how sensors should coordinate and reconfigure themselves to form a Δ-dense arrangement such that minimum energy is spent in reconfiguration.

Problem 3: This problem concerns incidentally mobile sensors. These sensors do not have control over where they move because they move under the influence of the external sources. Thus, energy is not an issue. However, the question is how these sensors should be deployed initially and how often they should collect the samples to obtain a Δ-dense arrangement. Given the incidental mobility model of nodes, the design question would be to find the number of nodes to be deployed, their initial distribution and their sampling strategies to guarantee a Δ-dense arrangement of samples. In Chapter 6, we showed that a Δ-dense arrangement guarantees that L_∞ coverage-discs around each sample cover the entire domain. Thus, coverage-discs around incidentally mobile sensors *sweep* the entire domain. In Chapter 3 we dealt with this situation when we discussed a coverage problem for floating event-detection sensors in rivers. We imposed the coverage constraint that the area swept by the coverage-discs around each floating sensor should not contain any holes.

[1] This problems was suggested by Prof. Gaurav Sukhatme at the University of Southern California during our discussion.

7.1.2 Random sensor arrangements

In Chapter 6, we discussed two types of random sensor arrangements for trigonometric polynomials. In random arrangements, samples are taken from a probabilistic distribution. Hence we can guarantee error-tolerance only in the probabilistic sense. Here we describe a problem related to incidental mobility as overlay-ed on the space of random sensor arrangements.

Sometimes, incidental mobility of a node is modeled stochastically. For instance, in Chapter 3, we modeled natural mobility of floating nodes in a river as a stochastic differential equation. This leads to random arrangements of samples which depend on the initial deployment, the incidental mobility model and the sampling strategy. For a given incidental mobility model, we ask the question: what should be the initial deployment of the nodes and the sampling strategy for each node in order to guarantee error tolerance with high probability?

We believe that there is a space of rich problems at the intersection of mobility and sampling. In this chapter, we attempted to discuss a only few problems related. We are currently working on some of these problems.

Chapter 8

Conclusions and Future Work

In this thesis, we considered coverage problems at the intersection of two sensing modalities, event-detection and estimation, and two mobility types, intentional and incidental. We summarize our conclusions on the problems we addressed here.

8.1 Conclusions

- We analyzed coverage and connectivity of a network of naturally-mobile event-detection sensors in rivers using simulations on 1) a mobility model for an idea river, and 2) a mesh model based on experimental data in real rivers. We showed that sufficient number of nodes *covering* the transverse cross-section of the river guarantee that no large holes are left in the region covered by sensors. We also showed that connectivity of sensors in the ad-hoc network settings in the central zone of the river is sustained for long periods.

- In case of reconfigurable camera networks, we showed that detection behavior of the camera depends on the surrounding conditions and is thus location dependent. We formulated a new type of locational optimization problem for sensors with location-dependent sensing performance function. We propose a distributed algorithm to obtain a coverage solutions. We present results of the algorithm in camera networks in indoor and outdoor pathways.

- We addressed the sensor arrangement problem for point estimation sensors – when and where to sample in order to guarantee that the estimation error is less than a pre-specified tolerance limit. We discussed a few deterministic and random classes of error-tolerant sensor arrangements for trigonometric polynomial fields.

8.2 Future Work

In future, we would like to extend our work in the following directions.

- In this thesis we considered river geometries that changed slowly. In some regions, river however meander and have sharp bends. In future we would like to incorporate effects of such geometries on the natural mobility and understand its impact on the network properties.

- Besides rivers, oceans and lakes are the biggest sources of natural mobility. We plan to analyze network properties in these domains.

- In reconfigurable camera networks, we considered pathways with just one loop. In future we would like to extend our work for pathways with multiple loops. Another interesting question relates to the minimum number of sensors required for such classes of sensors to guarantee minimum coverage.

- In case of estimation sensors, we considered various classes of error-tolerant sensor arrangements for trigonometric polynomial fields. In future we want to examine fields with other kinds of basis functions. We also plan to study how underlying physics of the process affects modeling of the field and geometries of sensor arrangements.

Bibliography

[1] Workshop: Sensors for environmental observatories. University of Washington, Seattle, 2004.

[2] I. F. Akyildiz, W. Su, Y. Sankarasubramaniam, and E. Cayirci. Wireless sensor networks: a survey. *Computer Networks*, 38(4):393–422, 2002.

[3] A. Aldroubi and K. Gröchenig. Nonuniform sampling and recontruction in shift-invariant spaces. *SIAM Review*, 43:585–620, 2001.

[4] R. F. Bass and K. Gröchenig. Random sampling of multivariate trigonometric polynomials. *SIAM Journal On Mathematical Analysis*, 36(3):773–795, 2004.

[5] M. A. Batalin, M. Rahimi, Y. Yu, D. Liu, A. Kansal, G. S. Sukhatme, W. J. Kaiser, M. Hansen, G. J. Pottie, M. B. Srivastava, and D. Estrin. Call and response: experiments in sampling the environment. In *SenSys '04: Proceedings of the 2nd international conference on Embedded networked sensor systems*, pages 25–38, New York, NY, USA, 2004. ACM Press.

[6] R. Beckwith, D. Teibel, and P. Bowen. Report from the field: Results from an agricultural wireless sensor networks. In *IEEE International Conference of Local Computer Networks, (LCN'04)*. IEEE Computer Society, 2004.

[7] G. Bennett. Probability inequalities for the sum of independent random variables. *Journal of the American Statistical Association*, 57(297):33–45, 1962.

[8] J. Burrell, T. Brooke, and R. Beckwith. Vineyard computing: Sensor networks in agricultural production. *IEEE Pervasive Computing*, 3(1):38–45, 2004.

[9] M. Cardei and J. Wu. *Coverage in Wireless Sensor Networks in Handbook of Sensor Networks.* CRC Press, 2004.

[10] O. Christensen. *An Introduction to Frames and Riesz Bases.* Applied and Numerical Harmonic Analysis. Birkhäuser, 2003.

[11] S. Coleri, S. Y. Cheung, and P. Varaiya. Sensor networks for monitoring traffic. In *Allerton Conference on Communication, Control and Computing*, 2004.

[12] T. H. Cormen, C. E. Leiserson, R. L. Rivest, and C. Stein. *Introduction to Algorithms, Second Edition.* The MIT Press and McGraw-Hill Book Company, 2001.

[13] J. Cortes, S. Martinez, T. Karatas, and F. Bullo. Coverage control for mobile sensing networks. In *IEEE Conference on Robotics and Automation*, pages 1327–1332, Arlington, VA, May 2002.

[14] J. Cortes, S. Martinez, T. Karatas, and F. Bullo. Coverage control for mobile sensing networks. *IEEE Transactions on Robotics and Automation*, 20(2):243–55, 04/ 2004.

[15] J. Cortes, S. Martinez, T. Karatas, and F. Bullo. Coverage control for mobile sensing networks. *IEEE Transactions on Robotics and Automation*, 20(2):243–255, 2004.

[16] I. Daubechies. *Ten Lectures on Wavelets.* CBMS-NSF Regional Conference Series in Applied Mathematics. SIAM, 1992.

[17] Z. Deng, V. P. Singh, and L. Bengtsson. Longitudinal dispersion coefficient in straight rivers. *Journal of Hydraulic Engineering*, 127(11):919–927, 2001.

[18] A. Deshpande and S. E. Sarma. Error tolerant arrangements of sensors for sampling fields. *American Control Conference, 2008*, pages 2401–2408, June 2008.

[19] A. Dhariwal, B. Zhang, B. Stauffer, C. Oberg, G. S. Sukhatme, D. A. Caron, and A. A. Requicha. Networked aquatic microbial observing system. In *IEEE International Conference on Robotics and Automation*, pages 4285–4287, Orlando, FL, May 2006. IEEE.

[20] R. Duffin and A. Schaeffer. A class of nonharmonic fourier series. *Transactions of American Mathematical Society*, 72(2):341–366, 1952.

[21] S. Dutch. Converting UTM to latitude and longitude (or vice versa). http://www.uwgb.edu/dutchs/UsefulData/UTMFormulas.htm.

[22] S. Eidenbenz, C. Stamm, and P. Widmayer. Inapproximability results for guarding polygons and terrains. *Algorithmica*, 31:79–113, 2001.

[23] D. Estrin, R. Govindan, J. Heidemann, and S. Kumar. Next century challenges: scalable coordination in sensor networks. In *MobiCom '99: Proceedings of the 5th annual ACM/IEEE international conference on Mobile computing and networking*, pages 263–270, New York, NY, USA, 1999. ACM.

[24] H. B. Fischer. Longitudinal dispersion and turbulent mixing in open-channel flow. *Annual Review of Fluid Mechanics*, 5:59–78, 1973.

[25] H. B. Fischer, E. J. List, R. C. Y. Koh, K. Imberger, and N. H. Brooks. *Mixing in inland and coastal waters.* Academic, 1979.

[26] D. W. Gage. Command control for many-robot systems. *Unmanned Systems*, Fall 1992.

[27] A. El Gamal, J. P. Mammen, B. Prabhakar, and D. Shah. Throughput-delay trade-off in wireless networks. In *INFOCOM*, 2004.

[28] D. Ganesan, S. Ratnasamy, H. Wang, and D. Estrin. Coping with irregular spatio-temporal sampling in sensor networks. *SIGCOMM Comput. Commun. Rev.*, 34(1):125–130, 2004.

[29] G. H. Golub and C. F. Van Loan. *Matrix Computations*. Johns Hopkins University Press, Baltimore, MD, USA, 1996.

[30] V. K. Goyal, J. Kovacevic, and J. A. Kelner. Quantized frame expansions with erasures. *Applied and Computational Harmonic Analysis*, 10(3):203–233, May 2001.

[31] V. K. Goyal, M. Vetterli, and N. T. Thao. Quantized overcomplete expansions in R-N: Analysis, synthesis, and algorithms. *IEEE Transactions on Information Theory*, 44(1):16–31, Jan 1998.

[32] R. M. Gray and D. L. Neuhoff. Quantization. *IEEE Transactions on Information Theory*, 44(6):2325–2383, Oct 1998.

[33] G. Grimmett and D. Stirzaker. *Probability and Random Processes, Third Edition*. Oxford, 2001.

[34] K. Gröchenig. Reconstruction algorithms in irregular sampling. *Mathematics of Computation*, 59(199):181–194, July 1992.

[35] K. Gröchenig. A discrete theory of irregular sampling. *Linear Algebra Applications*, 193(1):129–150, 1993.

[36] K. Gröchenig, B. M. Poetscher, and H. Rauhut. Learning trigonometric polynomials from random samples and exponential inequalities for eigenvalues of random matrices, 2007.

[37] K. Gröchenig and T. Strohmer. *Theory and Practice of Nonuniform Sampling*, chapter Numerical and theoretical aspects of non-uniform sampling of band-limited images, pages 283–322. Kluwer Academic/Plenum Publishers, 2000.

[38] C. Guestrin, A. Krause, and A. P. Singh. Near-optimal sensor placements in gaussian processes. In *ICML*, pages 265–272, 2005.

[39] P. Gupta and P. R. Kumar. Critical power for asymptotic connectivity in wireless networks. In W. M. McEneany, G. Yin, and Q. Zhang, editors, *Stochastic Analysis, Control, Optimization and Applications: A Volume in Honor of W.H. Fleming*, pages 547–566. Birkhauser, Boston, 1998.

[40] C. E. Heil and D. F. Walnut. Continuous And Discrete Wavelet Transforms. *SIAM Review*, 31(4):628–666, DEC 1989.

[41] H. Hemond. Personal communications, 2006.

[42] D. J. Holtschlag and S. A. Aichele. Visualization of drifting buoy deployments on st. clair river near public water intakes.

[43] D. J. Holtschlag and S. A. Aichele. Visualization of drifting buoy deployments on upper detroit river within the great lakes waterway from august 28-30, 2001.

[44] A. Howard, M. J. Matarić, and G. S. Sukhatme. Mobile sensor network deployment using potential fields: A distributed, scalable solution to the area coverage problem. In *Proceedings of the International Symposium on Distributed Autonomous Robotic Systems*, pages 299–308, 2002.

[45] B. Hull, V. Bychkovsky, Y. Zhang, K. Chen, M. Goraczko, A. Miu, E. Shih, H. Balakrishnan, and S. Madden. Cartel: a distributed mobile sensor computing system. In *SenSys '06: Proceedings of the 4th international conference on Embedded networked sensor systems*, pages 125–138, New York, NY, USA, 2006. ACM.

[46] T. Jaakkola. 6.867 machine learning class notes. http://courses.csail.mit.edu/6.867, 2007.

[47] J. M. Kahn, R. H. Katz, and K. S. J. Pister. Next century challenges: mobile networking for "smart dust". In *MobiCom '99: Proceedings of the 5th annual ACM/IEEE international conference on Mobile computing and networking*, pages 271–278, New York, NY, USA, 1999. ACM.

[48] T. Kailath, A. H. Sayed, and B. Hassibi. *Linear Estimation.* Prentice Hall, 2000.

[49] A. Kansal, W. J. Kaiser, G. Pottie, M. B. Srivastava, and G. S. Sukhatme. Reconfiguration methods for mobile sensor networks. *ACM Transactions on Sensor Networks*, 3(4):22–23, 2007.

[50] B. Krishnamachari. *Networking Wireless Sensors.* Cambridge University Press, January 2006.

[51] F. Lekien and N. E. Leonard. Non-uniform coverage and cartograms. *SIAM Journal on Control and Optimization*, in submission.

[52] N. E. Leonard, D. A. Paley, F. Lekien, R. Sepulchre, D. M. Fratantoni, and R. E. Davis. Collective motion, sensor networks, and ocean sampling. *Proceedings of the IEEE*, 95(1):48–74, 2007.

[53] B. Liu, P. Brass, O. Dousse, P. Nain, and D. Towsley. Mobility improves coverage of sensor networks. In *MobiHoc '05: Proceedings of the 6th ACM international symposium on Mobile ad hoc networking and computing*, pages 300–308, New York, NY, USA, 2005. ACM Press.

[54] D. G. Luenberger. *Optimization by Vector Space Methods.* John Wiley and Sons Inc., 1969.

[55] A. Mainwaring, D. Culler, J. Polastre, R. Szewczyk, and J. Anderson. Wireless sensor networks for habitat monitoring. In *WSNA '02: Proceedings of the 1st ACM international workshop on Wireless sensor networks and applications*, pages 88–97, New York, NY, USA, 2002. ACM Press.

[56] S. Meguerdichian, F. Koushanfar, M. Potkonjak, and M. B. Srivastava. Coverage problems in wireless ad-hoc sensor networks. *Proceedings IEEE INFOCOM 2001. Conference on Computer Communications. Twentieth Annual Joint Conference of the IEEE Computer and Communications Society*, vol.3:1380–1387, 2001.

[57] R. Motwani and B. Raghavan. *Randomized Algorithms.* Cambridge University Press, 1995.

[58] A. Nordio, C. Chiasserini, and E. Viterbo. The impact of quasi-equally spaced sensor layouts on field reconstruction. In *IPSN*, pages 274–282, 2007.

[59] A. Nordio, C. Chiasserini, and E. Viterbo. Quality of field reconstruction in sensor networks. In *INFOCOM*, pages 2406–2410, 2007.

[60] University of Alberta. River2d, two-dimensional depth averaged model of river hydrodynamics and fish habitat, available online.

[61] A. Okabe, B. Boots, and K. Sugihara. *Spatial Tessellations: Concepts and Applications of Voronoi Diagrams.* John Wiley & Sons Ltd., 1992.

[62] J. O'Rourke. *Art Gallery Theorems and Algorithms.* Oxford University Press, 1987.

[63] J. Paek, K. Chintalapudi, R. Govindan, J. Caffrey, and S. Masri. A wireless sensor network for structural health monitoring: Performance and experience. In *EmNetS-II: The Second IEEE Workshop on Embedded Networked Sensors*, pages 1–10. IEEE, May 2005.

[64] S. Poduri and G. S. Sukhatme. Constrained coverage for mobile sensor networks. *2004 IEEE International Conference on Robotics and Automation*, Vol.1:165 – 71, 2004.

[65] R. Pon, M. Batalin, J. Gordon, M. H. Rahimi, W. J. Kaiser, G. S. Sukhatme, M. B. Srivastava, and D. Estrin. Networked infomechanical systems: A mobile wireless sensor network platform. In *IEEE/ACM Fourth International Conference on Information Processing in Sensor Networks (IPSN-SPOTS)*, pages 376–381, Apr 2005.

[66] G. J. Pottie and W. J. Kaiser. Wireless integrated network sensors. *Commun. ACM*, 43(5):51–58, 2000.

[67] G. J. Pottie and W. J. Kaiser. *Principles of Embedded Networked Systems Design.* Cambridge University Press, 2005.

[68] H. Risken. *The Fokker-Planck Equation: Methods of Solutions and Applications.* Springer, second edition, 1996.

[69] M. Schwager, J. Slotine, and D. Rus. Decentralized, adaptive control for coverage with networked robots. In *International Conference on Robotics and Automation*, Rome, April 2007.

[70] S. Shakkottai, R. Srikant, and N. B. Shroff. Unreliable sensor grids: Coverage, connectivity and diameter. In *INFOCOM*, 2003.

[71] C. E. Shannon. Communication in the presence of noise. *Proceedings of the IEEE*, 86(2):447–457, 1998.

[72] T. Shermer. Recent results in art galleries. In *Proceedings of the IEEE*, volume 80, pages 1384–1399, 1992.

[73] A. Singh, R. Nowak, and P. Ramanathan. Active learning for adaptive mobile sensing networks. In *IPSN '06: Proceedings of the fifth international conference on Information processing in sensor networks*, pages 60–68, New York, NY, USA, 2006. ACM Press.

[74] M. Sipser. *Introduction to the Theory of Computation.* PWS Publishing Company, 1997.

[75] R. Szewczyk, A. Mainwaring, J. Polastre, J. Anderson, and D. Culler. An analysis of a large scale habitat monitoring application. In *SenSys '04: Proceedings of the 2nd international conference on Embedded networked sensor systems*, pages 214–226, New York, NY, USA, 2004. ACM.

[76] R. Szewczyk, E. Osterweil, J. Polastre, M. Hamilton, A. Mainwaring, and D. Estrin. Habitat monitoring with sensor networks. *Commun. ACM*, 47(6):34–40, 2004.

[77] G. Taylor. Dispersion of soluble matter in solvent flowing slowly through a tube. *Proceedings of the Royal Society of London. Series A, Mathematical and Physical Sciences*, 219(1137):186–203, 1953.

[78] G. Taylor. The dispersion of matter in turbulent flow through a pipe. *Proceedings of the Royal Society of London. Series A, Mathematical and Physical Sciences*, 223(1155):446–468, 1954.

[79] M. Unser. Sampling - 50 years after Shannon. *Proceedings Of The IEEE*, 88(4):569–587, APR 2000.

[80] Jorge Urrutia. Art gallery and illumination problems. In *Handbook of Computational Geometry (ed. J. R. Sack and J. Urrutia)*. North-Holland, 2000.

[81] Ecosystems Research Division U.S. Environmental Protection Agency. Environmental fluid dynamics code (efdc) manual, available online. 2002.

[82] I. Vasilescu, K. Kotay, D. Rus, M. Dunbabin, and P. Corke. Data collection, storage, and retrieval with an underwater sensor network. In *SenSys '05: Proceedings of the 3rd international conference on Embedded networked sensor systems*, pages 154–165, New York, NY, USA, 2005. ACM Press.

[83] X. Wang, G. Xing, Y. Zhang, C. Lu, R. Pless, and C. Gill. Integrated coverage and connectivity configuration in wireless sensor networks. In *SenSys '03: Proceedings of the 1st international conference on Embedded networked sensor systems*, pages 28–39, New York, NY, USA, 2003. ACM.

[84] X. Wang, G. Xing, Y. Zhang, C. Lu, R. Pless, and C. Gill. Integrated coverage and connectivity configuration in wireless sensor networks. *SenSys'03: Proceedings of the First International Conference on Embedded Networked Sensor Systems*, pages 28 – 39, 2003.

[85] G. Xing, X. Wang, Y. Zhang, C. Lu, R. Pless, and C. Gill. Integrated coverage and connectivity configuration for energy conservation in sensor networks. *ACM Trans. Sen. Netw.*, 1(1):36–72, 2005.

[86] N. Xu, S. Rangwala, K. K. Chintalapudi, D. Ganesan, A. Broad, R. Govindan, and D. Estrin. A wireless sensor network for structural monitoring. In *SenSys '04: Proceedings of the 2nd international conference on Embedded networked sensor systems*, pages 13–24, New York, NY, USA, 2004. ACM Press.

[87] J. L. Yen. On nonuniform sampling of bandwidth-limited signals. *IRE Trans. on Circuit Theory*, CT-3:251–257, December 1956.

[88] B. Zhang and G. S. Sukhatme. Adaptive sampling for estimating a scalar field using a robotic boat and a sensor network. In *IEEE International Conference on Robotics and Automation*, pages 3673–3680, 2007.

[89] F. Zhao and L. J. Guibas. *Wireless Sensor Networks: An Information Processing Approach.* Morgan Kaufmann, 2004.